
DEGREE PROJECT, IN ELECTROPHYSICS , SECOND LEVEL
*STOCKHOLM*, *SWEDEN 2014*

# Antenna for GNSS Reception in GEO-Orbit

PATRICK MAGNUSSON

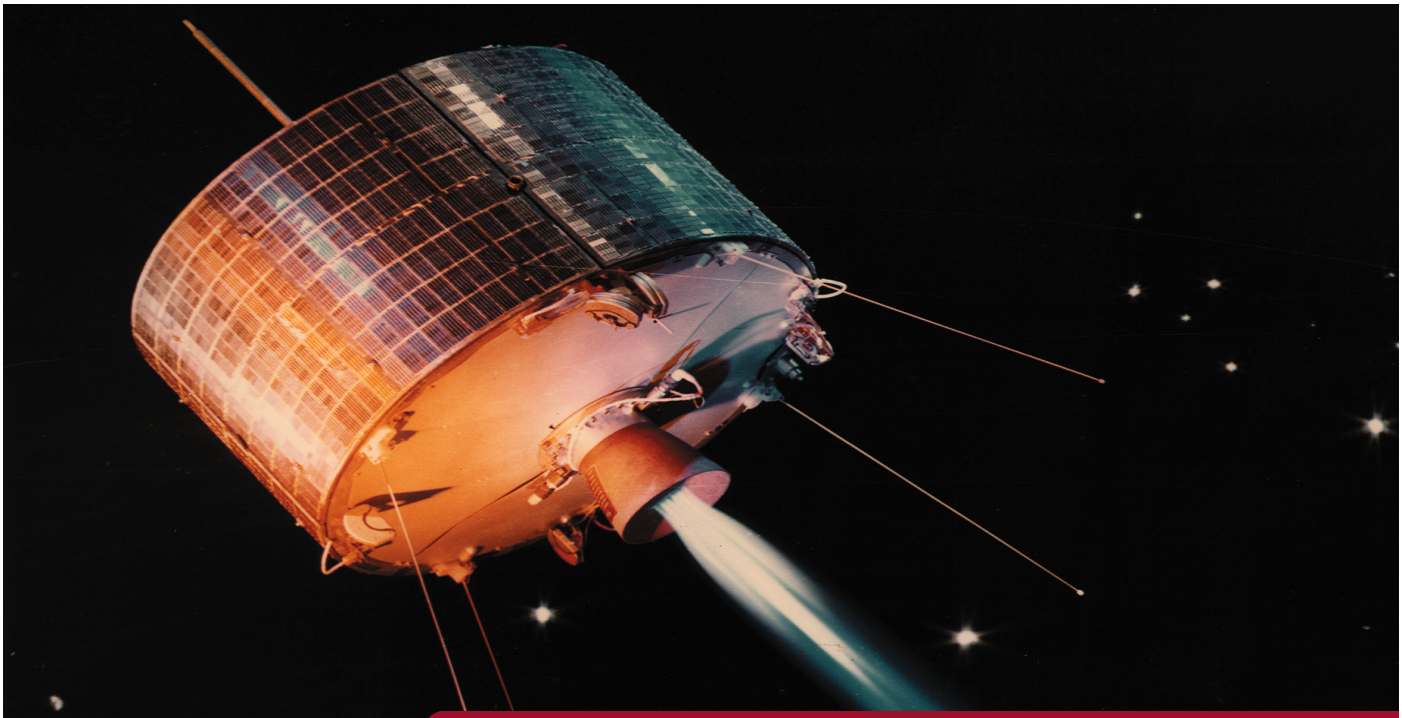

**KTH ROYAL INSTITUTE OF TECHNOLOGY**

**ELECTRICAL ENGINEERING, SPACE AND PLASMA PHYSICS DEPARTMENT**

TRITA XR-EE-SPP 2014:003


KTH Electrical Engineering

# Antenna for GNSS reception in GEO-orbit

**by**

**Patrick Magnusson**

**Master of Science Thesis**

**XR-EE-SPP 2014:003**

Royal Institute of Technology
Department of Electrical Engineering
Space and Plasma Physics

Stockholm 2014

## Abstract

There are a number of global navigation satellite systems (GNSS), in use or planed, which are used for navigation on earth but also for autonomous navigation of satellites in low earth orbit (LEO). It would be desirable to also have autonomous navigation in geosynchronous earth orbit (GEO) to reduce costs and make it possible to get higher accuracy on the position of the satellite. One part of the navigation system is the GNSS antenna which is examined in this master thesis.

The specifications of the antenna were first decided and then three antenna alternatives were investigated in greater detail: a monofilar helix antenna, a three element circular array antenna and a twelve element circular array antenna. The result was that they would all work as a GNSS antenna in GEO but none could be judged to be the best under all circumstances. The size requirement for the mission and the used GNSS receiver would primarily decide which fits the mission best.

## Sammanfattning

Det finns ett antal världstäckande navigeringssystem (GNSS), i användning och planerade, som används för navigation på jorden fast också för autonom navigation för satelliter i låg bana runt jorden. Det skulle också vara önskvärt att använda autonom navigation för satelliter i geostationär omloppsbana (GEO) för att reducera kostnaden och få högre positions noggrannhet. En del av navigationssystemet är GNSS antennen vilken är undersökt i detta examensarbete.

Specifikationerna för antennen bestämdes först och sedan undersöktes tre olika antennalternativ i detalj: en monofilär helixantenn, en tre elements cirkulär gruppantenn och en tolv elements cirkulär gruppantenn. Resultatet var att alla alternativen skulle fungera som en GNSS antenn i GEO-bana fast inget av alternativen är bäst i alla förhållanden. Storlekskraven för uppdraget och vilken GNSS mottagare som skall användas påverkar vilket av alternativen som passar uppdraget bäst.

## Keywords

GNSS antenna, GNSS, GPS, antenna, GEO, helical antenna, circular array, conical radiation pattern, link budget, monofilar helix,

## Acknowledgement

This master thesis was conducted at the company RUAG and I would like to thank RUAG and all the people working there for the opportunity and all the help I have received. I furthermore thank Johan Wettergren for being my supervisor at RUAG. I would also like to thank my supervisor at KTH, Nikolay Ivchenko, and the examiner at KTH, Tomas Karlsson. Acknowledgement goes to NASA for the cover picture of the first geosynchronous satellite, Syncom.

TABLE OF CONTENTS PAGE

## Abbreviations

| | |
|---|---|
| A/D | Analog-to-Digital |
| ADS | Advanced Design System |
| $C/N_0$ | Carrier-to-Noise Density |
| CNC | Computer Numerical Control |
| cx | Cross |
| EIRP | Equivalent Isotropically Radiated Power |
| ESA | European Space Agency |
| FDMA | Frequency-Division Multiple Access |
| FEM | Finite Element Method |
| GEO | Geosynchronous Earth Orbit |
| GIOVE | Galileo In-Orbit Validation Element |
| GLONASS | Globalnaya navigatsionnaya sputnikovaya sistema |
| GNSS | Global Navigation Satellite System |
| GOES | Geostationary Operational Environmental Satellite |
| GPS | Global Positioning System |
| HEO | High Earth Orbit |
| HFSS | High Frequency Structural Simulator |
| HPBW | Half Power Beamwidth |
| IGSO | Inclined Geosynchronous Satellite Orbit |
| IRNSS | Indian Regional Navigational Satellite System |
| LEO | Low Earth Orbit |
| LNA | Low-Noise Amplifier |
| LHC | Left-Hand Circular |
| MEO | Middle Earth Orbit |
| MMS | Magnetospheric Multiscale Mission |
| MoM | Method of Moment |
| N-GSO | Non-Geosynchronous Orbit |
| NASA | National Aeronautics and Space Administration |
| NF | Noise Figure |
| PEC | Patch excited cup |
| PSD | Power Spectral Density |
| QZSS | Quasi-Zenith Satellite System |
| RHCP | Right-Hand Circular Polarization |
| RMS | Root-Mean-Square |
| SMA | SubMiniature version A |
| TEAMSAT | Technology, science and Education experiments Added to Maqsat. |
| TM | Transverse Magnetic |
| VSWR | Voltage Standing Wave Ratio |
| XPD | Cross Polarization Discrimination |
| YES | Young Engineer’s Satellite |

# 1 INTRODUCTION

The global navigation satellite systems (GNSS) work by having multiple satellites transmit their position and the time the position message was sent. The receiver can then decide its position by using the transmitted signal and knowledge of how long the signal has propagated. The most common receivers use a least square method where signals from four GNSS satellites are used to calculate the position. Three satellites are needed to decide the position and a fourth is needed to accurately decide the time at the receiver. The antenna on the GNSS satellite is pointing towards the earth with a narrow beam in order not to waste power transmitting out to space.

A number of GNSSs are in operation or are planned to be put in operation. The first GNSS to be completed was the American GPS in 1993 with a full constellation of 24 satellites. Today, the GPS constellation consists of 31 active MEO satellites [1], [2]. Since then, the Russian GLONASS has also been completed in 1995 but, due to neglecting maintenance, the system degraded. GLONASS was later re-established and the constellation was again completed in 2012. Today GLONASS consists of 24 MEO satellites [3]. There are also two incomplete systems, GALILEO and BeiDou, previously called COMPASS. GALILEO is an ESA project planned to be fully operational before 2020 and will consist of 30 MEO satellites, of which four are currently in operation. The last GNSS is BeiDou controlled by China which currently has five GEO, five IGSO and four MEO satellites in operation. BeiDou currently provides regional coverage over China but is planned to reach global coverage by 2020. The BeiDou is planned to consist of five GEO, three IGSO and 27 MEO satellites [4], [5]. Beside these GNSSs there are also regional navigation systems such as Japan's QZSS and India's IRNSS which use GEO, N-GSO and IGSO satellites. The QZSS is planned to be used with the GPS to improve the accuracy of the position solution over Japan while IRNSS should be able to operate as its own navigation system over India, both QZSS and IRNSS are planned to consist of seven satellites [6], [7].

The GNSSs are first and foremost designed for navigation on earth but they are also extensively used for determining position and autonomous navigation of satellites in LEO [8]. Autonomous navigation is preferable to the otherwise more costly manual navigation and as such it would be desired to implement autonomous navigation with the help of a GNSS receiver for satellites in GEO and HEO as well. The accuracy of orbit determination with the help of a GNSS receiver is also better than the standard on the ground orbit determination and the fuel consumption could be optimized [9]. The GPS has furthermore specified the transmitted signal level at greater angle from the satellites and lowest received signal at GEO altitude, increasing the interest for using GPS for navigation at GEO.

In 1997 the experiment YES onboard TEAMSAT was the first to confirm GPS reception above the GPS constellation where GPS signal was received up to an altitude of 26 000 km. The GPS constellation is at an altitude of 20 200 km [2], [10]. Later in 1997 the Equator-s satellite was also able to track GPS signals. This time at an altitude of 34 000 km, which is close to the altitude of 35 786 km for a GEO satellite. Equator-s was also able to track signals from the GPS satellites side lobes and in 1998 was able to track a GPS signal at 61 000 km above earth [11]. Falcon-Gold also recorded and sent down GPS data in 1997 [12]. In [13], published in 2000, it is described how a satellite from the USA military actually was navigated using the GPS. In this specific case the received GPS signal was sent down to earth for processing. The AMSAT OSCAR-40 satellite was able to track four satellites simultaneously and it was later possible to calculate a position at ground. AMSAT OSCAR-40 was also able to measure the gain of the GPS antenna and the results was presented in 2002 [14]. The first position fix in orbit with an onboard GPS receiver above the GPS constellation was achieved on the retired GIOVE-A, a GALILEO demonstration satellite, at an altitude of 23 300 km in 2012 using the SRG-GEO receiver [15].

There are several projects which plan on using a GNSS receiver onboard for navigation in GEO or HEO orbit. This includes the small GEO mission which revolves around building a small geostationary satellite platform. The first satellite is scheduled to launch 2014 and will fly a GNSS receiver as an experiment and if it is successful the GNSS receiver will be included in the following satellites [16], [17]. The MMS mission, planned to be ready for launch in 2014, also plans to use a GPS receiver for primary navigation and includes four satellites in a HEO orbit [18]. Furthermore the GOES-R satellite planned for launch in 2016 is also planned to use a GPS receiver for navigation [19], [20].

## 1.1 Purpose

The purpose of this master thesis is to design an antenna for GNSS reception in GEO. This includes specifying requirements on the antenna to be able to operate in GEO. After the requirements are specified different antennas should be considered and investigated and a few should be chosen for further design and analysis. Tasks also include figuring out the feed for the antenna.

The chosen specifications are presented in Section 2. In Section 0 the antenna design is described which include choice of antennas, simulation result along with the details of the feed. After that there is the discussion in Section 4, where which antenna fits the requirement best is discussed, and then the conclusion is presented in Section 5.

# 2 SPECIFICATIONS

To decide the antenna specifications the performance of the system first has to be decided which is done in Section 2.1. After the performance is decided the bandwidth is specified in Section 2.2 and the radiation pattern in Section 2.3. Other electrical specifications are presented in Section 2.4 and mechanical and environmental requirements are presented in Section 2.5. A summary of the specifications can be found in Section 2.6.

## 2.1 Performance

A normal GEO satellite has a station keeping box that is 75 km wide which it has to be kept within. The satellite using on-ground orbit determination is usually allowed to drift from one side of the box to the other and then a manoeuvre is performed to get the satellite to drift towards the other end of the box which maximizes the time between manoeuvres. Ground based position determination for a GEO satellite, using one ground station, have good accuracy for the distance between the ground station and the satellite but worse in the longitude and inclination of the satellite. One technique for measuring the position of the satellite is interferometry which gives an accuracy of 220 m. From the measurement, and previous measurements, the orbit is estimated with an orbit determination algorithm and the typical performance for ground based orbit determination algorithms is 60 m in semi-major axis, 2.2 km in inclination and 1.4 km in longitude. In [16] it is also stated that the expected performance of the ground station position accuracy is somewhere between 0.2-2 km which is still within the requirements for the small GEO mission. Another example of performance requirement for a GEO satellite is 100 m for the GOES-R satellite which include daily manoeuvres [9], [21].

GNSS navigation is as stated in Section 1 not widely used in GEO but there are quite a few studies conducted on the viability of using GNSS for position determination. The studies usually only take into account GPS and in some cases also include GALILEO and range from determining how many satellites can be tracked during a certain time period to also include how the performance of an autonomous navigation system using GNSS would be. Some of the studies focus on using a specific receiver and some are more in general.

### 2.1.1 Number of satellites tracked

To be able to use GNSS for navigation purposes it is necessary to track satellites and to be able to track a satellite, the satellite signal first has to be acquired. The signal can be acquired if the received $C/N_0$, defined as the received signal strength compared to the noise density, is over the specific level required by the receiver. After acquisition the signal is tracked, this usually requires a lower $C/N_0$. In [9] the tracking threshold was set to 20 dBHz and the acquisition threshold was 27 dBHz and a simulation on the visible (above 20 dBHz) and usable (above 20 dBHz and have been acquired) satellites was performed. In the simulation it was assumed that the receiving antenna had 10 dBi in gain, 40 degree HPBW and was directed towards earth. The link budget for the simulation included the path loss, the GPS EIRP which was derived using the modelled antenna gain from the GPS and the minimum specification on power of the signal received on earth, the noise temperature based on an antenna looking at free space and losses in the front-end and A/D converter. Different constellations are considered, both different versions of the GPS satellite, block IIA, IIR and IIF, and the planned GALILEO constellation. The GPS constellation is simulated both with the guaranteed 24 satellites and the extended version with 27 satellites and the L1 band frequency was used for GPS and GALILEO. The result from [9] is presented in Table 1 which shows that only using GPS yield at least four satellites always available but using only GALILEO you would have less than four satellites at times.

**Table 1: The amount of visible and useable satellites from the simulation in [9]. The values were read out from graphs in [9].**

| Number of satellites | GPS (24) IIA | GPS (27) IIA | GPS (24) IIR | GPS (24) IIF | GAL (27) | GPS(24) IIA+ GAL(27) | GPS(27) IIA+ GAL(27) | GPS(24) IIR+ GAL(27) | GPS(24) IIF+ GAL(27) |
|---|---|---|---|---|---|---|---|---|---|
| Min visible | 9 | 11 | 9 | 7 | 6 | 16 | 18 | 16 | 14 |
| Mean visible | 11.5 | 13 | 11.5 | 10.5 | 7.5 | 19.5 | 21 | 20 | 19 |
| Max visible | 15 | 16 | 15 | 15 | 11 | 25 | 26 | 25 | 25 |
| Min usable | 6 | 7 | 9 | 7 | 2 | 9 | 10 | 12 | 10 |
| Mean usable | 8 | 9 | 11.5 | 10.5 | 4.5 | 13 | 14 | 16 | 15 |
| Max usable | 11 | 12 | 15 | 15 | 7 | 17 | 18 | 21 | 21 |

In [22] only the visibility of GPS satellites of block IIA with a constellation of 27 satellites is taken into account where the visibility is defined as when the received $C/N_0$ is above a specified level. The differences in the link budget compared to [9] are that the used receiver antenna has 9 dBi gain over -30 to +30 degrees, the additional losses from the receiver are stated to be 2 dB, the side lobes are lowered 2 dB due to uncertainty and the noise temperature is calculated based on an antenna looking exclusively on earth. The results from [22] are presented in Table 2 and show that the result is worse than the ones from [9], probably because of a more conservative link budget. On the other hand in another article, [23], using a receiving antenna with 9.2 dBi gain, 2.9 dB additional losses and noise temperature based on an antenna looking at earth gives the result in Table 3 which is considerately better than [22] even though that the presented parts of the link budget are very similar. The difference in result could be due to different orbits of the GEO satellite.

**Table 2: The probability to see x amount of satellites using GPS, GALILEO or both constellations with different threshold values on $C/N_0$. The values were read out from graphs in [22].**

| Probability of number of satellites visible | GPS 20 dBHz | GAL 20 dBHz | GPS 25 dBHz | GAL 25 dBHz | Both 25 dBHz | GPS 28 dBHz | GAL 28 dBHz | Both 28 dBHz | Both 35 dBHz |
|---|---|---|---|---|---|---|---|---|---|
| 1 | 1 | 1 | 1 | 1 | 1 | 0.9 | 0.9 | <1 | 0.9 |
| 2 | 1 | 1 | <1 | 0.8 | 1 | 0.6 | 0.6 | 0.9 | 0.7 |
| 3 | 1 | 1 | 0.9 | 0.5 | 1 | 0.4 | 0.2 | 0.6 | 0.3 |
| 4 | 1 | 1 | 0.6 | 0.3 | <1 | <0.1 | <0.1 | 0.2 | 0.1 |
| 5 | 1 | 1 | 0.3 | <0.1 | 0.9 | 0 | 0 | <0.1 | 0 |
| 6 | <1 | <1 | 0.1 | 0 | 0.7 | 0 | 0 | 0 | 0 |
| 7 | <1 | 0.8 | <0.1 | 0 | 0.5 | 0 | 0 | 0 | 0 |
| 8 | 0.9 | 0.7 | 0 | 0 | 0.3 | 0 | 0 | 0 | 0 |
| 9 | 0.9 | 0.5 | 0 | 0 | 0.2 | 0 | 0 | 0 | 0 |
| 10 | 0.7 | 0.3 | 0 | 0 | 0.1 | 0 | 0 | 0 | 0 |

**Table 3: Values from [23] where the probability to see more than one or more than four GPS satellites is computed for different thresholds of $C/N_0$.**

| **Threshold dBHz** | **Probability of time more than/equal to one satellite is visible** | **Probability of time more than/equal to four satellites is visible** |
|---|---|---|
| 35 | 0.780 | 0.041 |
| 30 | 0.989 | 0.603 |
| 28 | 1 | 0.850 |

There is also [24] which investigates the performance with all the planned and built GNSSs. [24] only investigates which satellites lie in the main beam of the GNSS satellites and does not consider any link budget. The results are that using more GNSSs greatly increases the amount of satellites visible, for example depending on the position of the GEO satellite it was between 69-97% that four or more satellites were visible if all the four GNSSs were used.

### 2.1.2 GNSS receivers

To be able to decide the threshold for $C/N_0$, different GNSS receivers have to be investigated. There are many different receivers on the market right now for space use. Most of them have some mentioning of the use in GEO even if the main market for them is LEO satellites. There are several receivers which can handle low $C/N_0$ in particular NASA's navigator where they have stated that perhaps in the future the acquisition threshold could be improved to 10-12 dBHz [25]. Some examples of receivers and their stated $C/N_0$ are presented in Table 4.

**Table 4: A selection of different kinds of receivers for space use and comparison of there $C/N_0$ thresholds.**

| Name | Acquisition | Tracking | Bands | Notes |
|---|---|---|---|---|
| MosaicGNSS [26] | 30 dBHz | 26 dBHz | GPS L1 C/A | Requires to track two satellite to update the Kalman filter. |
| LAGRANGE [27] | 31 dBHz for L1<br>43 dBHz for L2 | 28 dBHz for L1<br>40 dBHz for L2 | GPS L1 L2<br>GLONASS L1 L2 | GLONASS is optional |
| Lion [28] | ? | ? | GPS L1 L2C L5<br>GALILEO E1 E5 | GLONASS/BeiDou optional. Successor of Mosaic so probably lower/same tracking/acquisition thresholds. |
| SGR-GEO [29] | ? | ? | GPS L1 C/A | Has achieved position fix (more than four satellites tracked at same time) above GPS constellation [15]. |
| TOPSTAR 3000 [30] | Warm start: 35 dBHz<br>After first fix: 19 dBHz | Code and carrier: 29 dBHz<br>Code only: 19 dBHz | GPS L1 C/A | After first fix acquisition allows reacquire signals when moved from main lobe to side lobe. |
| Navigator [31] | Down to 22 dBHz | Down to 22 dBHz | GPS L1 C/A | L2 and L5 GPS in the future based on [25] from early 2010. |
| RUAG GPS receiver [32] | ? | L1 C/A tracking: 32 dBHz | GPS L1 L2 | Will fly on Sentinel-3. |

### 2.1.3 Position accuracy

To calculate the position a Kalman filter is used. The Kalman filter does not need to track four satellites to be able to use the GNSS for position calculations, it is able to use information from a single satellite. The more satellites tracked the better the accuracy is of course. Besides the information from the GNSS receiver other information is also taken into consideration when estimating the position. Usually information regarding current orbit, model of the acceleration for different manoeuvres and different sensors like accelerometer or gyro are used.

The position accuracy, stated in [9], for using both GPS (IIA) and GALILEO was an average error of below 0.5 m and a standard deviation of below 15 m. The average velocity error was below 1 mm/s and the standard deviation was below 10 mm/s. Along with the GNSS measurements data from an attitude sensor, an accelerometer, models of the current orbit and thrusters were also used. Another study of the position accuracy is presented in [33] where the number of satellites tracked is much lower than in the case from [9]. The number of satellites tracked was never higher than three which it was only 7% of the time and no satellites were tracked 37% of the time, the threshold for a visible satellite is in this case 35 $C/N_0$. The orbit and thrusters were modelled but no extra sensors were used. The mean position error in a manoeuvre-free reference solution was 10 m and the max error was 32 m.

[33] also includes how the error is affected by different manoeuvres. The three different manoeuvres investigated are momentum unload to keep the satellite at correct attitude which happens daily in this case, East-West station keeping for making sure that the satellite is at correct longitude which happens monthly and North-South station keeping for keeping the correct latitude which happens yearly. The manoeuvres were initiated at two different time periods, at T1 where zero satellites are tracked but is close to a time period with one to two satellites visible and T2 which starts with tracking zero satellites and where there is two hours before next visible satellite. The result for the momentum unload at time T1 is that the max error slightly exceeds 100 m for a short time period after the momentum unload and then after a few hours falls back to same values as for the static case. For the momentum unload at time T2 the results were similar. The maximum error for East-West station keeping were 230 m at T1 and 700 m at T2 and the error stayed above 100 m for a few hours after the manoeuvre. For North-South station keeping the maximum error reached 2 km for T1 and 8.3 km for T2, the error stayed above 100 m for several hours.

Furthermore in [31] the navigator GPS receiver together with a Kalman filter was tested with a GPS simulator. Between four to ten satellites were tracked normally and the maximum position error was 12 m and the mean error was 4 m, the max velocity error was 1.6 mm/s and the mean error was 0.6 mm/s. In [16] the performance of the navigation system for the small GEO mission was investigated using a GPS simulator. The receiver for the small GEO system was a MOSAIC receiver and it has access to star trackers for attitude control. For the test it was able to track between one to three satellites normally and the position RMS error was 60 m.

Given these results where using a GNSS receiver with relatively high threshold, a $C/N_0$ of 35 dBHz for acquiring the signal, gives good results in navigation, an error of less than 100 m, it is possible to say that the use of GNSS for navigation in GEO is possible. The goal for the full system performance is chosen to be 100 m accuracy with a receiver with acquisition and tracking threshold of 30 dBHz which is a bit conservative as there exists receivers which can acquire signals at $C/N_0$ of 22 dBHz.

## 2.2 Bandwidth

The only fully established and open frequencies are currently L1 C/A for GPS and L1OC and L2OC for GLONASS. All GNSSs are planning to transmit several open signals and these are the interesting ones for this project. One thing to note is that in [34] it was reported that the BeiDou system is planned to switch frequencies around 2020. As no official documents were found it is not 100 % clear if there is a switch or if it instead is an addition of signals. It should also be noted that GLONASS is currently using the FDMA channel access technique where the centre frequency is different between the GLONASS satellites. Only two satellites use the same frequency which are on opposite side of the earth so users on earth never receives more than one signal at a time. The chance to receive signals from two satellites with the same frequency in GEO orbit, assuming that the radiation pattern is similar to the one GPS satellites, is very low. The open signals are summarized in Table 5 and the spectrum is visually shown in Figure 1 where all but the GLONASS signals under study are presented. Beside the GNSSs the regional QZSS sends the same signals as the GPS and IRNAS also uses the L5 frequency band.

**Table 5: A list of the different signals which are sent or are planned to be sent by the GNSSs. *in 2014-04-10**

| Name | Centre frequency | Bandwidth | Note |
|---|---|---|---|
| **GPS** | | | |
| L1 [35], [36] | 1575.42 MHz | +-10.23 MHz | On all GPS satellites. The L1 band contains the civilian L1 C/A signal. |
| L2 [35], [36] | 1227.6 MHz | +-10.23 MHz (+-15.35 MHz in the future) | On eleven satellites now*, on 24 satellites in 2018. The L2 band contains the civilian L2 C signal. The expanded bandwidth will be on 24 satellites in 2026. |
| L5 [35], [37] | 1176.45 MHz | +-12 MHz | On four satellites now*, on 24 satellites in 2021 |
| L1 C [35], [38] | 1575.42 MHz | +- 15.35 MHz | Not used yet, 24 satellites in 2026. |
| **GALILEO** | | | |
| E1 [39], [40] | 1575.42 MHz | +- 12.276 MHz | Four satellites currently*, 18 in mid decade and full constellation (30) 2020. |
| E5 A [39] | 1176.450 MHz | +- 10.23 MHz | -“- |
| E5 B [39] | 1207.14 MHz | +- 10.23 MHz | -“- |
| **BeiDou** | | | |
| B1I [4], [5] | 1561.098 MHz | +-2.046 MHz | 14 satellites currently send this signal*. Possibly changed 2020 when the system is completed (35 satellites). |
| B2I [5] | 1207.14 MHz | +- 12 MHz | -“- |
| B1-$C_d$ [5] | 1575.42 MHz | ? | Taken into operation 2020 |
| B2-$a_d$,$a_p$,$b_d$,$b_p$ [5] | 1191.795 MHz | ? | -“- |
| **GLONASS** | | | |
| L1OF [41] | 1598,0625-1605,375 MHz | +-0.511MHz | 24 satellites*, fully operational, FDMA |
| L2OF [42] | 1242,9375 - 1248,625 MHz | +-0.511MHz | -“- |
| L3OC [3] | 1202.025 | ? | Satellites launched from 2014 transmit this signal |
| L1OC [3] | 1600.995 | ? | Satellites launched from 2015 transmit this signal |
| L2OC [3] | 1248.06 | ? | -“- |
| L5OCM [3] | 1176.45 MHz | ? | Under study |
| L1OCM [3] | 1575.42 MHz | ? | -“- |

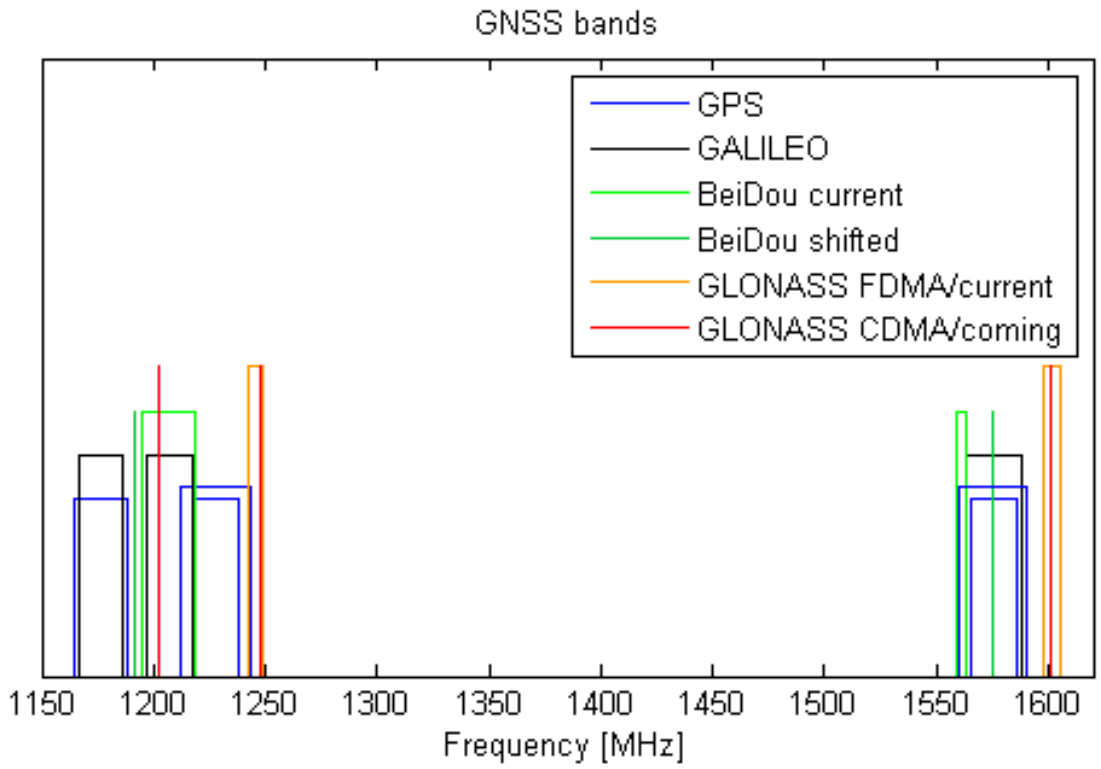


**Figure 1: Spectrum of the different GNSS signals where future signals without a specification on bandwidth are symbolized by a peak at the centre frequency. The GLONASS signals under study are excluded.**

Beside the GNSS transmission the L-band is also used for satellite radio and satellite phones. There are also plans for starting a 4-G wireless network using satellites which would transmit close to the GPS L1 frequency. The plan is for now stopped due to fear of it interfering with the GPS. Even if the 4-G network was to be implemented it is unknown if it would affect the GEO satellite [42]. From [43] it seems like some of the beams from the first 4-G satellite leaks over the earth and could cause interference.

The open GNSS frequencies are separated in two regions and the goal is to cover both regions with a single antenna, it could perhaps also be done with two antennas but it is not the goal. The first region is chosen to be between 1559 to 1606 MHz which would cover both the fully operating GPS L1 band and the GLONASS L1OF band. The GALILEO E1 band and the BeiDou B1 would be covered as well. Furthermore the coming GPS L1C, BeiDou B1-$C_d$ and GLONASS L1OC bands would also be covered. The second region the antenna should cover is 1164 – 1238 MHz where both the GPS L2 and L5 frequency are located but it would be preferable to also cover the GLONASS L2OF band ending at 1249 MHz. Advantages with choosing several frequencies from the same GNSS is that it is possible to use signals passing through the ionosphere and that the radiation pattern is different for the different frequencies. This means that side lobes are at different angles increasing the chance to see the satellites. Interference would probably not be a problem right now as there are no reported issues but if the 4-G network would be put in operation it would be necessary to make sure that the filters can remove the unwanted signal.

## 2.3 Radiation pattern

The basic requirement on the radiation pattern is to make GNSS reception possible and to do that it is important to look at the geometry of the signal path. The GNSS satellites direct their main beam towards earth and very little is transmitted out to space. As the GEO satellite is not in an orbit below the GNSS satellites the only signal received is from satellites on the opposite side of the earth and the geometry of this is presented in Figure 2. As presented a theta angle of 0° means that the satellite, and antenna, is pointing straight at earth. Furthermore satellites which send their signal through the ionosphere are usually not used because of uncertainty of the delay caused by the ionosphere. When using more than one frequency, from the same satellite, it is possible to calculate the delay and use those signals as well. In [9] it is stated that less than 5% of the signals reaching the GEO satellite passed through the ionosphere so the gain of being able to use them too is not very high.

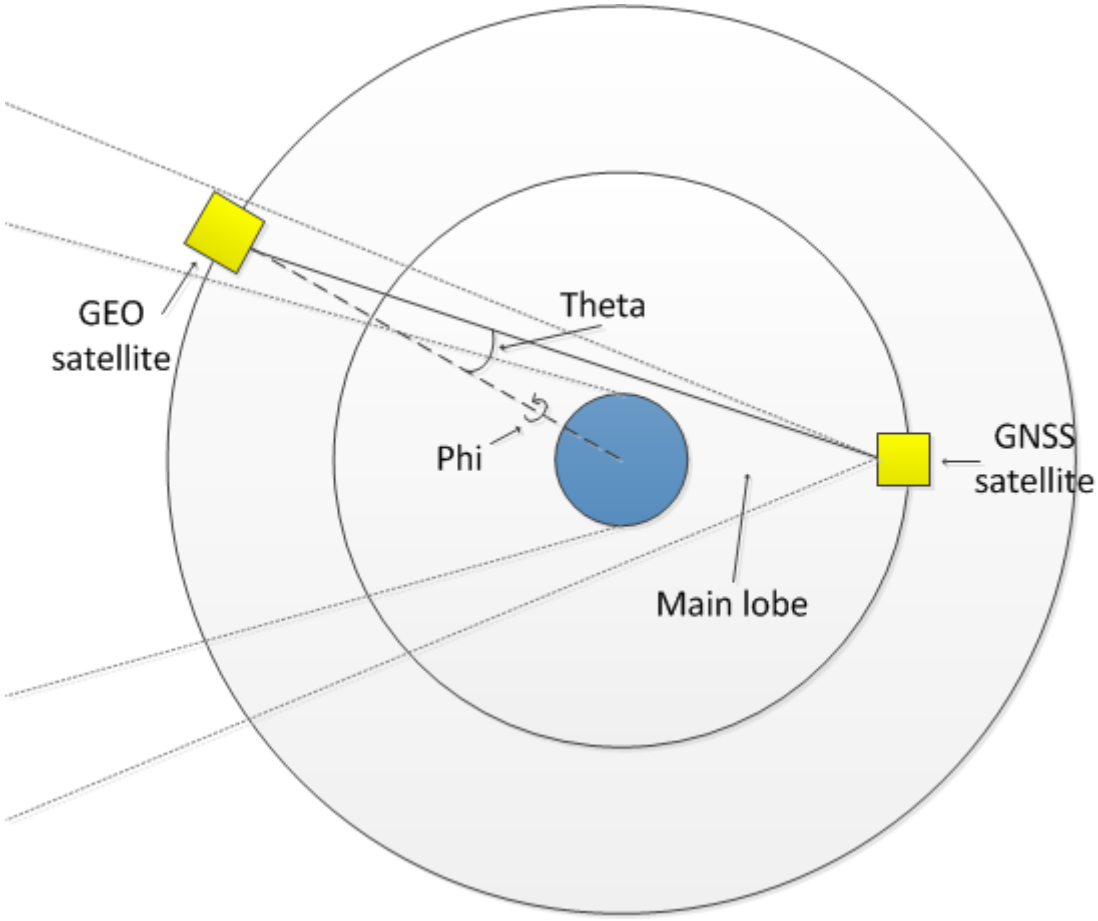


**Figure 2: The geometry of the signal path from the main lobe where the signal is sent from a GNSS satellite on the other side of the earth to the GEO satellite.**

### 2.3.1 Link budget

Beside the main lobe the GNSS satellites also have side lobes. By also using the side lobes the number of visible satellites increases. The radiation pattern on the designed antenna should allow for side lobe reception. A link budget was created to be able to decide the minimum requirement and is presented in Table 6. The link budget was created by using the calculated mean EIRP for the GPS IIA antenna from [9]. The free space loss was calculated for the different angles. The antenna temperature was calculated with the earth brightness temperature set to 190 K, [44], and the background temperature set to 5 K [45]. The resulting antenna temperature was 29 K when the gain over earth was 13 dBi, not taking into account the sun and moon. The sun affects the noise more severely and according to [46] the temperature increase from the sun at 2800 MHz can be as high as 40 K during solar maximum for a 10 dB gain antenna, so with 13 dBi gain the increase would be 80 K. The additional noise temperature from the cable and a LNA was also taken into account. The physical temperature of the cable was set to 150 °C because part of the cable is on the outside of the satellite. In Table 7 the increase in noise power due to the extra noise from earth is presented with and without the sun and with and without the 3 m cable, in other words the LNA is placed close to the antenna in the case with no cable. As presented there is little advantage to limit the gain over earth.

In Figure 3 the calculated $C/N_0$ versus the angle the GEO satellite sees the GPS satellite is presented where the blue graph is for a receiving antenna with 10 dBi gain over 0-35°. The black graph in Figure 3 is for the case before the receiving antenna gain is accounted for or rather with an receiving antenna with 0 dBi gain. The red horizontal line marks the receiver's acquisition threshold and the red vertical line marks where the edge of the earth is. The magenta vertical line marks the ionosphere which should be excluded if not several frequencies from the same satellite are used.

**Table 6: The link budget between the GPS satellites and the GEO satellite. The L1 C/A signal was used.**

| Name | Value | Note |
|---|---|---|
| **GPS side** | | |
| EIRP | | Extracted from figure 4-3 in [9] |
| **Propagation** | | |
| Free space loss | | Calculated with Friis transmission equation |
| **GEO side** | | |
| Gain | 10 and 0 dBi, over 0-35° | "Two alternatives" |
| Polarization loss | 0.14 dB | For 15 dB XPD |
| Received power | | EIRP+Free space loss + Gain – Polarization loss |
| **Noise** | | |
| Cable losses | 1.12 dB | Cable 3 m, type 41/5D [47] at 150°C |
| Receiver NF | 2.55 dB | RUAG LNA for E1 and E5, including filters |
| Receiver noise temperature | 231.7 K | 290×(10^(NF/10)-1) |
| Antenna observation temperature | 109.0 K | 13 dB gain over earth and sun, 80 K from sun. |
| Antenna losses | 1 dB | Estimation |
| Antenna temperature | 173.6 K | $(T\_A_{obs}/Loss_A)+(Loss_A-1)/Loss_A \times T\_A_{Physical}$ for 150°C physical temperature |
| System temperature | 597.9 K | $T\_Antenna+(Loss_c-1) \times T\_C_{phys}+ Loss_c \times T\_Receiver$ for a physical temperature of the cable of 150°C |
| Noise Power | -200.83 dB | $10 \log10(k_b T_{sys})$ |
| **$C/N_0$** | Presented in Figure 3 | Received power - Noise power |

**Table 7: Comparison of the noise power with and without the noise from earth for four different cases. The case without the cable losses means that the LNA is placed close to the antenna.**

| Case | Antenna temperature with earth | Noise power with earth | Antenna temperature without earth | Noise power without earth | Difference in noise power |
|---|---|---|---|---|---|
| **With sun and cable** | 109 K | -200.83 dB | 85 K | -200.97 dB | 0.15 dB |
| **Without sun with cable** | 29 K | -201.32 dB | 5 K | -201.47 dB | 0.15 dB |
| **Without cable and sun** | 29 K | -203.26 dB | 5 K | -203.51 dB | 0.25 dB |
| **With sun without cable** | 109 K | -202.52 dB | 85 K | -202.73 dB | 0.21 dB |

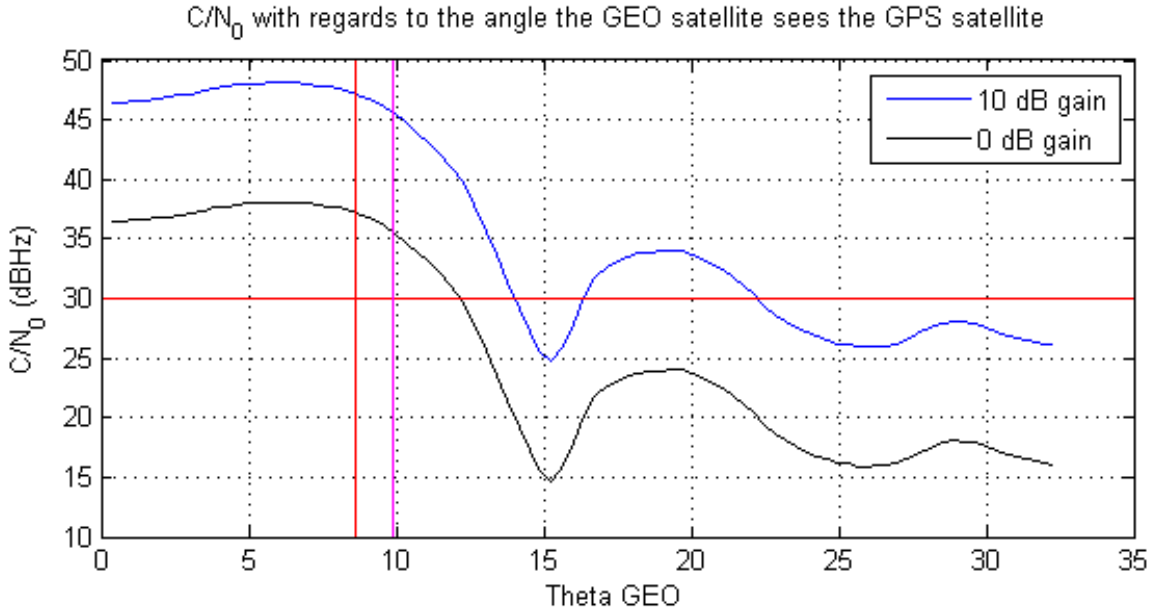


**Figure 3: The $C/N_0$ at the receiver depending on from what angle the GEO satellite sees the GPS satellite. The horizontal line marks the 30 dBHz $C/N_0$ threshold for the receiver and the vertical line marks the edge of the earth. The magenta line is the end of the ionosphere. The calculations are based upon the EIRP of a GPS IIA satellite at the L1 frequency.**

### 2.3.2 Gain specifications

Based on the link analysis the minimum and wanted specifications in Table 8 are chosen, the specification on the gain is also shown in Figure 4. The requirements would allow for reception in the first side lobe. A pointing error of the satellite of 0.1° is furthermore taken into account in the requirement. It should be noted that the mean gain is used. In reality the gain of the GPS antenna changes azimuthally. The different blocks of GPS satellites are a bit different as well, here IIA was used as it had the lowest modelled side lobes. It should be noted that this is for the L1 C/A signal and that the other signals have slightly different patterns.

**Table 8: Minimum requirements of the gain for the antenna.**

| Angle [°] | Gain [dBi] | Note |
|---|---|---|
| **Wanted specifications** | | |
| 8.5 -11 | Over 0 dBi | Allow acquisition of main lobe |
| 11-12.5 | Over 4 dBi | Allow acquisition of main lobe |
| 12.5-16.5 | Over 7 dBi | Allow acquisition of main lobe. Covers a dip in the pattern, but could allow reception of main lobe on other signals, i.e. L2 and L5, which have wider main lobe. |
| 16.5-22.5 | Over 10 dBi | Allow side lobe reception. The max gain should preferable be placed at either ends of this region. |
| 22.5-30 | Over 0 dBi | The second side lobe of the IIR satellites was reported to be quite high, [14], and together with better receiver, reception of second side lobes could be possible. |
| **Minimum specifications** | | |
| 8.5 -11.5 | Over 0 dBi | Same as above |
| 11.5-12.5 | Over 3 dBi | |
| 12.5-16.5 | Over 6 dBi | |
| 16.5-21.5 | Over 8 dBi | |
| 21.5-25 | Over 0 dBi | |

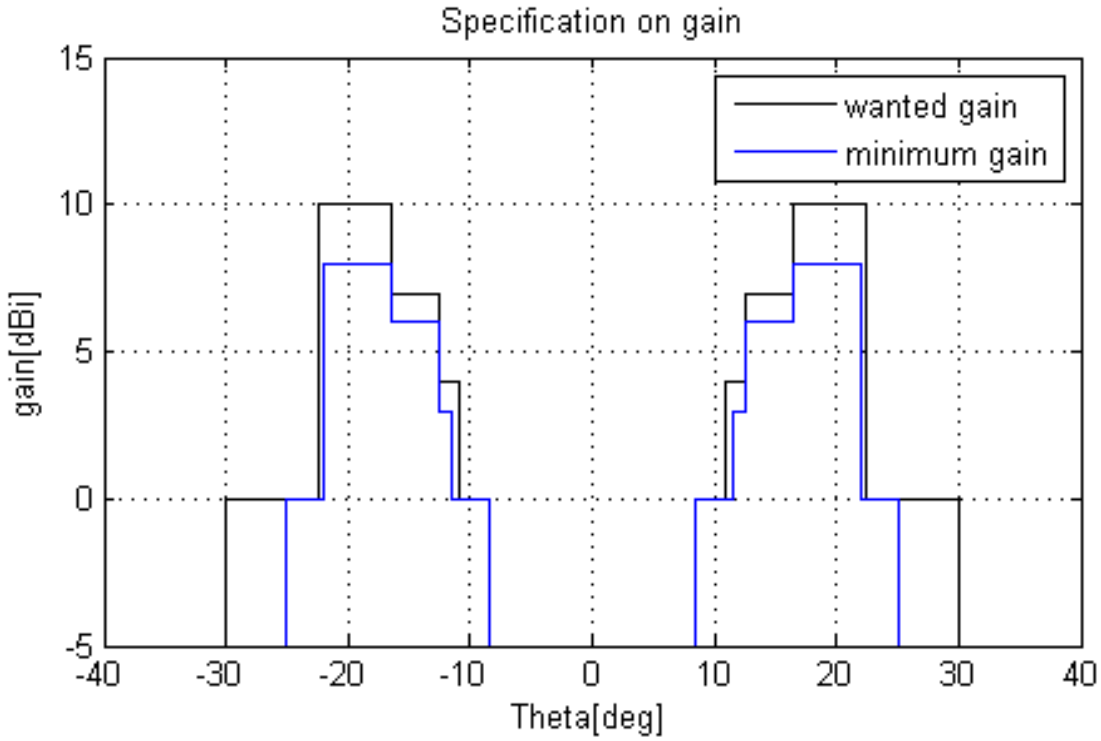


**Figure 4: The specified minimum and wanted gain plotted against the angle.**

## 2.4 Other electrical specifications

Besides the radiation pattern and bandwidth; polarization, matching, phase centre stability and group delay stability also have to be specified. The polarization is right hand circular polarization and the allowed cross polarization discrimination, XPD, is chosen to be >15 dB which is the same as in [48], [48] is a specification from ESA for a GNSS antenna for GEO use. The matching requirement in [48] is a VSWR of 1.1 which corresponds to a return loss of 26.4 dB but here the requirement is set to 20 dB but higher, over 25 dB, is desirable.

Phase centre stability means the stability of the point where it seems like the antenna receives the signal from. Phase centre usually varies somewhat with the angle the signals are received from. The effect of a big phase centre movement is that you do not really know where the signals were collected. A phase centre shift of 1 m for example means that you would have a 1 m uncertainty. In [48] the phase centre stability is specified to be <5° (2.5 mm) but the position specification is of an accuracy of 100 m and in the best case an accuracy of 0.5 m. Therefore the specification on the phase centre stability was chosen to be <0.25 m over the angles -40 to 40 °.

Group delay is the time delay from the wave reaching the antenna to that it is output from the port. The group delay stability does not affect normal least square method as the time at the receiver is estimated there [49]. When receiving from one GNSS satellite and possible for two and three satellites it would affect the position performance. Group delay is defined as minus the change in phase divided by the change in frequency. Group delay can be different for different angles, change over frequency and over temperature, due to that the antenna itself expands when the temperature is increased. To later calculate the group delay variation due to temperature the change in frequency over temperature first has to be calculated. The linear expansion of aluminium is for example 0.66 % for a temperature difference of 300°C which then would cause a shift of 0.66 % in frequency for the antenna, an 11 MHz shift at 1.6 GHz. The group delay variation is checked over the frequency bands in this report, group delay variation over theta is checked over the L1OC band and the L5 band. Here the specification is set to <0.83 ns which corresponds to <0.25 m in position same as for phase centre stability. This requirement is 0.50 ns, or 0.15 m, more than [48].

## 2.5 Mechanical and environmental requirements

Beside the electrical specifications the size, mass, interfaces as well as environmental requirements have to be specified. The environmental requirements are made so that the antenna would be able to withstand the conditions for a GEO satellite. The temperature range specified in [48] is -150 - 150 °C and the same is set for this specifications. The antenna should furthermore be able to handle vacuum. The antenna also needs to be able to handle the launch and should therefore be able to sustain vibrations. In [48] an example of the vibration requirement is presented and the same will be used here and is shown in Table 9 where M is the mass and PSD is the power spectral density.

**Table 9: The vibration requirements for the GNSS antenna which is the same as in [48]. M is the mass of the antenna and PSD is the power spectral density.**

| **Out of Plane** | |
|---|---|
| 20-100 Hz | + 3dB/octave |
| 100-300 Hz | PSD(M)=0.12 $g^2$/Hz×(M+20)/(M+1) |
| 300-2000 Hz | -5 dB/octave |
| **In Plane** | |
| 20-100 Hz | + 3dB/octave |
| 100-300 Hz | PSD(M)=0.05 $g^2$/Hz×(M+20)/(M+1) |
| 300-2000 Hz | -5 dB/octave |

The size of the antenna is to be decided later but it should be considered during the antenna design. [48] specifies the size to be 0.25x0.25x0.5 m (width x length x height) which makes it a quite high antenna, a more flat antenna but larger in width and length could also be desirable. The mass is decided to be <1 kg which is the same as [48]. The electrical interface is a SMA connector and the mechanical interface is to be decided later.

## 2.6 Summary of the specifications

The specifications for the antenna are summarized in Table 10 below.

**Table 10: The specifications for the GNSS antenna.**

| | | |
|---|---|---|
| Electrical requirement | | |
| Frequency band | | 1164 – 1238 MHz (preferable to 1249 MHz) , 1559 -1606 MHz |
| GAIN specifications (Preferable specifications shown in Section 2.3.2 ) | | |
| | 8.5-11°(GEO satellite boresight) | More than 0 dBi |
| | 11-12.5° | More than 4 dBi |
| | 12.5-16.5° | More than 7 dBi |
| | 16.5-22.5 ° | More than 10 dBi |
| | 22.5-30° | More than 0 dBi |
| Polarization | | Right hand circular polarization |
| XPD | | >15 dB |
| Return loss | | >20 dB (>25 dB is preferable) |
| Phase centre stability | | <0.25 m over -40 -40° |
| Group delay stability | | <0.83 ns (<0.25 m) |
| Mechanical requirements | | |
| Size | | Not decided yet |
| Mass | | <1 kg |
| Interface requirements | | |
| Electrical interface | | SMA |
| Mechanical interface | | Not decided yet |
| Environmental requirements | | |
| Temperature range | | -150  -150 °C |
| Vibration | | |
| | Out of plane | |
| | 20-100 Hz | + 3dB/octave |
| | 100-300 Hz | PSD(M)=0.12 $g^2$/Hz×(M+20)/(M+1) |
| | 300-2000 Hz | -5 dB/octave |
| | In Plane | |
| | 20-100 Hz | + 3dB/octave |
| | 100-300 Hz | PSD(M)=0.05 $g^2$/Hz×(M+20)/(M+1) |
| | 300-2000 Hz | -5 dB/octave |

# 3 Antenna design

The antenna was designed by first choosing what type of antenna is suitable and should be investigated further. As presented in Section 3.2 array antennas and helix antennas were chosen. The array option was first investigated and the distribution of the elements was investigated by both searching in papers for suitable element distributions and trying different designs by calculating the array factor, presented in Section 3.3. The investigation of the helix antenna is presented in Section 3.4 and the most promising design, monofilar helix antenna with ground plane, was simulated in HFSS. In Section 3.5 an antenna from RUAG which is intended to be used for GPS navigation on a GEO satellite is presented. The final performance of the designed antenna types is presented first, in Section 3.1 in Table 11, to be able to give the reader a quick comparison between the specifications and the performance.

## 3.1 Antenna trade-off table

A comparison between the final performance for the three different antenna choices and the specifications are presented in Table 11.

**Table 11: A summary of the performance of the investigated antennas. (*) Not known as the HFSS model was not matched.**

| | | **Specification** | | **12 element array** | | **3 element array** | | **Monofilar helix antenna** | |
|---|---|---|---|---|---|---|---|---|---|
| Frequency | | | | | | | | | |
| | | 1164–1238 MHz (preferably to 1249 MHz) , 1559-1606 MHz | | GPS L1 and L2 | | GPS L1 and L2 | | 1164 – 1249 MHz, 1559 - 1606 MHz | |
| Gain [dBi] | | Min | Wanted | 1164 MHz | 1610 MHz | 1164 MHz | 1610 MHz | 1164 MHz | 1605 MHz |
| | 7° | n/c | n/c | 4.8-4.9 | 9.1-9.3 | 11.9-12.1 | 12.8 | 10.9-11 | 11-11.5 |
| | 12° | 3 | 4 | 8.5-8.7 | 12.2-12.5 | 11.5-11.8 | 12.1-12.2 | 10.4-10.7 | 10.4-11.1 |
| | 17° | 8 | 10 | 10.1-10.4 | 12.6-13.1 | 10.8-11.3 | 11.1-11.2 | 9.7-10.1 | 9.5-10.4 |
| | 22° | 0 | 10 | 10.4-10.9 | 11-12.1 | 9.9-10.5 | 9.7-9.9 | 8.8-9.3 | 8.4-9.5 |
| | 30° | n/c | 0 | 8.7-9.7 | 3.6-7 | 8.1-8.9 | 6.7-7.1 | 7-7.7 | 5.8-7.9 |
| XPD [dB] | | | | 1164 MHz | 1610 MHz | 1164 MHz | 1610 MHz | 1164 MHz | 1605 MHz |
| | 0° | 15 | | 45.5 | 44.5 | 45.5 | 44.5 | 25.8 | 15.4 |
| | 30° | | | 20.9-38.1 | 21.7-43.1 | 20.9-38.1 | 21.7-43.1 | 15.6-37.8 | 11.9-28.3 |
| Return loss [dB] | | Min | Wanted | | | | | 100% yield | 80% yield |
| Maximum | | -20 | -25 | < -20 | | < -20 | | -18.5 | -20 |

| Phase centre stability | | 1164 MHz | 1610 MHz | 1164 MHz | 1610 MHz | 1164 MHz | 1605 MHz |
|---|---|---|---|---|---|---|---|
| Over Theta | 250 mm | 11.4 mm | 23.3 mm | 12.9 mm | Below 10.4 mm to 30° | 7 mm | 10 mm |
| Over frequency | | 0.1 mm from 1164 – 1605 MHz | | 1.3 mm from 1164 – 1605 MHz | | 117 mm from 1164 – 1605 MHz | |
| Group delay variation | | 1164 MHz | 1610 MHz | 1164 MHz | 1610 MHz | 1164 MHz | 1605 MHz |
| Over Theta | 0.83 ns | 0.3 ns at 40° | 0.5 ns at 30° | 0.25 ns at 40° | 0.7 ns at 40° | Below 0.83 ns to 40° | Below 0.83 ns to 21° |
| Over frequency | | * | | * | | 1.4 ns over B2I, 1.2 ns over E5B, 0.9 ns over L1 C, otherwise below 0.83 ns | |
| Mechanical | | | | | | | |
| Maximum diameter | n/c | 540 mm | | 300 mm | | 158 mm | |
| Maximum Height | n/c | 20.5 mm | | 20.5 mm | | 437 mm | |
| Weight | 1 kg | 0.859 kg | | 2528 kg | | 0.826 kg | |

## 3.2 Antenna type choice

As presented in Table 8, a conical radiation pattern is desired and there are several types of antenna which radiate in a conical pattern. A couple of examples are helix antennas, a slot on a cone, single patch elements, a dielectric resonator antenna and array antennas. A short overview of each option is listed below:

- A helix antenna can radiate in a conical pattern when the diameter of the turns is larger than what is required for axial mode radiation as described in [50]. The helix antenna can produce RHCP but the problem would be to fulfil the requirement on the pattern over the wanted bandwidth and the matching. One option is to use one antenna for each frequency range but that is not further investigated.

- In [51] a dielectric resonator antenna is presented but it is linearly polarized, has low gain, the beam is directed at too high angles and furthermore the material of the dielectric has to be able to withstand the conditions in space.

- A slot along the circumference of a cone also radiates in a conical mode as shown in [52] but how to mechanically assemble it along with getting RHCP and the wanted bandwidth is problematic.

- Patch antennas can produce conical pattern if the $TM_{0n}$ mode is excited as explained in [53]. The patterns presented in [53] show that the angle for the maximum gain is too big for our purposes and it could be difficult to create a single element which fulfils the other requirements as well.

- An array could with the right configuration create a conical pattern. In an array the elements would greatly affect requirements like bandwidth and polarization and with suitable elements the antenna would be able to fulfil the requirements. The negative point with using an array is that it could have relatively large footprint.

Even if a conical pattern is optimal, an isoflux or flattened radiation pattern could also fulfil the specifications. The isoflux pattern can be achieved with for example choke ring antennas as presented in [54]. A choke ring antenna can have RHCP and the correct pattern, but is quite large. Helix antennas and array antennas can also achieve both isoflux and flattened pattern as well.

The array antenna and helix antenna are judged to be the best solutions and are further investigated. They were chosen as RHCP is possible, relative high gain in a conical or isoflux pattern is achievable and the size of the solutions is relatively small. The other options had problems within these fields or no information could be found with these options fulfilling for example RHCP.

## 3.3 Array dimensioning

There are a few concepts of how to choose the position, phase and amplitude to be able to create a conical pattern with an array. One specific method is to place leaky wave antennas in a circle and feed them with the same phase and amplitude as presented in [55]. The problem with this configuration is how to achieve RHCP. Another method, and the one to be further investigated, is to use a circular array, similar to the leaky wave antenna method but with arbitrary kind of elements. The phase shift of the elements is the same as the angle in the circle the elements are placed in. This arrangement produces a conical pattern as presented in [56]. A circular array has also been suggested to be used for receiving GPS signal in GEO orbit [57]. Another benefit with using this arrangement is that the array by itself is somewhat circularly polarized [58].

The array was dimensioned by first calculating the array factor for different configurations where the number of elements and the radius of the circle were changed. Using a circle of nine elements along with a circle of three elements inside was also investigated and a top view of that array is presented in Figure 5, theta is 0° along the z-axis which points straight upwards from the plane viewed in Figure 5. An element factor was multiplied with the array factor to be able to calculate the gain. The element pattern used was a Gaussian one and the results from using an element factor with a gain of 7.5 dBi in different configurations are presented in Table 12. As presented, the smallest possible array fulfilling the minimum requirement is 0.46 m in diameter with elements that are 0.13 m in diameter. The best result of the tried configurations yielded the one with the most elements, twelve, which also was the largest configuration with a diameter of 0.56 m. The radiation pattern for this configuration is presented in Figure 6 and 7 for 1164 MHz and 1610 MHz, respectively. Noteworthy is that as the diameter, in wavelengths, is increased the beamwidth decreases and the angle for the maximum gain is decreased.

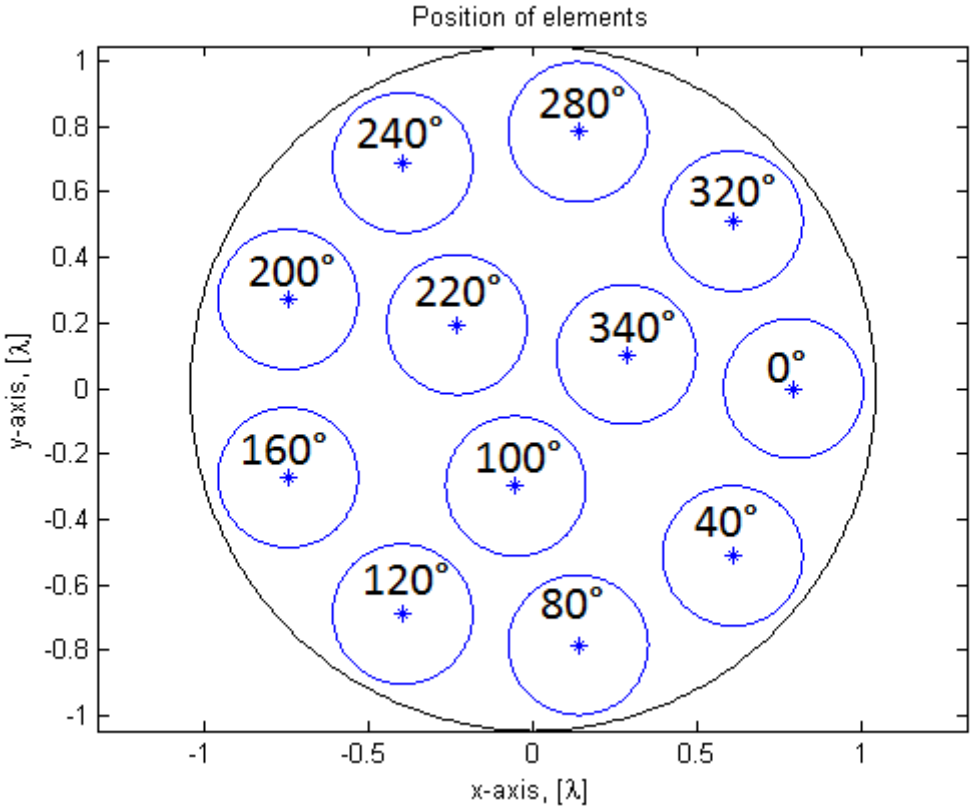


**Figure 5: The ring elements placed in the twelve element array along with the tracing of the physical size of the array. The electrical phase shift in degrees between elements is marked. The scale is in wavelengths at 1164 MHz.**

**Table 12: The gain at different theta angles for different configurations of a circular array. The element factor used was Gaussian and had 7.5 dBi gain. The twelve element configuration had nine elements in an outer circle and three elements in an inner circle. f1 is 1164 MHz and f2 is 1610 MHz.**

| | Gain in dBi at different theta angles,[min/max] | | | | | Diameter |
|---|---|---|---|---|---|---|
| Configuration | 7° | 12° | 17° | 22° | 30° | Size [m] |
| 4 elements, f1 | 0.5/0.7 | 4.4/4.8 | 6.2/7.1 | 6.7/8.4 | 5.7/8.9 | 0.44 |
| 4 elements, f2 | 2.8/3.2 | 6.2/7.1 | 7/8.9 | 6.1/9.6 | 0.2/8.7 | |
| 5 elements, f1 | 2.5 | 6.4/6.5 | 8.3/8.5 | 8.9/9.3 | 8/9.2 | 0.47 |
| 5 elements, f2 | 4.6 | 8/8.1 | 8.9/9.4 | 8.1/9.4 | 2.1/7.3 | |
| 6 elements, f1 | 3.7 | 7.7 | 9.5 | 10/10.1 | 9/9.3 | 0.49 |
| 6 elements, f2 | 6.1 | 9.4 | 10.2/10.3 | 9.2/9.5 | 2.9/5.2 | |
| 7 elements, f1 | 4.4 | 8.3 | 10 | 10.4 | 9.3 | 0.51 |
| 7 elements, f2 | 7.3 | 10.5 | 11.1 | 9.9/10 | 3.3/4.3 | |
| 7 e [small], f1 | 2.1 | 6.1 | 8.2 | 9.1 | 8.9 | 0.45 |
| 7 e [small], f2 | 5.9 | 9.5 | 10.8 | 10.6/10.7 | 7.8/8.1 | |
| 8 elements, f1 | 4.9 | 8.6 | 10.3 | 10.6 | 9.1/9.2 | 0.52 |
| 8 elements, f2 | 8.1 | 11.2 | 11.7 | 10.2/10.3 | 2.8/3.1 | |
| 9 elements, f1 | 5.2 | 8.9 | 10.5 | 10.7 | 9 | 0.53 |
| 9 elements, f2 | 7.1 | 11.3 | 11.6 | 10 | 1.3 | |
| 12 elements, f1 | 4.8/4.9 | 8.5/8.7 | 10.1/10.4 | 10.4/10.9 | 8.7/9.7 | 0.54 |
| 12 elements, f2 | 9.1/9.3 | 12.2/12.5 | 12.6/13.1 | 11/12.1 | 3.6/7 | |

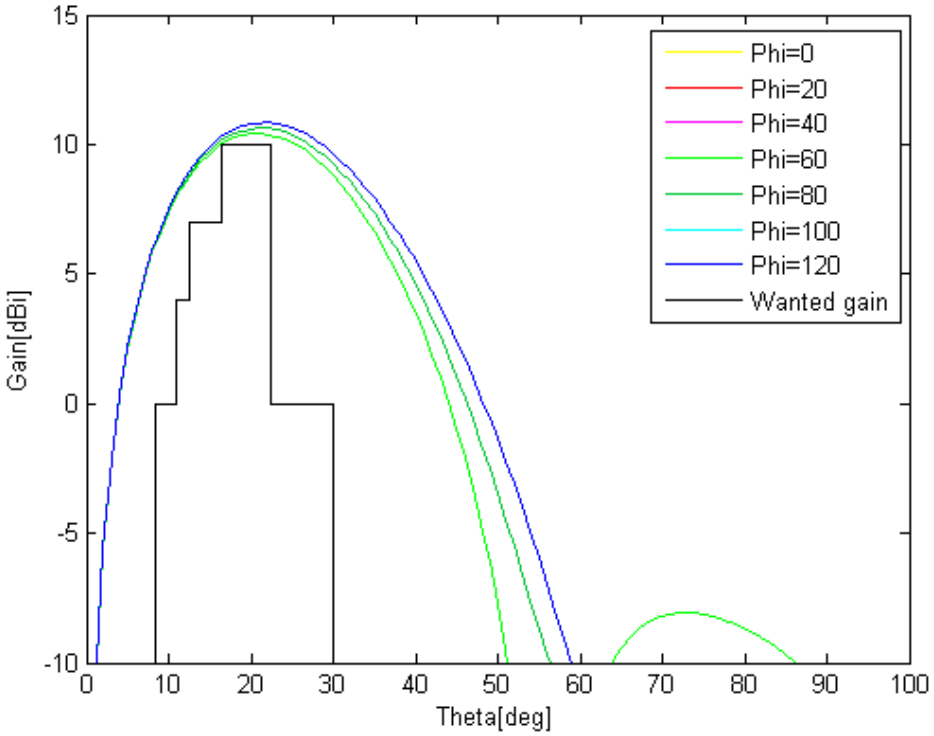


**Figure 6: Gain for the simulated array with twelve elements, where the elements had 7.5 dBi gain for 1164 MHz.**

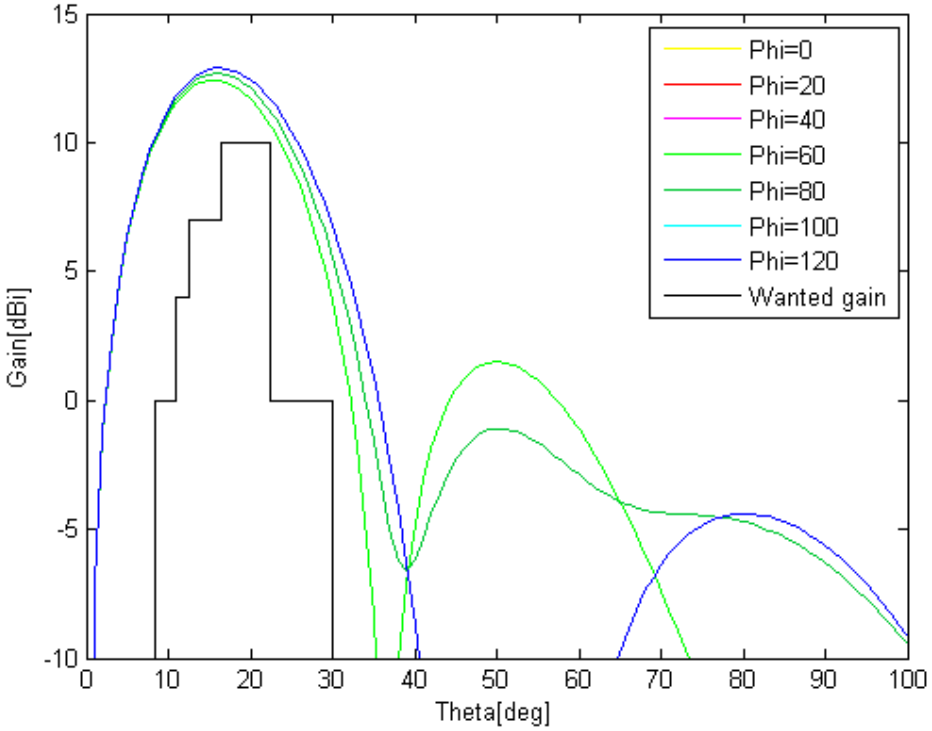


**Figure 7: Gain for the simulated array with twelve elements, where the elements had 7.5 dBi gain for 1610 MHz.**

A global optimization script using a genetic algorithm, [59], was utilized to try to find better configurations. For the twelve element configuration the outer ring was split into three rings and the radius of those three rings along with the radius of the inner ring were allowed to be varied along with the excitation amplitude of the rings and the multiplicity of the phase. The phase and amplitude could be regulated separately for the two frequencies. The optimizations were run with an element with 6.75 dBi in gain but the results presented here are with an element gain of 7.5 dBi. In Table 13 results from two different optimizations along with the original configuration are presented. In the first, (Opt 1), the cost was focused on higher gain in the area 17-22 ° while the other run, (Opt 2) focused on covering a wider angle and the resulting geometry is presented in Figure 8 for the case with focus on wider angle. The pattern for the (Opt 2) case is shown in Figure 9 and 10 for 1164 MHz and 1610 MHz, respectively. The results show that the optimized configurations have larger omni variation but have higher top values on the gain at the interesting angles. The larger omni variation was considered to yield a decline in system performance and therefore the focus was set on the original arrangement.

**Table 13: The gain at different theta angles for the original twelve element configurations from Table 12 compared to two optimized configurations. For [Opt 1] the costs in the optimization were set as to increase the beamwidth and for [Opt 2] the costs were set as to increase the gain between 17-22°. f1 is 1164 MHz and f2 is 1610 MHz.**

| | Gain in dBi at different theta angles,[min/max] | | | | | Diameter |
|---|---|---|---|---|---|---|
| Configuration | 7° | 12° | 17° | 22° | 30° | Size [m] |
| 12 e, [original] f1 | 4.8/4.9 | 8.5/8.7 | 10.1/10.4 | 10.4/10.9 | 8.7/9.7 | 0.54 |
| 12 e, [original] f2 | 9.1/9.3 | 12.2/12.5 | 12.6/13.1 | 11/12.1 | 3.6/7 | |
| 12 e, [Opt 1] f1 | 5.2/5.9 | 8.6/9.8 | 9.7/11.6 | 9.4/11.9 | 6.6/10.5 | 0.59 |
| 12 e, [Opt 1] f2 | 8.3/9.2 | 10.9/12.5 | 10.9/13.2 | 8.8/12 | 0/6.5 | |
| 12 e, [Opt 2] f1 | 3.7/4.3 | 7.3/8.4 | 8.8/10.3 | 8.9/10.9 | 7.1/10.1 | 0.54 |
| 12 e, [Opt 2] f2 | 6.4/7.2 | 9.5/10.9 | 10.2/12.2 | 9.3/12 | 5.2/9.3 | |

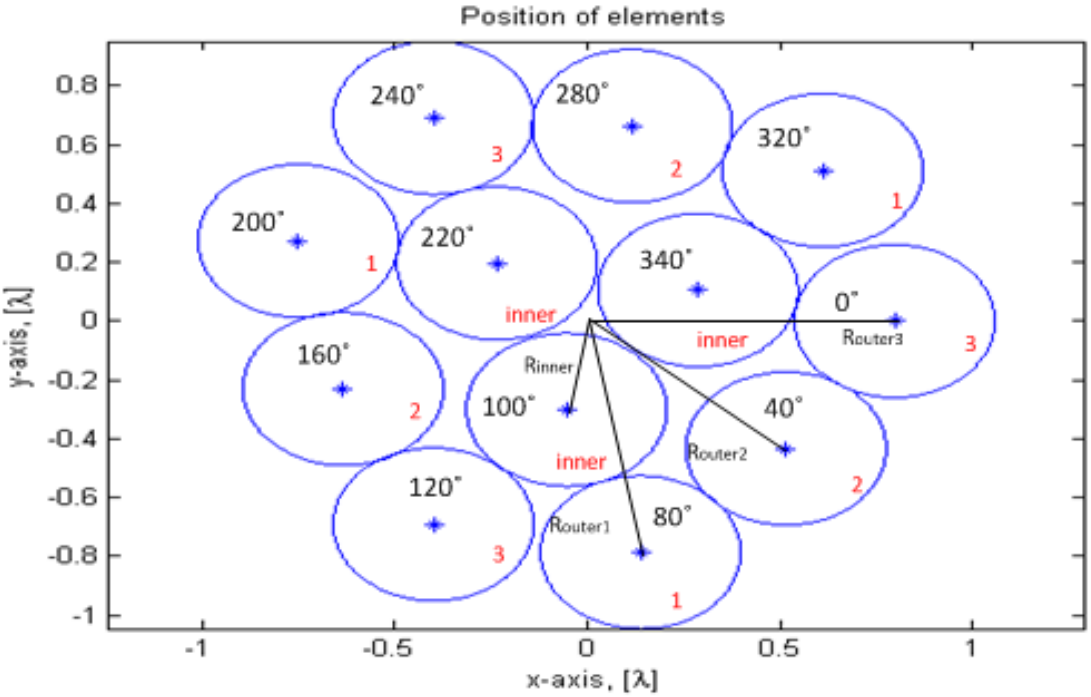


**Figure 8: The element position after optimization had been performed where the costs were set as to increase the beamwidth. The electrical phase shift in degrees between elements is marked. The different groups the elements are divided in is marked in red (1, 2, 3 and inner) and radius for each group is also shown in the figure (Rinner, Router1, Router2 and Router3). The scale is in wavelengths at 1164 MHz.**

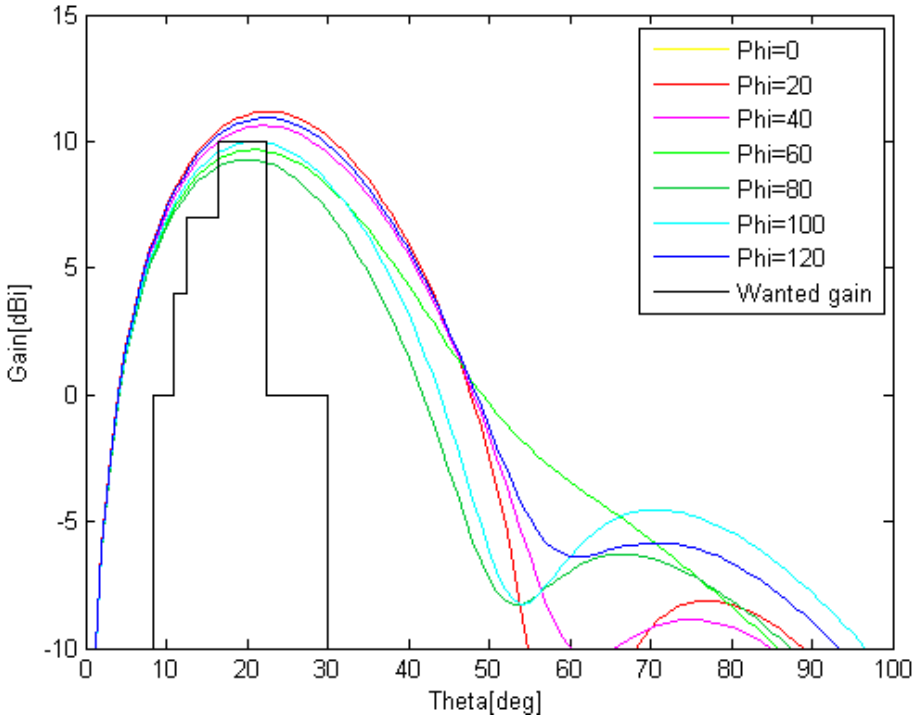


**Figure 9: Gain for the optimized array with twelve elements, where the elements had 7.5dBi gain for 1164 MHz. The costs in the optimization were set as to increase the beamwidth.**

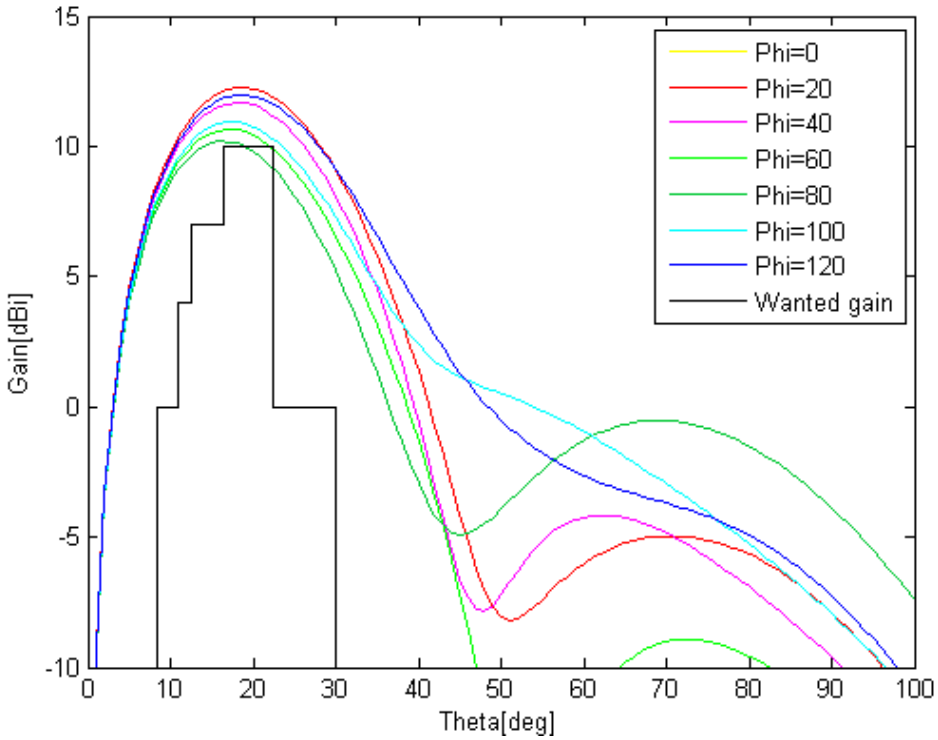


**Figure 10: Gain for the optimized array with twelve elements, where the elements had 7.5 dBi gain for 1610 MHz. The costs in the optimization were set as to increase the beamwidth.**

Furthermore it was investigated if a linear array in close to end-fire could fulfil the requirements. The optimizer was used where the position of the elements, phase and amplitude were able to be changed. The phase and amplitude could be different for the two different frequencies. The optimization was done mainly to see the possibilities with a linear array and the elemental spacing was set to 0.1 λ at 1164 MHz. Another element factor was used with maximum gain at theta angle 90°, it was Gaussian but having only 1.6 dBi in gain. The results were that there are no nulls at 0°, the radiation pattern was either flattened or isoflux. The results are presented in Table 14 and as shown the configurations have a worse pattern than for the circular arrays but on the other hand they have a smaller footprint. For the 10 element case the radiation pattern at 1164 MHz is presented in Figure 11 and the radiation pattern at 1610 MHz is presented in Figure 12.

**Table 14: The gain at different theta angles for different sized, optimized, linear arrays radiating in close to end-fire. The element factor used was Gaussian with 1.6 dBi gain. f1 is 1164 MHz and f2 is 1610 MHz.**

| | Gain in dBi at different theta angles,[min/max] | | | | | Height |
|---|---|---|---|---|---|---|
| Configuration | 7° | 12° | 17° | 22° | 30° | Size [m] |
| 7 elements, f1 | 10.6 | 10.4 | 10 | 9.5 | 7.7 | 0.55 |
| 7 elements, f2 | 9,9 | 10 | 9,9 | 9,5 | 7,7 | |
| 5 elements, f1 | 8,8 | 8,7 | 8,5 | 7,9 | 5,5 | 0.63 |
| 5 elements, f2 | 8,2 | 8,1 | 7,9 | 7,2 | 4,3 | |
| 10 elements, f1 | 10,9 | 10,6 | 9,9 | 9,1 | 7,1 | 0.25 |
| 10 elements, f2 | 10,8 | 10,5 | 10 | 9,2 | 7,3 | |

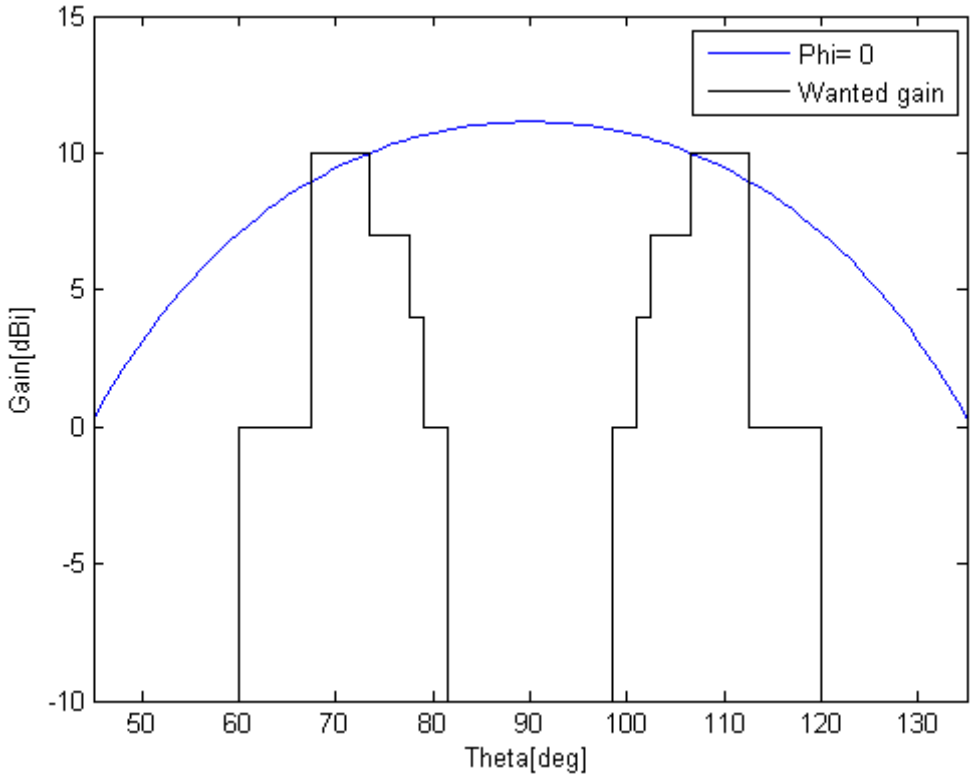


**Figure 11: Gain for the optimized linear array with ten elements, where the elements had 6.75 dBi gain for 1164 MHz.**

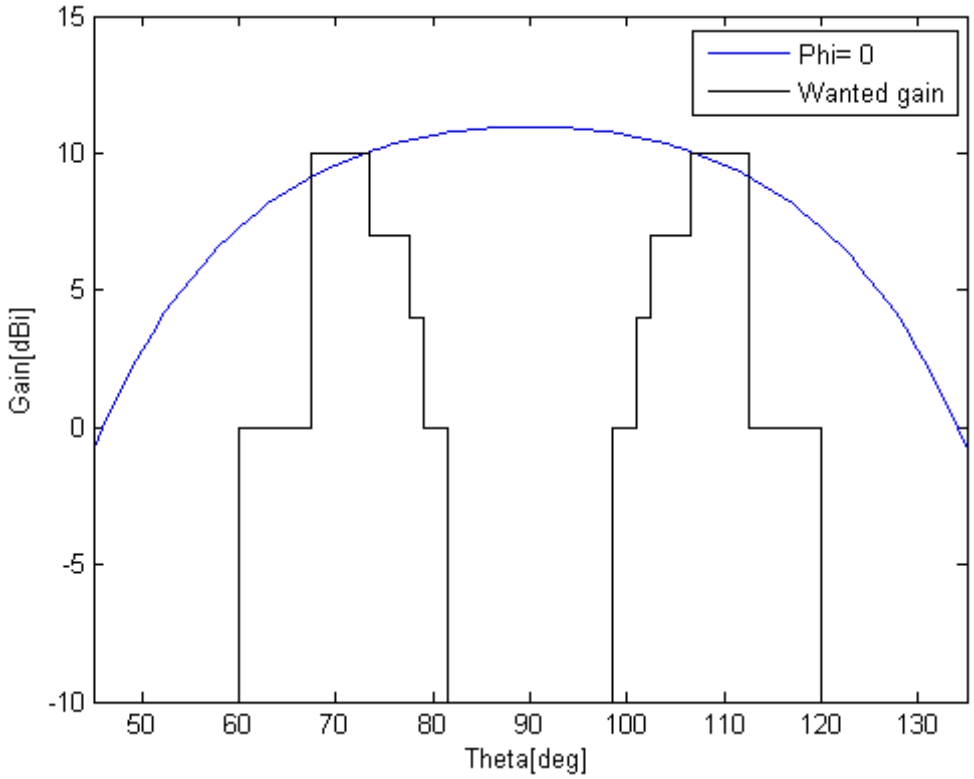


**Figure 12: Gain for the optimized linear array with ten elements, where the elements had 6.75 dBi gain for 1610 MHz.**

The linear arrays were more of a theoretical test to see what was possible with a linear array. The pattern turned out to be quite bell like so it was also investigated what was possible to do with a circular array where the elements were fed with the same phase to create a broadside pattern. The number of elements used was three or four to be able to get as small footprint as possible. The results are presented in Table 15 and the pattern is also shown in Figure 13 and 14 for the smallest configuration that fulfil the minimum specifications. The pattern is very similar to the one from the linear array indicating that it is what is possible to do with a clocklike pattern.

**Table 15: The gain at different theta angles for different circular arrays where the elements are feed the same phase. f1 is 1164 MHz and f2 is 1610 MHz.**

| | Gain in dBi at different theta angles,[min/max] | | | | | Diameter |
|---|---|---|---|---|---|---|
| Configuration | 7° | 12° | 17° | 22° | 30° | Size [m] |
| 3 e [dia 1] f1 | 10.6 | 10.2 | 9.6 | 8.9 | 7.3 | 0.29 |
| 3 e [dia 1] f2 | 12.3 | 11.7 | 10.8 | 9.6 | 7.0 | |
| 3 e [dia 2] f1 | 11 | 10.6 | 10 | 9.1 | 7.3 | 0.30 |
| 3 e [dia 2] f2 | 12.6 | 11.9 | 10.9 | 9.5 | 6.4/6.5 | |
| 3 e [dia 3] f1 | 11.4 | 11 | 10.3 | 9.3 | 7.3/7.4 | 0.31 |
| 3 e [dia 3] f2 | 12.7 | 11.9 | 10.8 | 9.2 | 5.6/5.8 | |
| 4 e f1 | 12.2 | 11.7 | 10.9 | 9.8/9.9 | 7.3/7.6 | 0.33 |
| 4 e f2 | 13.7 | 12.8/12.9 | 11.4/11.5 | 9.4/9.7 | 4.3/5.7 | |

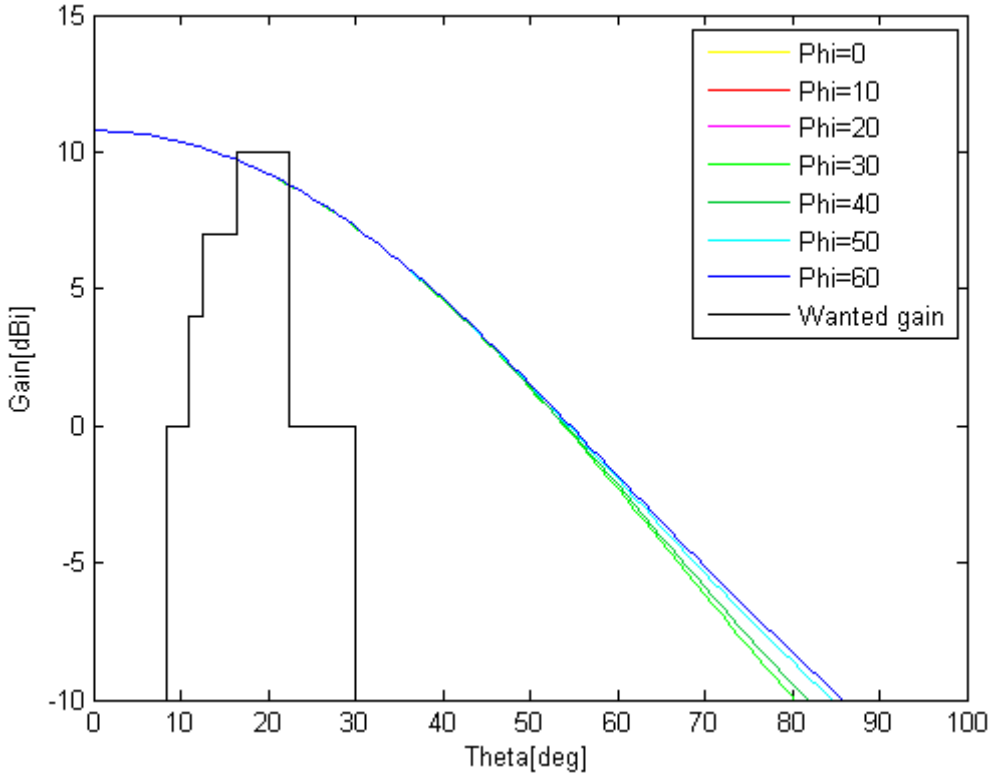


**Figure 13: Gain for the circular array with three elements and same phase on all elements. The elements had 7.5 dBi gain, the total diameter was 0.3 m and the frequency was 1164 MHz.**

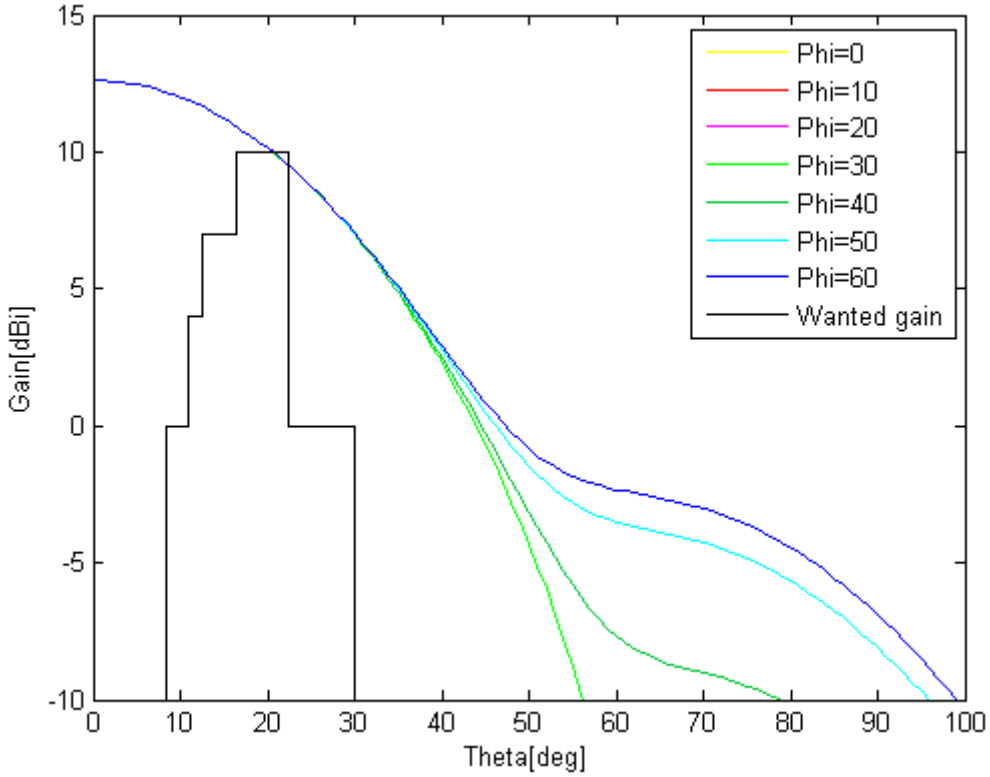


**Figure 14: Gain for the circular array with three elements and same phase on all elements. The elements had 7.5 dBi gain, the total diameter was 0.3 m and the frequency was 1610 MHz.**

As the circular array with the conical pattern needs the same phase shift over the whole frequency interval to achieve the wanted pattern, the possibilities to achieve a wideband phase shift was investigated. As it is only possible to achieve a wideband phase shift of 90 degrees the rest of the phase shift has to be made with strip line which gives a varying shift over frequency. The wanted phase shifts were set at the centre frequency, 1.387 GHz, and the consequences of the change in phase for 1164 MHz and 1610 MHz were simulated. The results are presented in Table 16 and in Figure 15 and 16 for 1164 MHz and 1610 MHz, respectively, as shown the change in the pattern is small.

**Table 16: The gain at different theta angles for the original arrangement with perfect phase shifts on both frequencies and a simulation, marked [PS], where the only wideband phase shift possible was 90° and the rest changed with frequency. f1 is 1164 MHz and f2 is 1610 MHz.**

| | Gain in dBi at different theta angles,[min/max] | | | | | Diameter |
|---|---|---|---|---|---|---|
| Configuration | 7° | 12° | 17° | 22° | 30° | Size [m] |
| 12 e, [original] f1 | 4.8/4.9 | 8.5/8.7 | 10.1/10.4 | 10.4/10.9 | 8.7/9.7 | 0.54 |
| 12 e, [original] f2 | 9.1/9.3 | 12.2/12.5 | 12.6/13.1 | 11/12.1 | 3.6/7 | |
| 12 e, [PS] f1 | 4.1/5.5 | 8.1/9.1 | 9.8/10.7 | 10.2/11.2 | 8.6/10.1 | 0.54 |
| 12 e, [PS] f2 | 8.7/9.7 | 12/12.7 | 12.5/13.4 | 10.8/12.4 | 3.3/7.8 | |

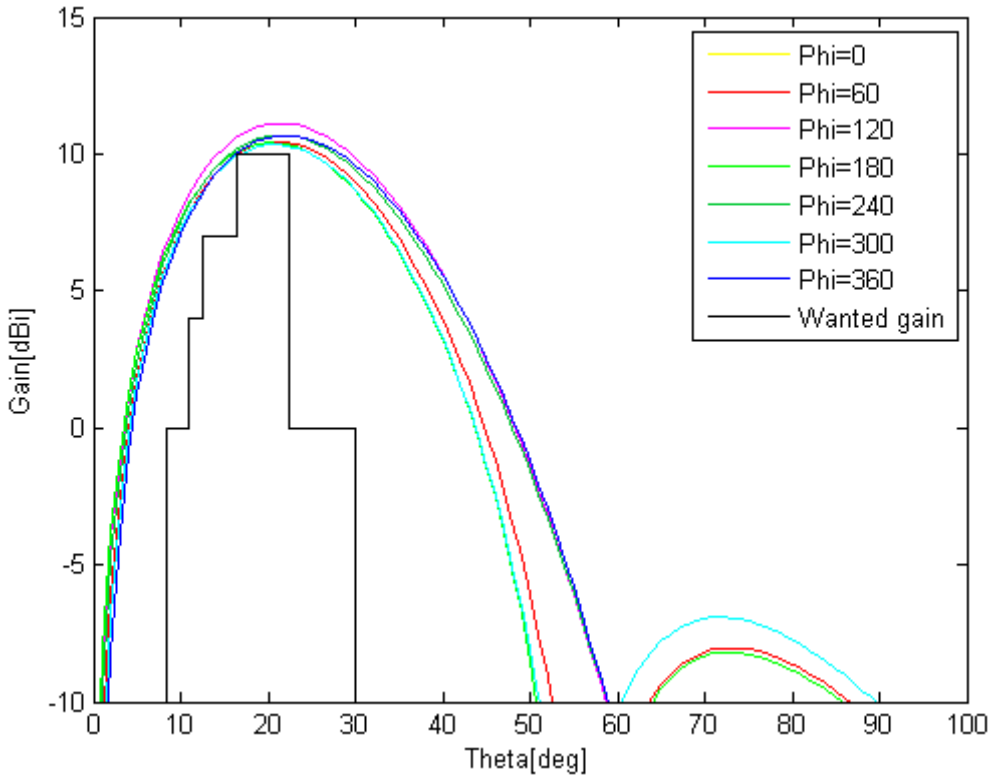


**Figure 15: Gain for the original twelve element array where the phase shift is dependant on frequency. The elements had 7.5 dBi gain for 1164 MHz.**

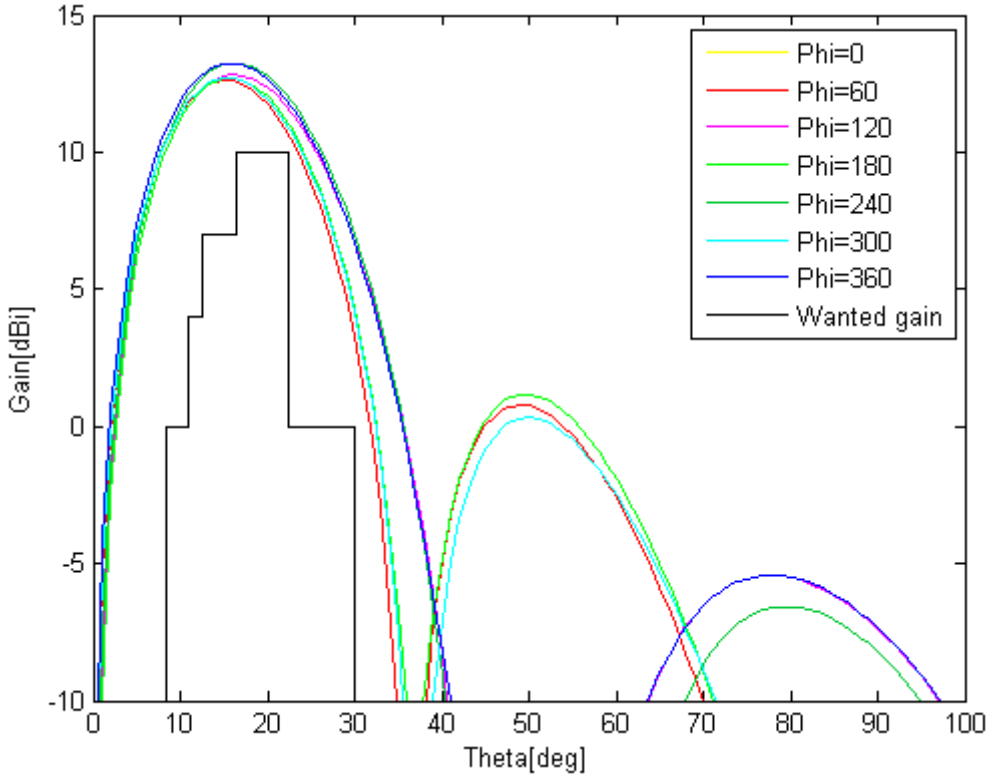


**Figure 16: Gain for the original twelve element array where the phase shift is dependant on frequency. The elements had 7.5 dBi gain for 1640 MHz.**

### 3.3.1 Array element

There are several different antenna elements that could be used to create these arrays. The requirements for the elements would be to have right hand circular polarization (this requirement could possibly be skipped for the twelve element array), have at least 7.5 dBi in Gain and be able to be placed within a half wavelength ,129 mm, at the lowest frequency. Having a reflection coefficient within specification along with good phase centre stability and low group delay variation would also be required. It could be possible to use elements which require larger spacing but then the array factor would be different from what have been used here.

There are a number of elements that could possibly satisfy these requirements like helices or patch elements. In this report the focus is on an already developed element from RUAG, a ring element in a cup. The ring element, shown in Figure 17, is two rings in a cup excited by two pairs of slots, one pair for each frequency band. The ports are phase shifted 90° between each other in each pair to create right hand circular polarization. As there are two pairs of excitation an array of these elements needs two distribution nets which mean that either a diplexer is needed before the port or two coax cables to the filter. As there are currently two filters, one for each frequency, along with a diplexer at the LNA it might be an advantage to have two distribution nets. The circular cup is 110 mm in diameter and the height of the element including the feed is 20.5 mm.

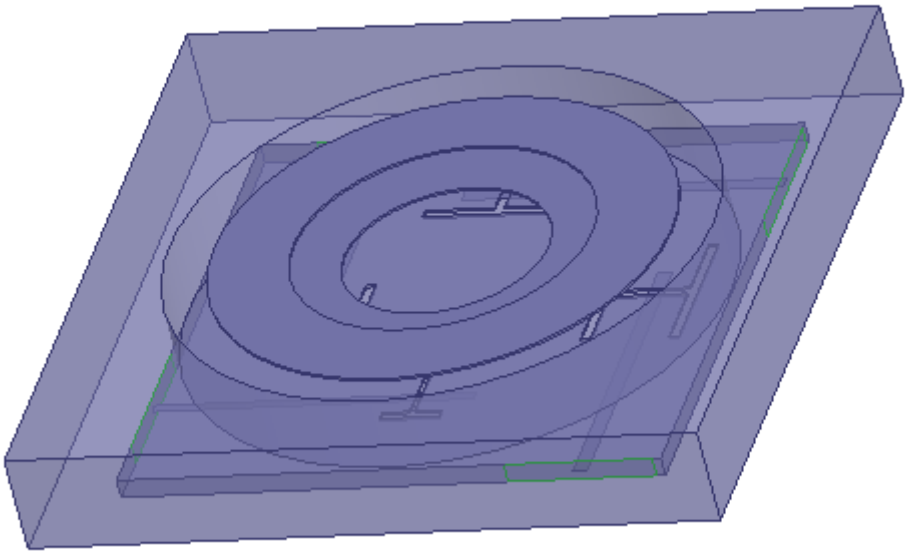

**Figure 17: The ring element model which was simulated in HFSS.**

The model presented in Figure 17 was not matched but simulated in HFSS anyway. The gain, XPD, phase centre, phase centre variation over theta and group delay variation over theta should not have been greatly affected by the missmatch of the element. In the simulation one pair of ports was excited for each frequency band. The gain for the ring element is presented in Figure 18. The gain is 7.5 dB at the lower band and 8.4 dB at the upper band which is above the requirement on the gain for the element. The element is right hand circularly polarized and the XPD is presented in Figure 19. No figure or plot was found of the return loss but the element is not expected to have much more bandwidth than to cover the L1 and L2 GPS bands, there is a possibility that it covers the whole upper band but not the lower band. Even if only the L1 and L2 GPS band is supported by the element, the array and element results are presented at the lowest frequency and highest frequency of the wanted frequency span.

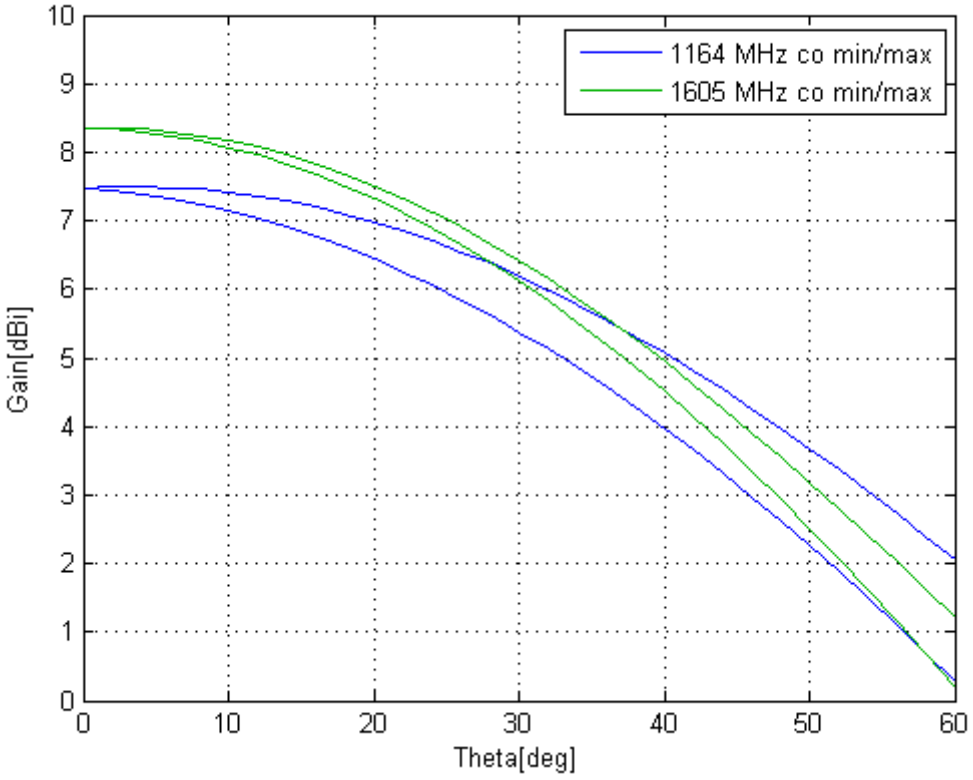


**Figure 18: The min/max gain for RHCP (co) of the ring element model in HFSS.**

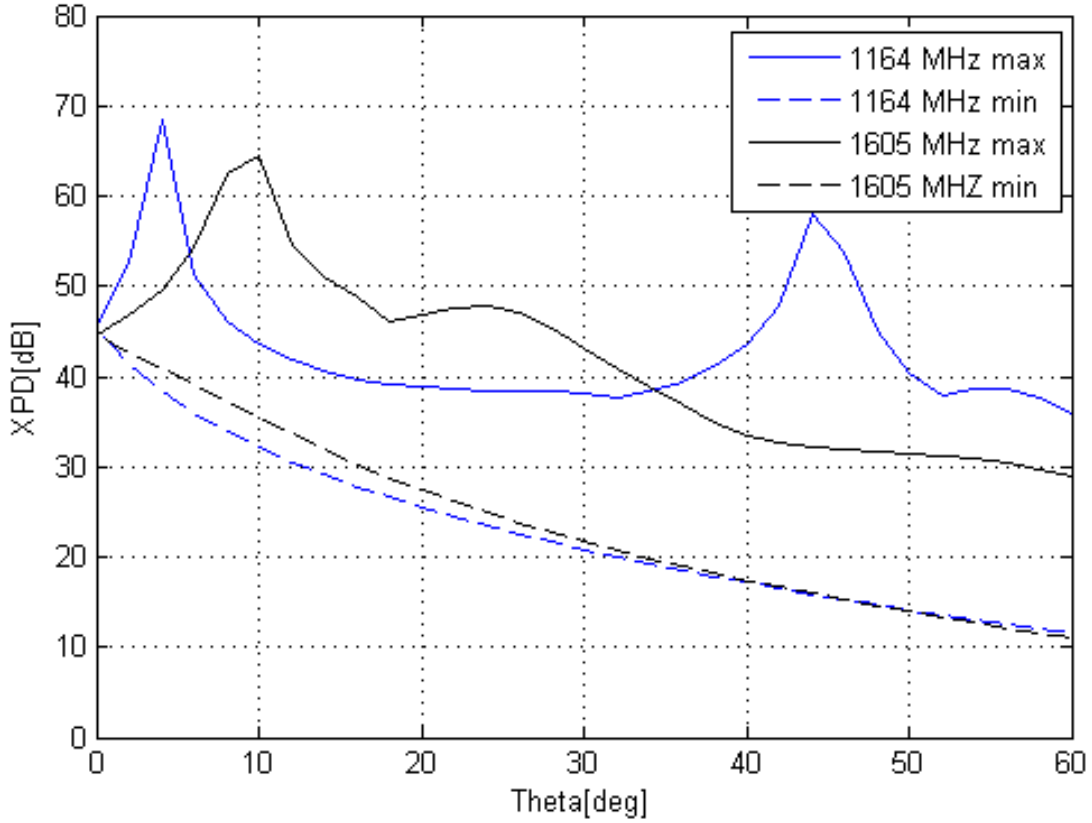


**Figure 19: The minimum/maximum XPD for RHCP at 1164 MHz and 1605 MHz for the HFSS model of the ring element.**

RUAG also has a PEC element which is presented in [60]. This element has a wider bandwidth which covers all the bands, at least for the measured results, but the element has a diameter of 161 mm which would require the array to be made bigger. The gain at L5 centre frequency is around 7.5 dBi and the gain at L1 centre frequency is a bit above 7.5 dBi, otherwise the height of the element is 55 mm and it weighs 320 g.

### 3.3.2 Final performance for the three element array

Using the results for the ring element, the total field was calculated in HFSS without simulating the whole array and thus not taking the coupling between elements into account. The three element array with 0.3 m diameter was used and the gain is presented in Figure 20. The result is better than when only the simple model with a Gaussian radiation pattern with 7.5 dBi gain was used, especially for the lower frequency. The XPD is presented in Figure 21 and the XPD is above 16.8 dB at 40°.

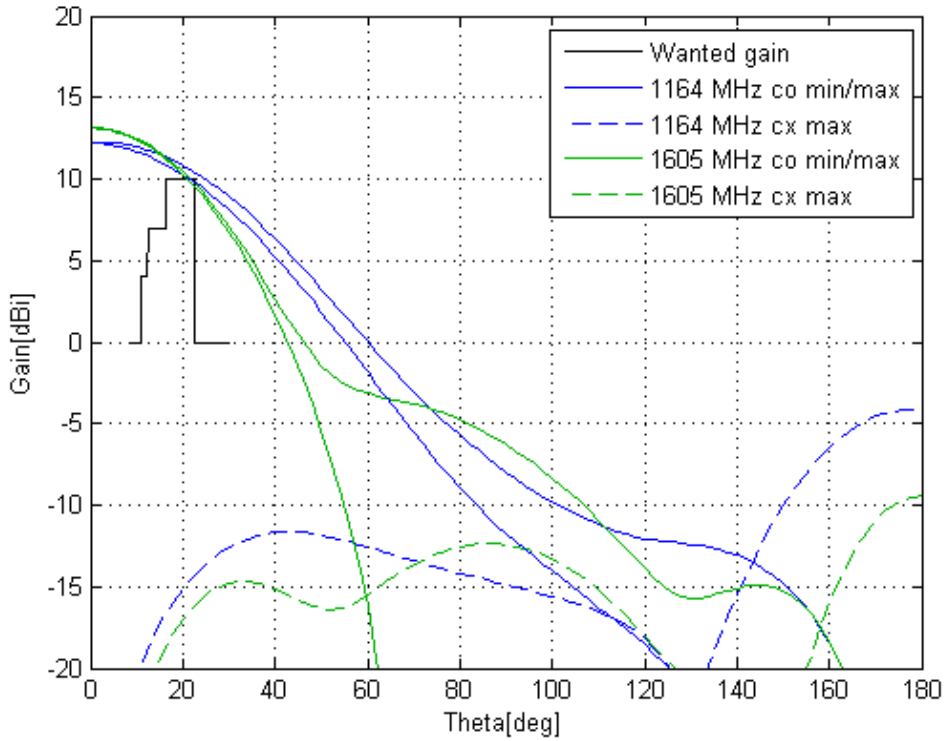


**Figure 20: Gain for the circular array with three elements and same phase on all elements. The element used was the ring element.**

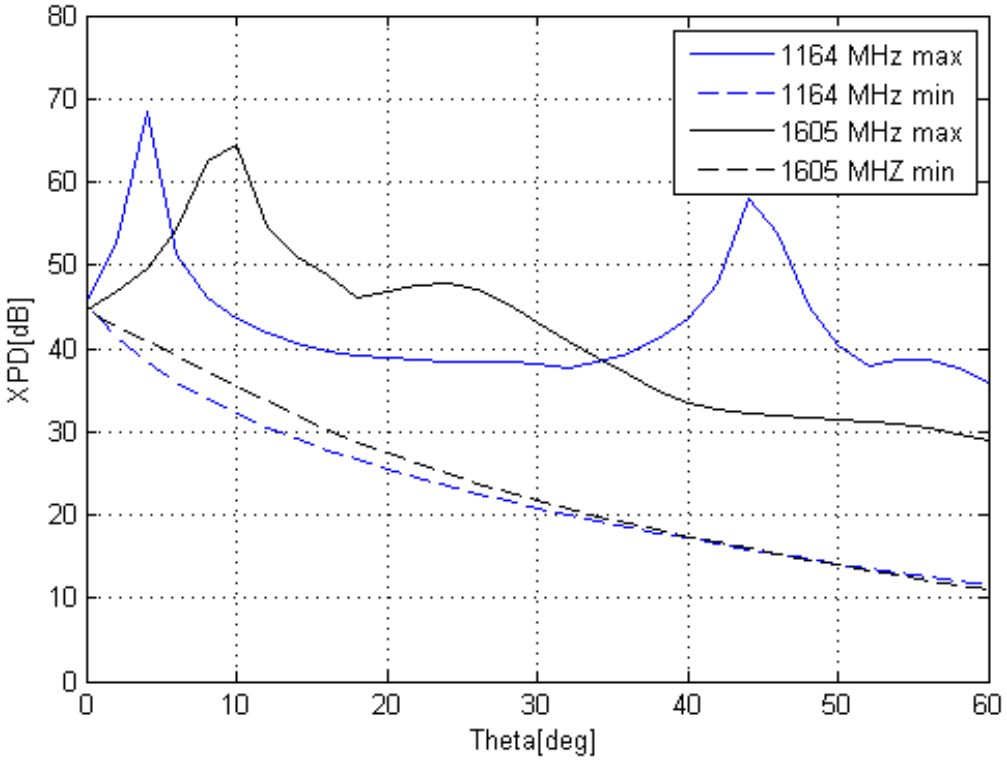


**Figure 21: The minimum/maximum XPD for RHCP at 1164 MHz and 1605 MHz for the HFSS model of the ring element in the three element array setup.**

3.3.2.1 Phase centre and group delay

The phase centre, defined here as the spot where the phase difference between -40° to 40° in theta is the smallest along the z-axis, was 25.4 mm above the antenna at 1164 MHz and 25.3 mm at 1606 MHz which gives very high phase centre stability over frequency. The distance is defined 0.5 mm below the floor of the cup. The phase variation over theta at 1164 MHz is presented in Figure 22 and the maximum variation at 40° in theta is 16°, corresponding to 11.4 mm. In Figure 23 the phase variation at 1606 MHz is presented and the maximum variation at 40° in theta is 45° which is 23.3 mm in distance.

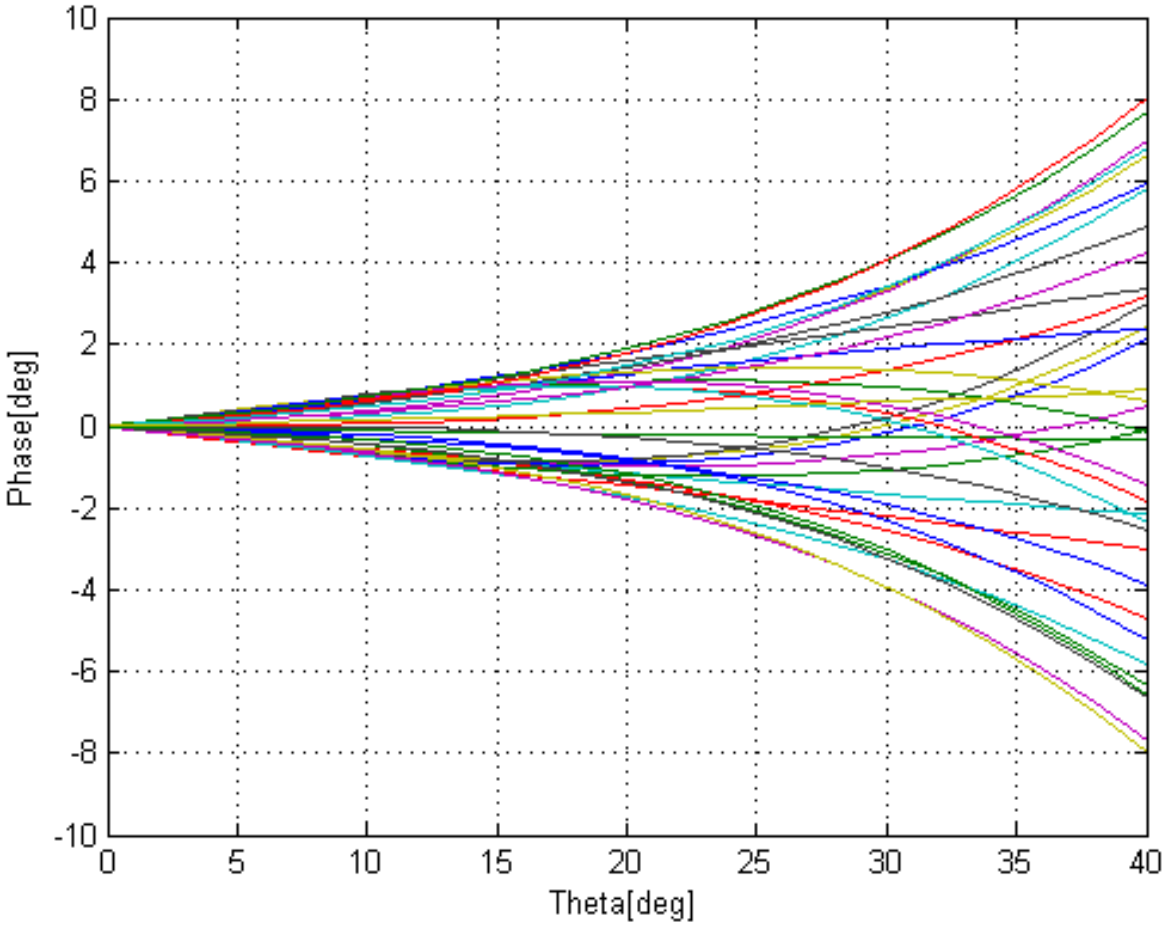


**Figure 22: The phase radiation pattern of the three element array with the ring element at 1164 MHz. Colour represents different phi cross sections, with a step of 10 degrees.**

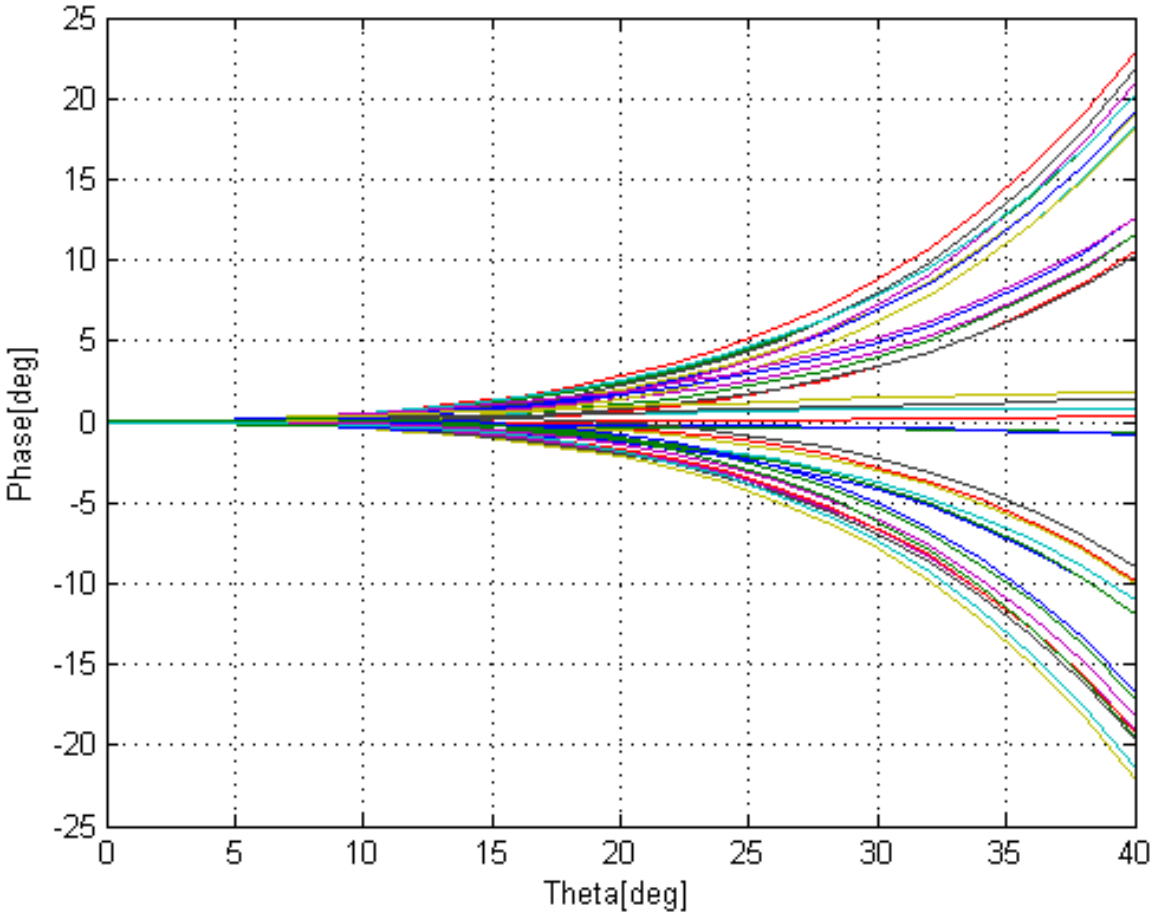


**Figure 23: The phase radiation pattern of the three element array with the ring element at 1606 MHz. Colour represents different phi cross sections, with a step of 10 degrees.**

The group delay variation over theta between 1164-1188 MHz is presented in Figure 24 and between 1598-1606 MHz in Figure 25. The specification is fulfilled. The group delay over frequency though, is worse as seen in Figure 26 and the specifications would not be fulfilled on practically any band but it should be taken into account that the antenna is not matched at all and the huge group delay variation is most likely because of this, in a real case the antenna would of course be matched and this would not be a problem.

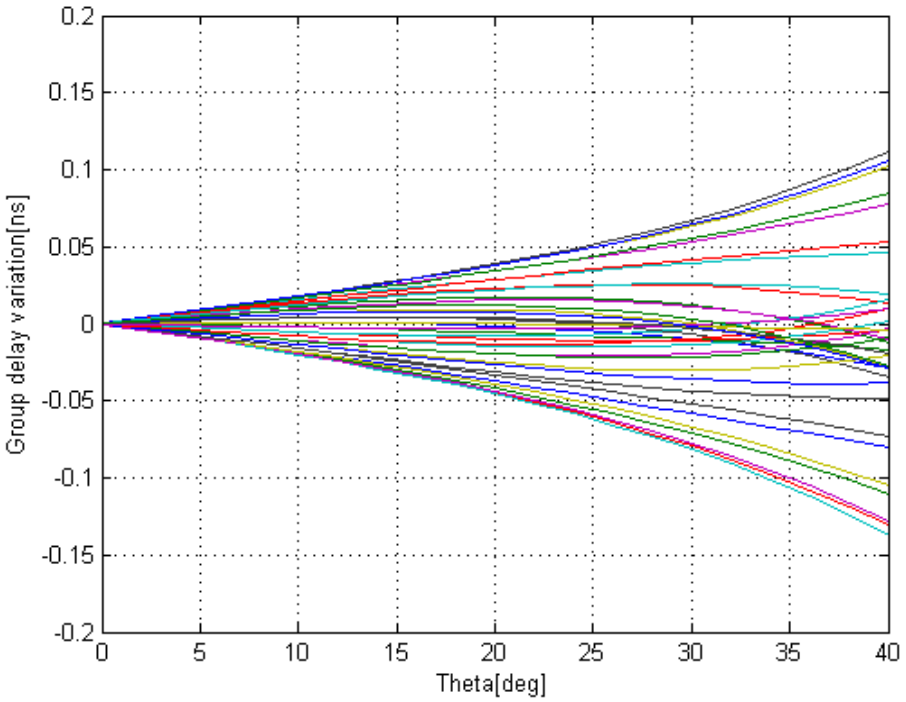


**Figure 24: The group delay variation over theta on the GPS L5 band (1164 - 1188 MHz) for the three element array with ring elements. Colour represents different phi cross sections, with a step of 10 degrees.**

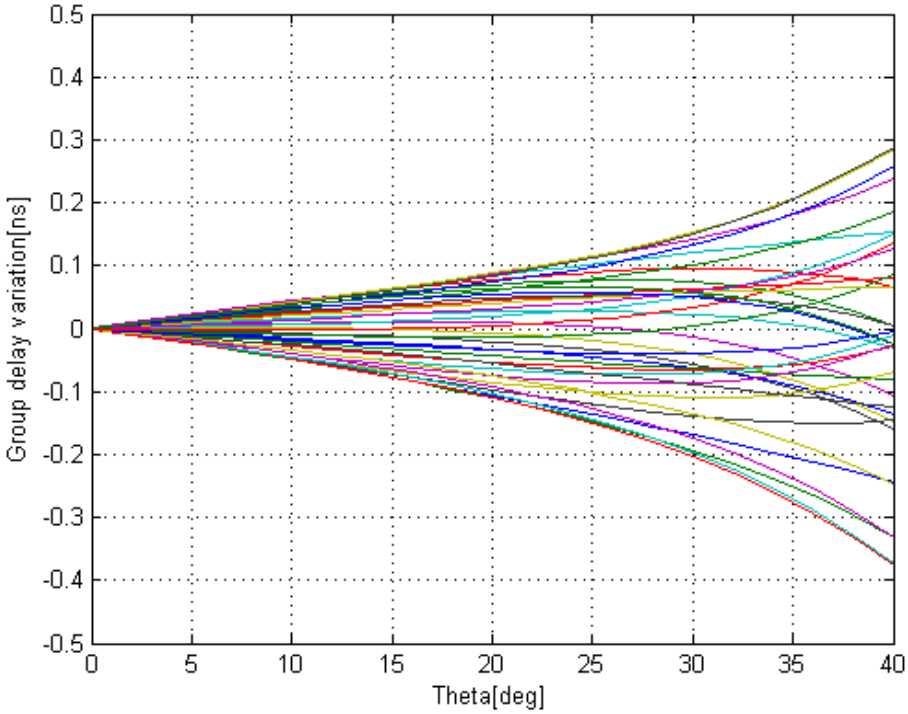


**Figure 25: The group delay variation over theta on the GLONASS L1OF band (1598 - 1606 MHz) for the three element array with ring elements. Colour represents different phi cross sections, with a step of 10 degrees.**

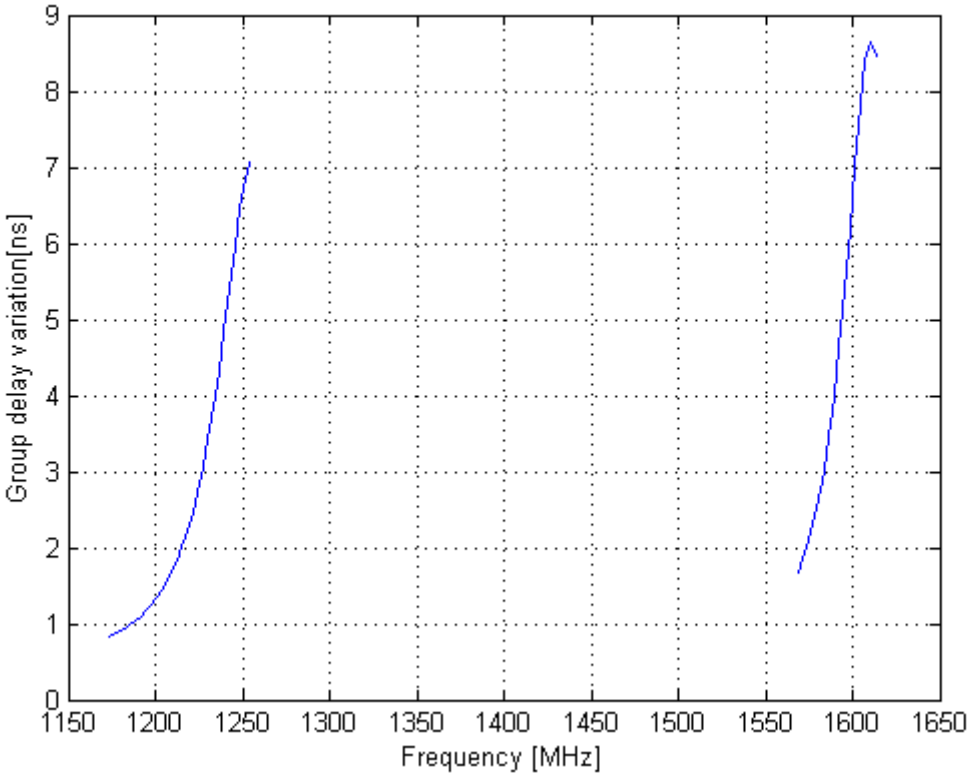


**Figure 26: The group delay variation over frequency for the three element array with ring elements.**

### 3.3.3 Final performance for the twelve element array

The radiation pattern for the twelve element array was calculated the same way as for the three element array in Section 3.3.2. The gain for the twelve element array is presented in Figure 27 and it has slightly larger margin to the mask than when the reference element pattern was used. The XPD is presented in Figure 28 and is the same as for the element and three element cases.

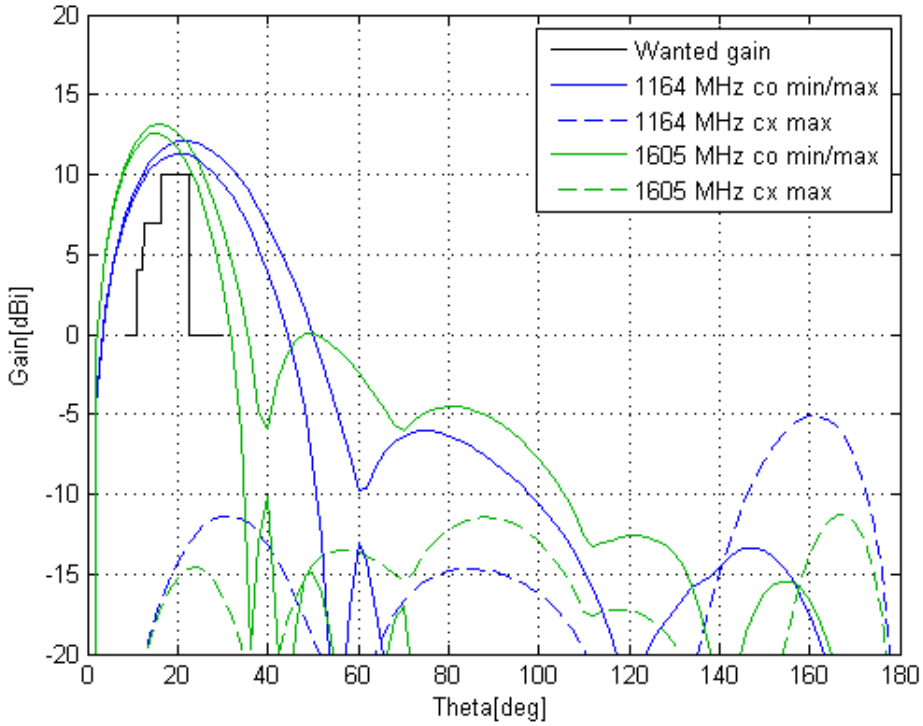


**Figure 27: Gain for the circular array with twelve elements. The element used was the ring element.**

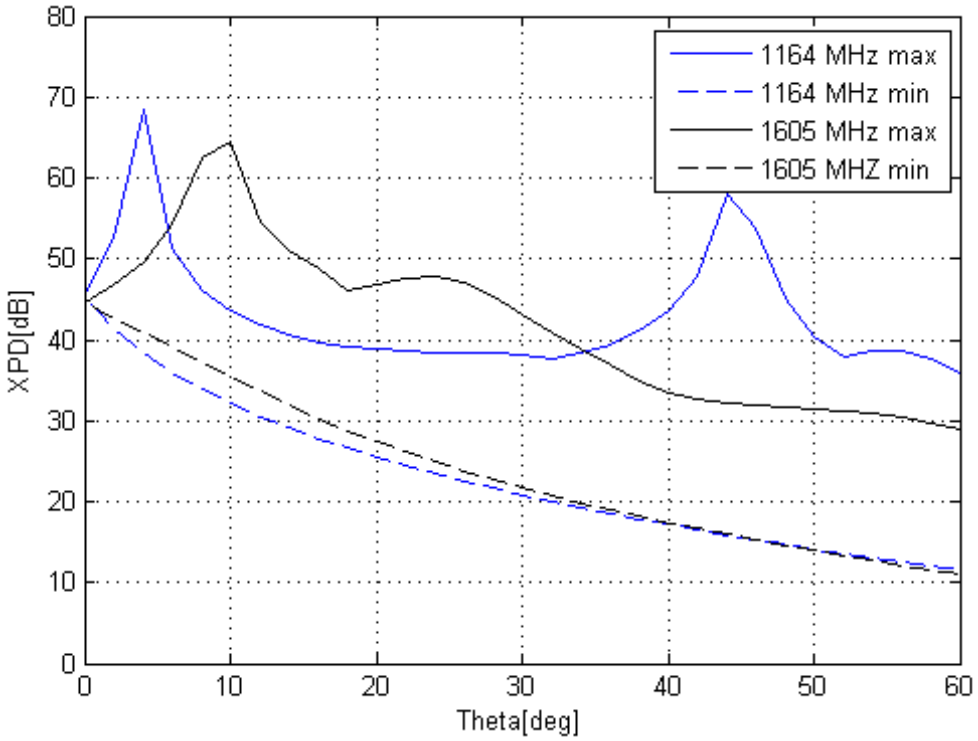


**Figure 28: The minimum/maximum XPD for RHCP at 1164 MHz and 1605 MHz for the HFSS model of the ring element in the twelve element array setup.**

### 3.3.3.1 Phase centre and group delay

The phase centre was 22.6 mm above the antenna at 1164 MHz and 21.3 mm at 1606 MHz which is within specifications for the phase centre stability over frequency. The phase variation over theta for 1164 MHz is presented in Figure 29 and the maximum variation at 40° in theta is 18° in phase, corresponding to 12.9 mm. The phase variation for 1606 MHz is presented in Figure 30 and is less than 20° at around 30° in theta, which is 10.4 mm in distance, after 30° in theta the phase variation increase rapidly to around 360° (one wavelength, 188 mm) at 40°, probably due to the fact that there is a null there in the radiation pattern.

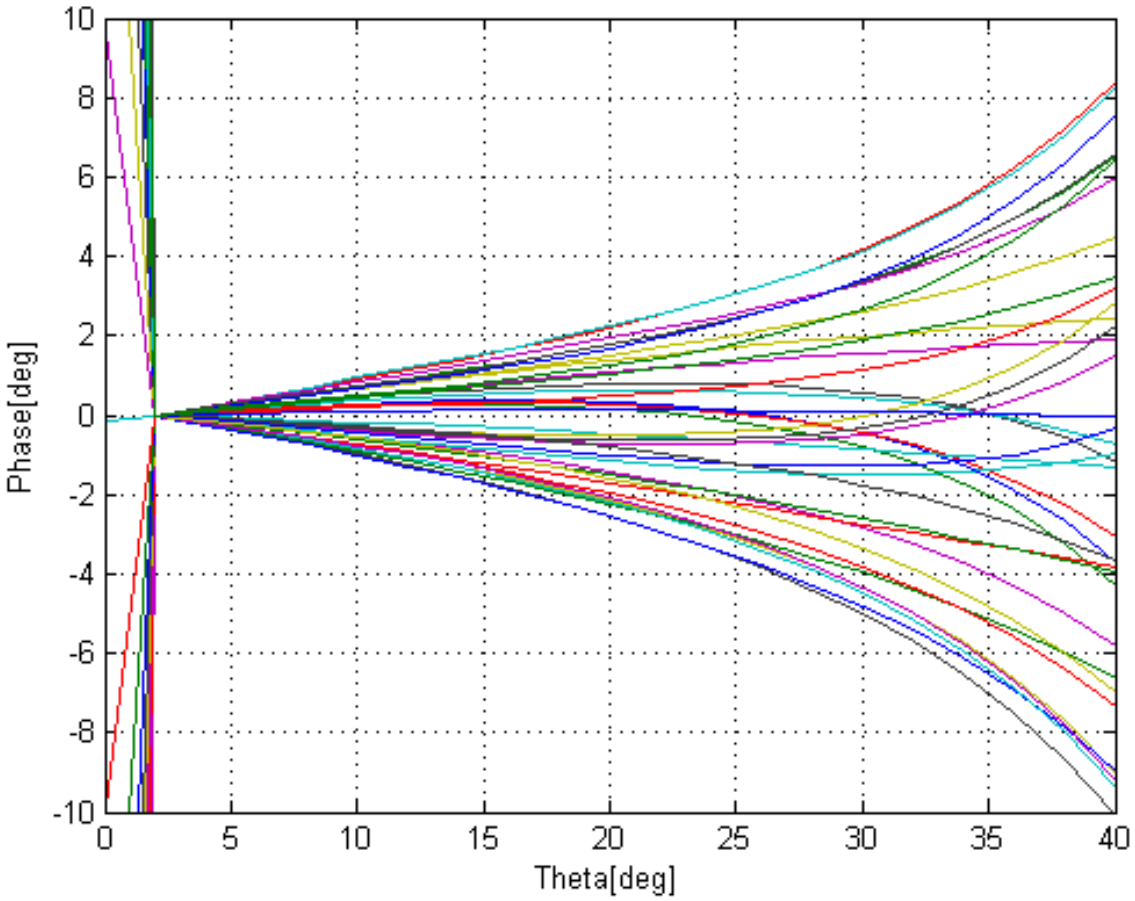


**Figure 29: The phase radiation pattern of the twelve element array with the ring element at 1164 MHz. Colour represents different phi cross sections, with a step of 10 degrees.**

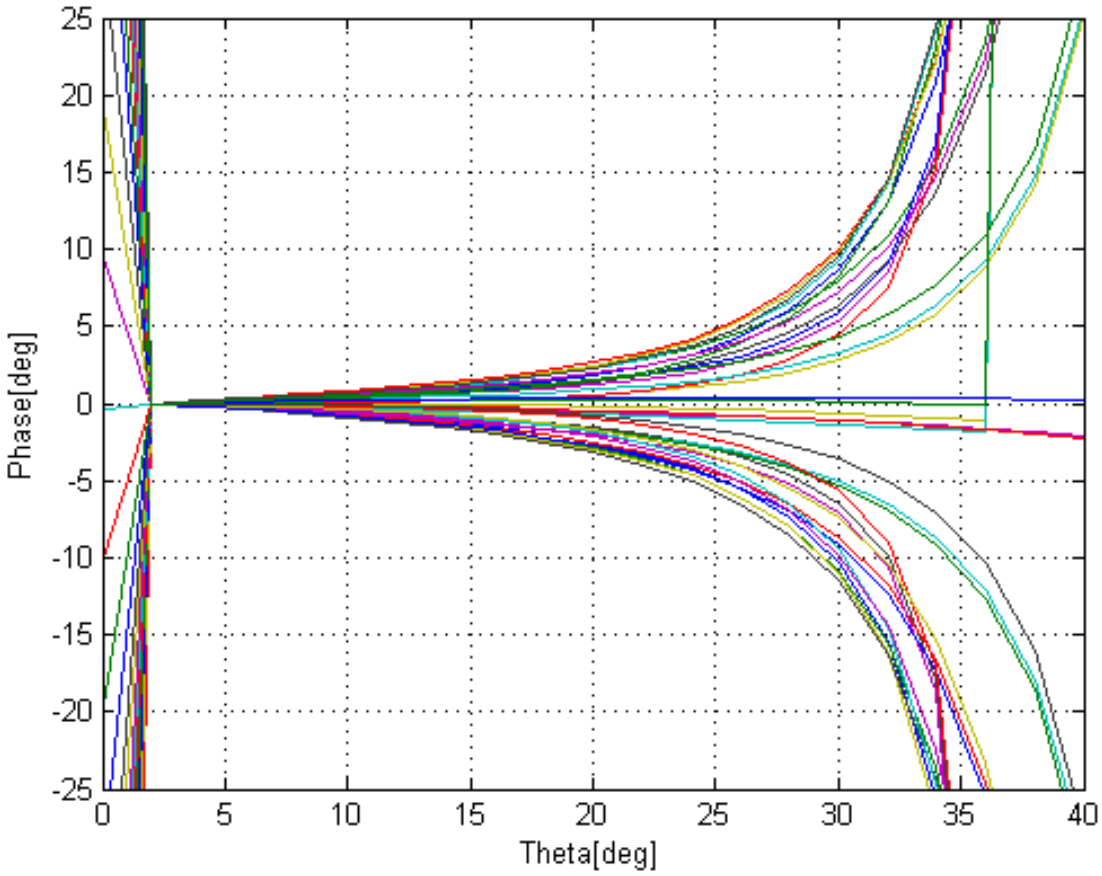


**Figure 30: The phase radiation pattern of the twelve element array with the ring element at 1606 MHz. Colour represents different phi cross sections, with a step of 10 degrees.**

The group delay variation with respect to theta between 1164 - 1188 MHz and between 1598 - 1606 MHz is presented in Figure 31 and Figure 32, respectively. The group delay variation is around 0.3 ns at 40° theta at the lower band which satisfies the requirements with large margin. At the upper band the same phenomenon as for the phase variation is visible with a large increase in group delay above 30° in theta. At 30° the group delay variation at the upper band is below 0.5 ns. For the group delay over frequency, presented in Figure 33, it is basically the same as for the three element array case which indicates further that it is because the element is not matched.

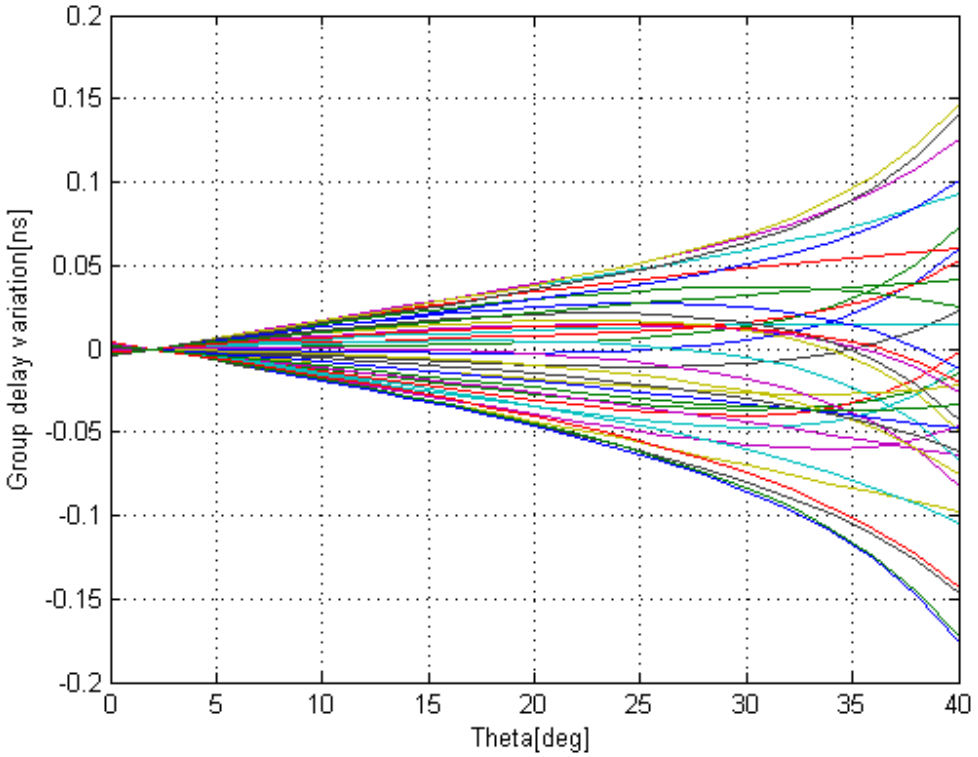


**Figure 31: The group delay variation over theta on the GPS L5 band (1164 - 1188 MHz) for the twelve element array with ring elements. Colour represents different phi cross sections, with a step of 10 degrees.**

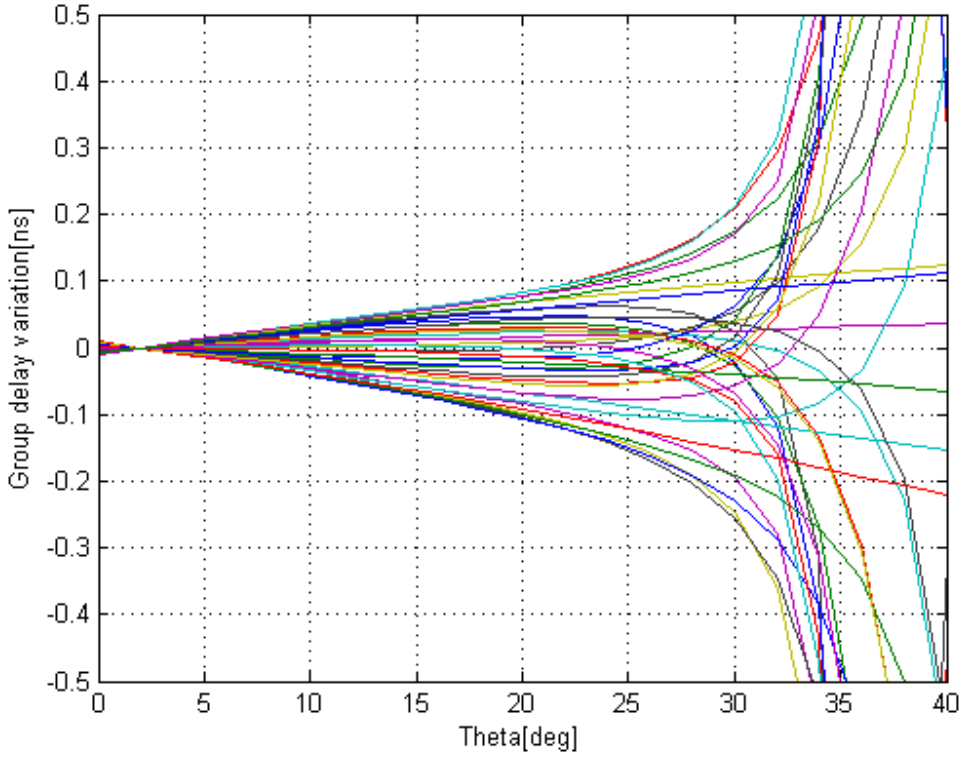


**Figure 32: The group delay variation over theta on the GLONASS L1OF band (1598 - 1606 MHz) for the twelve element array with ring elements. Colour represents different phi cross sections, with a step of 10 degrees.**

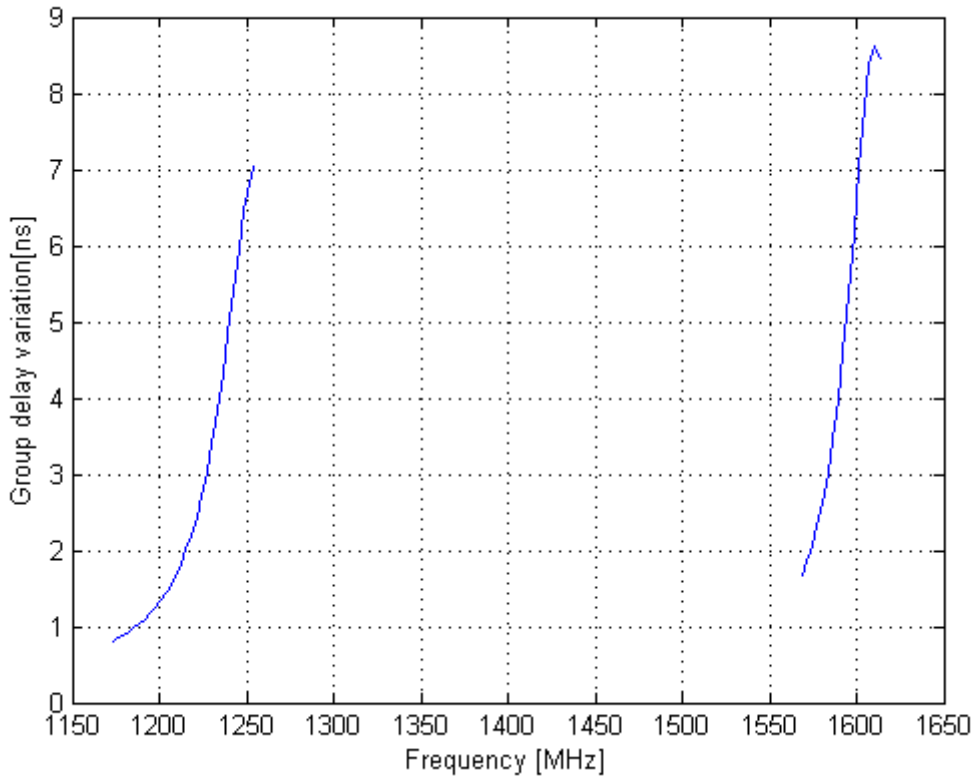


**Figure 33: The group delay variation over frequency for the twelve element array with ring elements.**

### 3.3.4 Mechanical construction

The array antenna is here thought of as round even if it probably could be made smaller and the view from above is presented in Figure 34 for the three element array and in Figure 5, in Section 3.3, for the twelve element array. The phases for the elements are marked in the figure and the amplitude is the same for all elements.

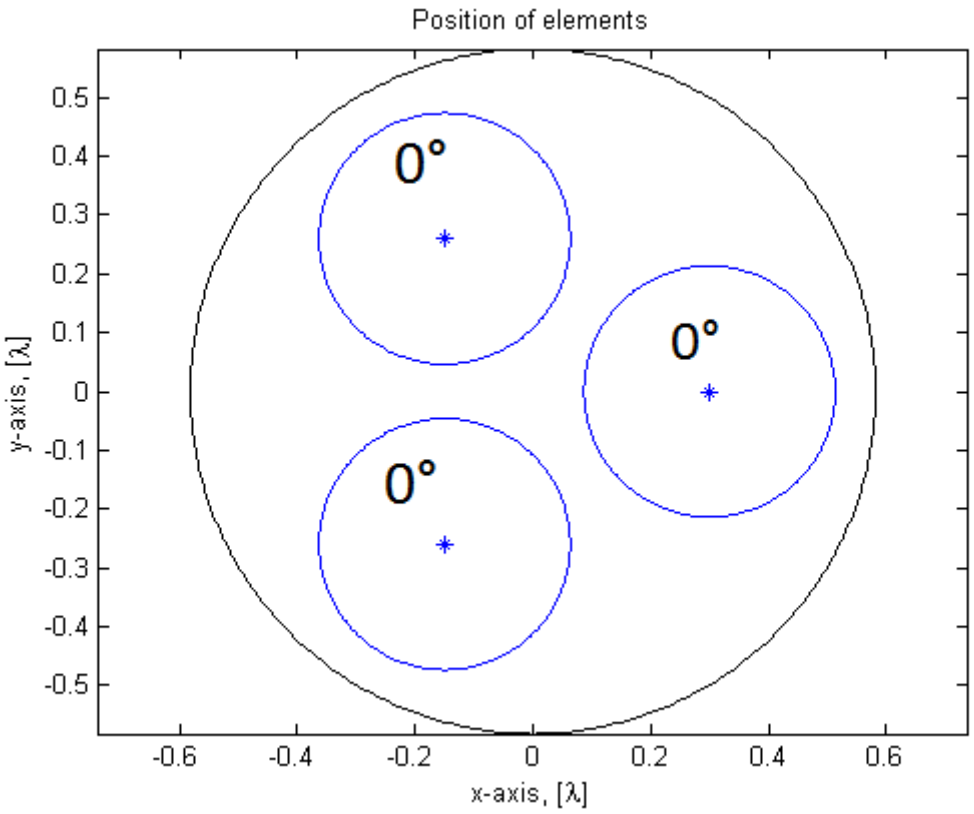


**Figure 34: The ring elements placed in the three element array along with the tracing of the physical size of the array. The electrical phase shift in degrees between elements is marked. For this case all elements are fed in phase. The scale is in wavelengths at 1164 MHz.**

The imagined cross-section of the arrays is presented in Figure 35, the rings inside the element is not shown here. The dark grey part, the base, is thought to be a single aluminium peace which has been produced by numerical drilling, CNC. The black parts are two separate lids. Along the outside of the element walls and the inside of the outer array wall there is a notch which the upper lid rests upon. The upper lid is connected to the base by screws, it is estimated that four screws per element are necessary along with three/nine extra screws placed at the edge of the lid for the three/twelve element array. The thickness of 2 mm for the wall takes into account that the wall needs to be a bit thicker where the screws are placed. Below the element is the distribution net, the distribution is thought of as a trace with two aluminium walls on each side. The walls are estimated to have an average thickness of 2 mm and one screw is placed every quarter wavelength on each wall. As traces can lie next to each other and thus not need to have two walls per trace, the total wall length is an overestimation so the quarter wavelength is based on 1164 MHz which gives fewer screws than if the upper frequency had been used. The bottom lid is screwed to the walls of the distribution network and rests on a ledge at the outer array wall. The ring elements and the distribution network are suspended on plastic supports.

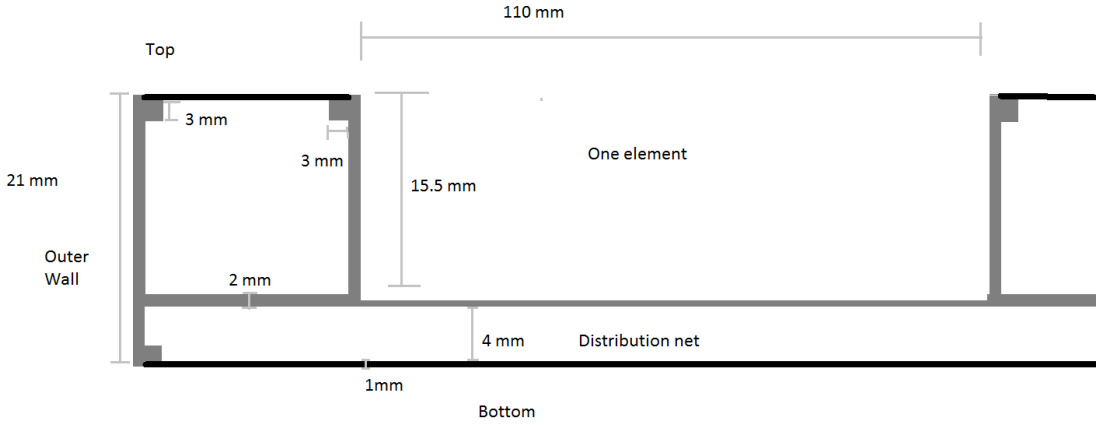


**Figure 35: A cross-section of the array antenna. The rings and support are not shown in the picture, neither the distribution network in detail.**

The total trace length was estimated by finding the average distance from a feed of an element to the edge of the array by summing the distance in X-axis and the distance in Y-axis. This is not the closest route but one where only 90 degree corners are used. It was then assumed that the power dividers are equally spaced and add up the distance for all traces. I am treating the case where the antenna has two ports, one for the upper band and one for the lower band. For the three element array case I assume that there is one power divider step which divides the power in three and then one more division for the element, this gives a total trace length of 205 mm. For the twelve element array it was assumed that it has 5 division steps (1 trace, 2, 4, 8, 12, 24) and the length of the traces became 627 mm. In Table 17 the weight is summarized where the walls for the matching network is considered a part of the large CNC'd piece of metal.

**Table 17: The weight of the individual parts and the total weight of the three element array and twelve element array.**

| Part | Weight of part [g] | Number of parts for 3 element array | Weight for 3 element array [g] | Number of parts for 12 element array | Weight for 12 element array [g] |
|---|---|---|---|---|---|
| Structure | n/c | 1 | 404 | 1 | 1153 |
| Top lid | n/c | 1 | 191 | 1 | 249 |
| Bottom lid | n/c | 1 | 103 | 1 | 618 |
| Rings | 9 | 3 | 17 | 12 | 108 |
| Support for rings | 5 | 3 | 15 | 12 | 60 |
| Network trace | n/c | 1 | 10 | 1 | 30 |
| Screws for bottom lid | 1 | 64 | 64 | 195 | 195 |
| Screws for upper lid | 1 | 15 | 15 | 57 | 57 |
| Screws for Satellite | 3 | 8 | 24 | 14 | 42 |
| SMA Connectors | 4 | 2 | 8 | 2 | 8 |
| Connectors screws | 1 | 8 | 8 | 8 | 8 |
| Total weight | | | 859 | | 2528 |

## 3.4 Helix dimensioning

There are several different helix antennas, for example quadrifilar helix antennas which have four arms and monofilar helix antennas which have one arm. Here, a quadrifilar helix antenna and a monofilar helix antenna are investigated. The quadrifilar antenna is top fed and is first designed simply as four wires with no regard for how the feed is to be constructed and is called the single layer case. A second layer of wires was later added to the quadrifilar design to allow the helix to be fed at the bottom and the design is called double layer qudrifilar helix antenna.

A number of monofilar helix antenna designs were tested and the one which turned out the best was one with a circular ground plane. This was also the helix antenna design which was judged best to continue evaluating and which was simulated in HFSS.

### 3.4.1 Single layer quadrifilar helix antenna

A quadrifilar helix antenna was first judged to be the best option to be able to fulfill the requirements as best as possible, among helix antennas. A quadrifilar helix antenna, has four arms/helixes, is a resonant antenna in contrast to a monofilar helix, having one arm/helix, which is a traveling wave antenna. The quadrifilar helix was dimensioned by using the genetic optimization algorithm together with the program WireMoM which is a simulation program using the method of moments.

The first model which was tried was a top-feed quad helix with short-circuit rings on top and bottom. How the feeds were connected to the top, cables inside the helix, were not included in the model. The helix was split into four segments where the height and number of turns could be changed by the optimizer. Different pitch angle of the turns on different sections help to match the antenna for several frequency bands as shown in [61] where the pitch angle on two sections of the antenna were changed to match the antenna to two different frequency bands. Furthermore the helix could be made conical and the cone angle can be varied along with the bottom radius. This could be advantageous as a conical helix can radiate in axial mode over a wider frequency span [62].

The resulting parameters are presented in Table 18 and a visualization of the quad helix is presented in Figure 36, theta is 0° along the symmetry axis of the helix. As presented the antenna is quite high but has smaller diameter than the array options investigated. The directivity at different frequencies is presented in Figure 37 and as shown, assuming high efficiency, the helix almost fulfils the wanted requirement on the gain and it fulfils the minimum requirement. It is also shown that the XPD is lower than 15 dB for 0-40 ° in theta. In Figure 38 the Smith chart is presented and in Figure 39 a magnification of the interesting area of the Smith chart is shown. It is shown that the helix is not very well matched to 50 Ω, which is the impedance of the distribution network and the normalized impedance of the Smith chart, but possibly could be matched to 50 Ω as the change in impedance over frequency is relatively small.

**Table 18: The parameters for the quadrifilar helix antenna generated by the optimization algorithm.**

| Parameters | Value | | | |
|---|---|---|---|---|
| Wire radius | 0.5 mm | | | |
| Bottom radius | 63.7 mm | | | |
| Cone angle | 8.2 ° | | | |
| Total Height | 322 mm | | | |
| Total number of turns | 6.1 turns | | | |
| | #1 | #2 | #3 | #4 |
| Height of segments | 52.6 | 97 | 69.9 | 102.6 |
| Turns per segment | 0.91 | 1.65 | 1.27 | 2.28 |
| Turns/Height×100 | 1.73 | 1.70 | 1.82 | 2.22 |

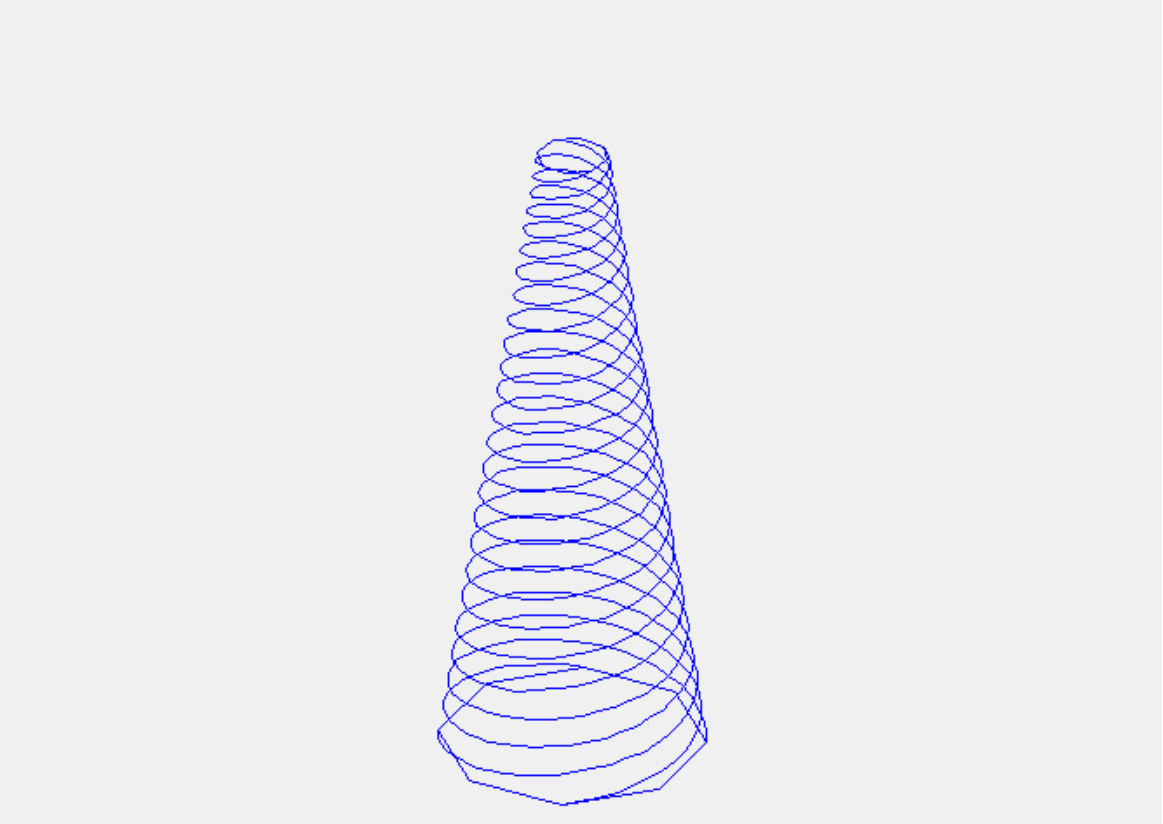

**Figure 36: A 3-D representation of the quadrifiliar helix model with a single layer.**

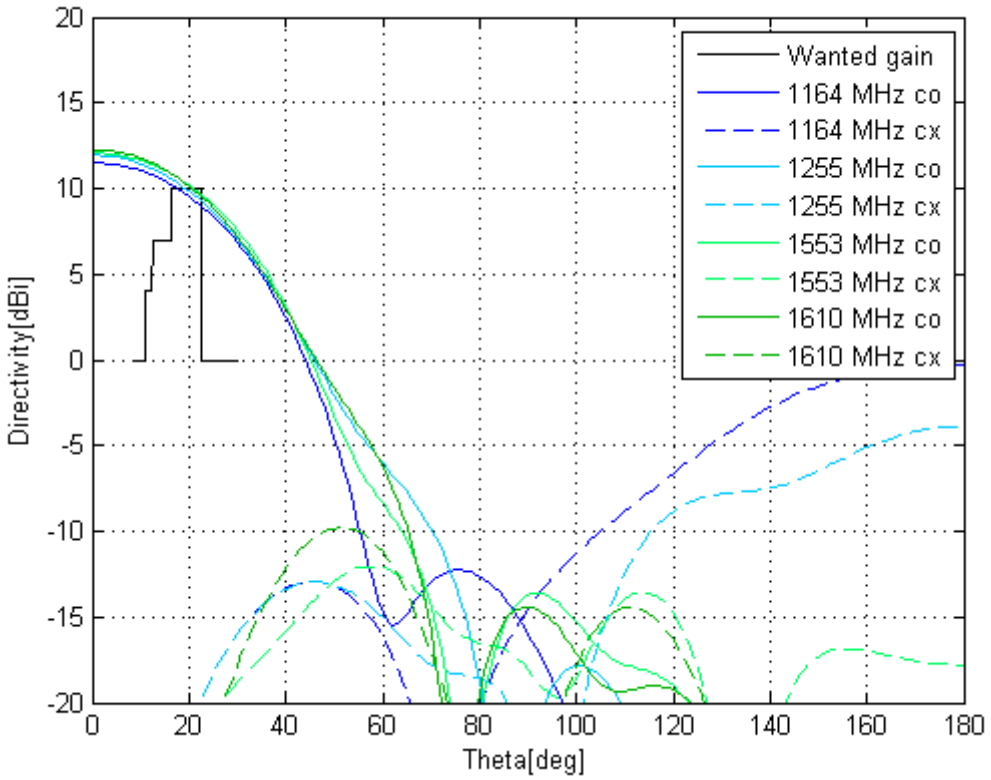


**Figure 37: The minimum directivity for RHCP (co) and maximum directivity for LHCP (cx) of the resulting quadrifilar helix antenna with single layer.**

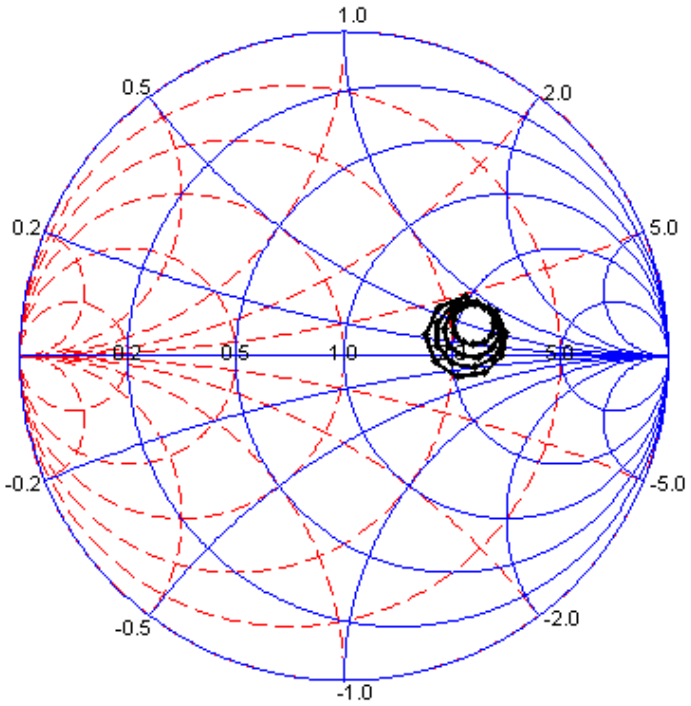


**Figure 38: The Smith chart for the quadrifilar helix antenna with single layer. The impedance is normalized to 50 Ω which is the impedance for the distribution net.**

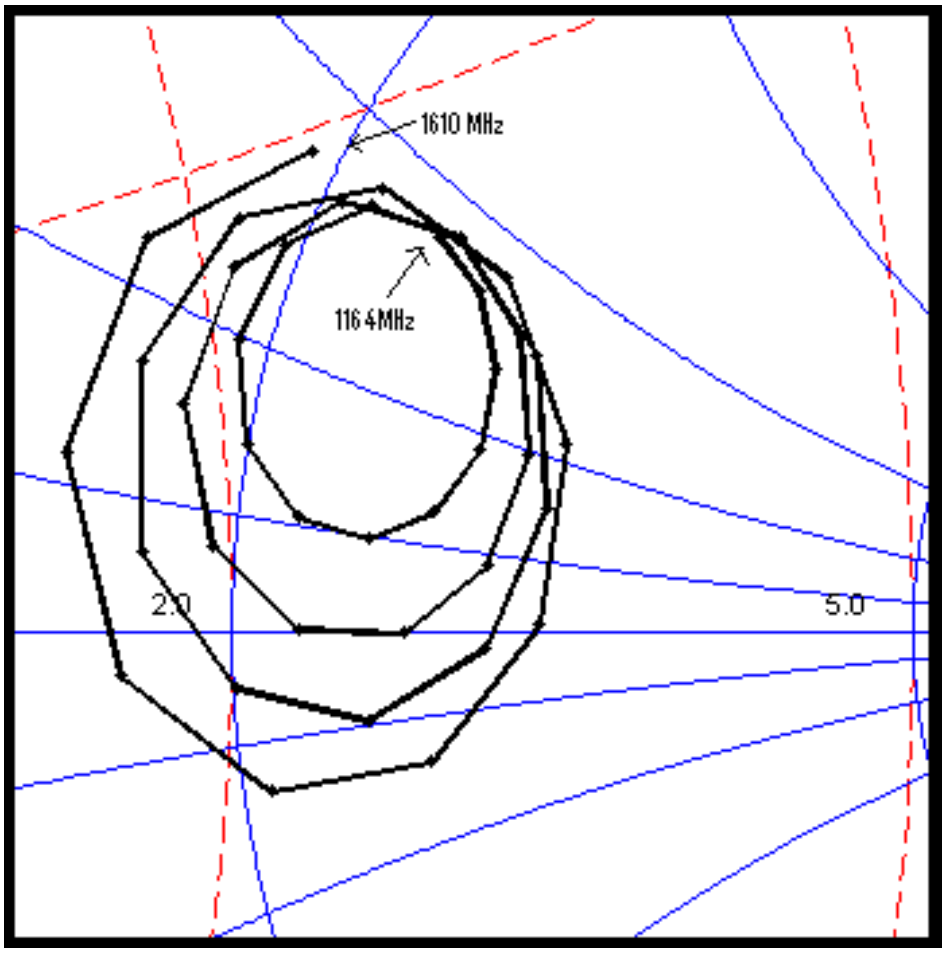


**Figure 39: Zoom-in on the Smith chart in Figure 38 for the quadrifilar helix antenna with single layer. The impedance is normalized to 50 Ω which is the impedance for the distribution net.**

### 3.4.2 Double layer quadrifilar helix antenna

After the initial optimization of the helix antenna a more complex version of the helix antenna was simulated. In the more complex version there are two layers of the wires where the inner layer is fed at the bottom. The inner layer is short circuited at the top while the outer layer at the top is left open. Furthermore, the outer layer is short circuited at the bottom. The short-circuit of the inner layer at the top changes the phase of the reflected current by 180 degrees and as the phase is not changed at the open end in the outer layer the return currents will be in phase. This makes the bottom fed double layer quad helix act as a top fed quad helix [63]. There are studs as well at the top of the helix to tune the antenna. In Figure 40 the top of the resulting double layer helix is presented to showing the studs. The double layer helix design is patented by RUAG space.

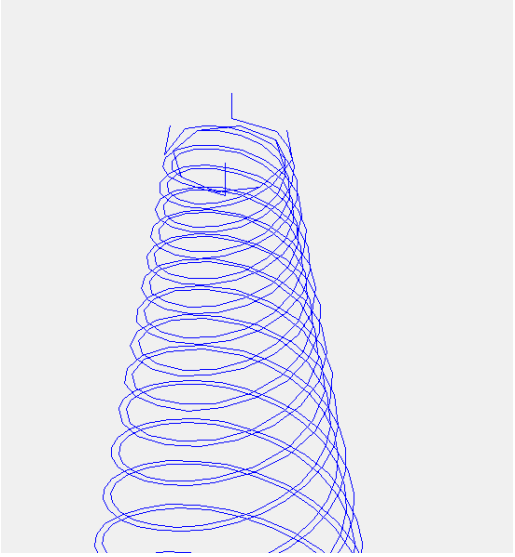

**Figure 40: A magnification of the 3-D representation of the quadrifiliar helix model with dual layer where the studs and the dual layer can be seen more clearly.**

As the double layer helix would have at least twice the number of elements and thus would take much longer to compute only a small variance from the values gotten from the single layer were input into the optimization. In addition to the parameters from the single layer design it was also possible to vary a height displacement between the inner and outer layer along with the length of the stubs which were varied over a larger interval.

The resulting parameters after the optimization are presented in Table 19 and a 3-D representation of the helix are presented in Figure 41.. The optimized design is quite similar to the single layer variant in total height, radius, cone angle and number of turns but the pitch angle for the different sections is a bit different. The directivity for different frequencies are presented in Figure 42 and in Figure 43 the Smith chart is presented, with relevant frequencies in Figure 44. It should be noted that only for a small portion over the wanted frequency bands the directivity was as low as presented for 1164 and 1553 MHz. Even though the lower frequencies are slightly below the result from the single layer case, they fulfil the minimum requirement. The impedance though as presented in Figure 44 is not very stable and it would be hard to achieve matching. A model without studs was simulated as well and the results were similar.

**Table 19: The parameters for the dual layer quadrifilar helix antenna generated by the optimization algorithm.**

| Parameters | Value | | | |
|---|---|---|---|---|
| Wire radius | 0.325 mm | | | |
| Bottom radius | 63.6 mm | | | |
| Cone angle | 8.2 ° | | | |
| Layer distance in radius | 2 mm | | | |
| Layer displacement in z | 3.54 mm | | | |
| Stud length | 0.97 mm | | | |
| Total Height | 323 mm | | | |
| Total number of turns | 6.4 turns | | | |
| | #1 | #2 | #3 | #4 |
| Height of segments | 49.2 | 96.2 | 91.3 | 86.22 |
| Turns per segment | 0.99 | 1.67 | 1.42 | 2.36 |
| Turns/Height×100 | 2.00 | 1.74 | 1.56 | 2.74 |

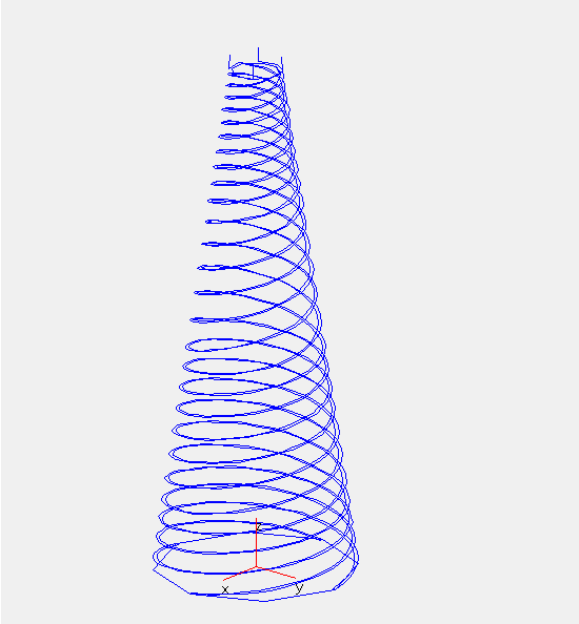

**Figure 41: A 3-D representation of the quadrifiliar helix model with dual layer.**

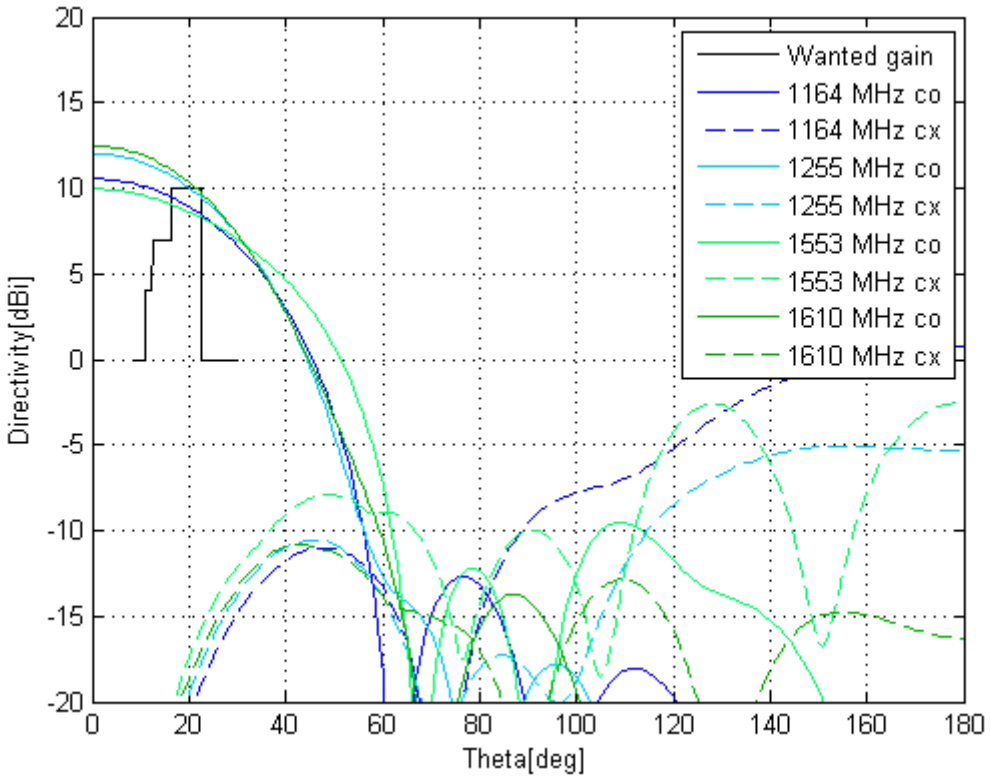


**Figure 42: The minimum directivity for RHCP (co) and maximum directivity for LHCP (cx) of the resulting quadrifilar helix antenna with dual layer.**

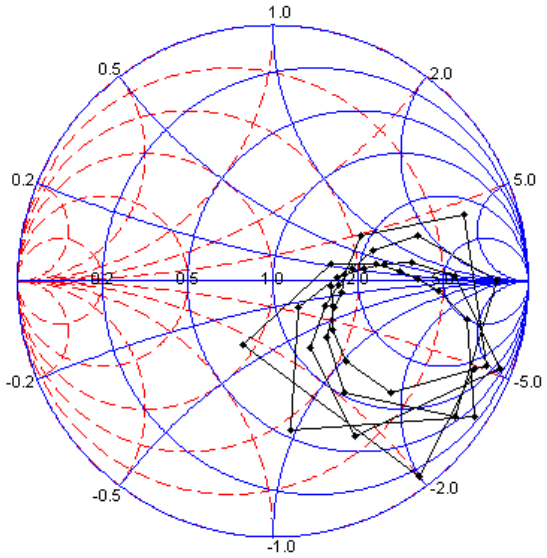


**Figure 43: Smith chart for the quadrifilar helix antenna with dual layer. The impedance is normalized to 50 Ω which is the impedance for the distribution net.**

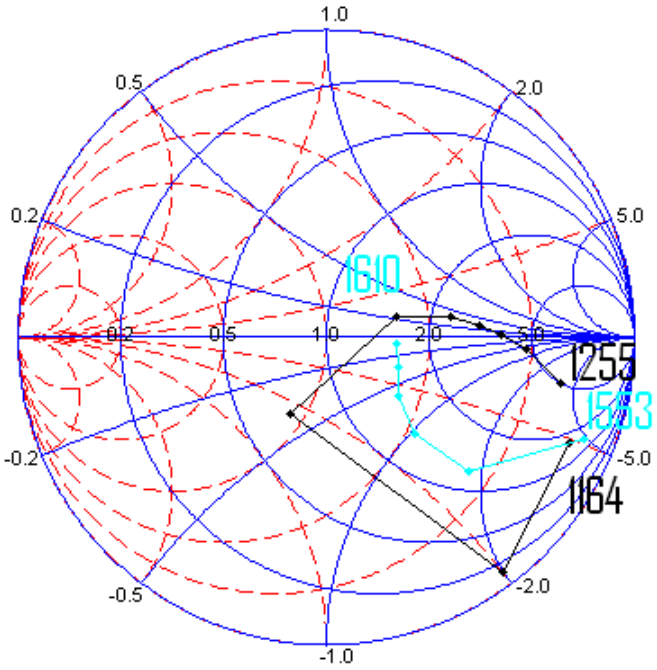


**Figure 44: The Smith chart in Figure 43 for the quadrifilar helix antenna with dual layer but with only the interesting frequency regions plotted. The impedance is normalized to 50 Ω which is the impedance for the distribution net.**

### 3.4.3 Monofilar helix antenna

It was also decided that a monofilar helix should be investigated. A first optimization run was performed without any ground plane and as in the quad helix case changing the height and number of turns of four sections along with cone angle and the bottom radius. The resulting parameter values are presented in Table 20. The first generated design was not able to reach the required gain as presented in Figure 45, at least not over the wanted bandwidth.

**Table 20: The parameters for the monofilar helix antenna without ground plane generated by the optimization algorithm.**

| Parameters | Value | | | |
|---|---|---|---|---|
| Wire radius | 0.5 mm | | | |
| Bottom radius, helix | 52.6 mm | | | |
| Cone angle | 4.5° | | | |
| Total Height | 257 mm | | | |
| Total number of turns | 12.4 turns | | | |
| | #1 | #2 | #3 | #4 |
| Height of segments | 41.8 | 73 | 63 | 79.2 |
| Turns per segment | 2.56 | 2.47 | 1.73 | 5.69 |
| Turns/Height×100 | 6.12 | 3,39 | 2.75 | 7.18 |

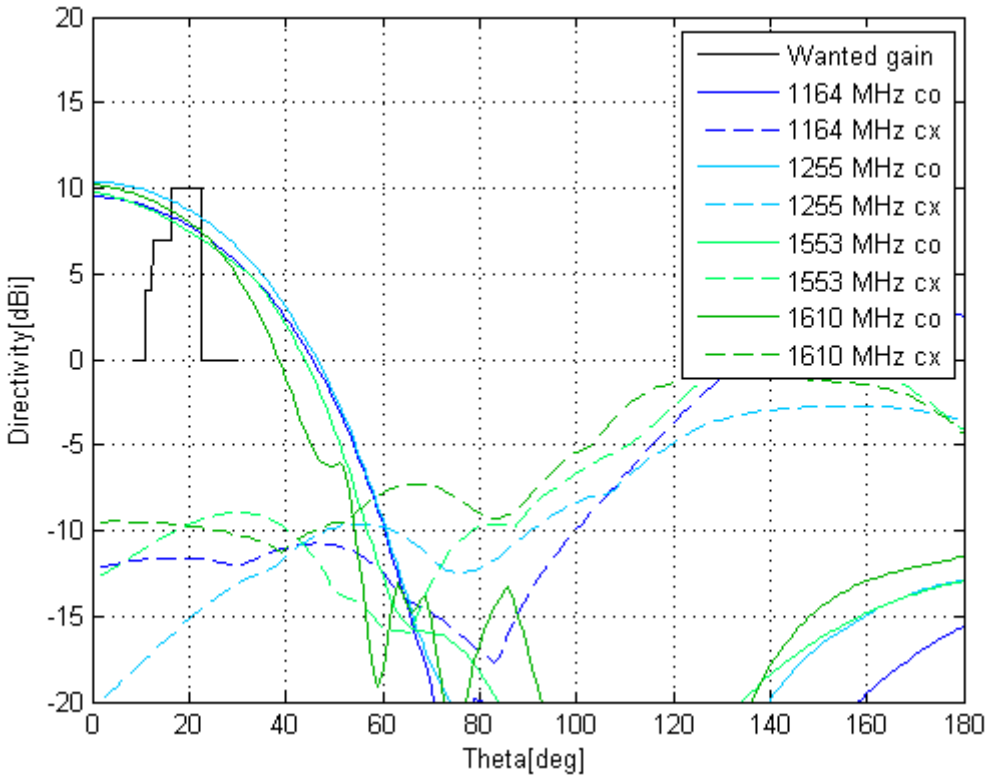


**Figure 45: The minimum directivity for RHCP (co) and maximum directivity for LHCP (cx) of the resulting monofilar helix antenna.**

#### 3.4.3.1 Monofilar helix antenna with ground plane

A circular ground plane was added to the design in hope that it would improve the results. A ground plane makes the antenna more broadband according to [64] where they were using an infinite ground plane and image theory to show that for lower frequencies the image contributes more than the real structure to the radiation pattern.

The size of the ground plane and the distance between the ground plane and the antenna could be optimized and the result from the optimizer is presented in Table 21 and the model is shown in Figure 47. The difference in turns and length is probably due to that the design without ground plane could not reach the wanted bandwidth and so increasing the number of turns did not improve the gain at both frequencies while it did that for the design with ground plane.

With this design the minimum requirements for the gain were fulfilled and the wanted requirements were almost fulfilled as presented in Figure 46 and the XPD is greater than 15 dB from 0-34 °. The Smith chart is presented in Figure 48 and as presented the impedance is 109 - 780j Ω at 1164 MHz and is 118 - 565j Ω at 1610 MHz which means that the antenna has to be matched if this design is to be used.

Furthermore, the current distribution along the helix arm shows some interesting phenomena, the normalized amplitude and normalized phase of the current is presented in Figure 49 and 50 for 1164 MHz and 1610 MHz respectively. The phase is normalized so that -1 is an outward travelling TEM wave in free space along the wire and the amplitude is normalized to one. As mentioned in [65] there are normally two distinct regions in the current distribution on a helix, one where the current decays, at the few lowest turns, and one region with constant amplitude but lower phase change. At the end of the wire there is a standing wave due to a reflection of the current at the end. For the lower frequencies this seems to be true but for the upper frequency the current does not decrease before the second change in turn/length. Before this region the amplitude is almost constant and the phase change is the same as a TEM wave along the helix, indicating that it could be a slow wave which does not radiate.

**Table 21: The parameters for the monofilar helix antenna with ground plane generated by the optimization algorithm.**

| Parameters | Value | | | |
|---|---|---|---|---|
| Wire radius | 0.5 mm | | | |
| Bottom radius, helix | 45 mm | | | |
| Cone angle | 5° | | | |
| Ground radius | 79 mm | | | |
| Distance between ground plane and start of helix | 17 mm | | | |
| Total Height | 309 mm (326 mm including distance to ground) | | | |
| Total number of turns | 20.4 turns | | | |
| | #1 | #2 | #3 | #4 |
| Height of segments | 36.6 | 82.8 | 96 | 93.6 |
| Turns per segment | 3.12 | 4.35 | 4.03 | 8.9 |
| Turns/Height×100 | 8.52 | 5.25 | 4.20 | 9.51 |

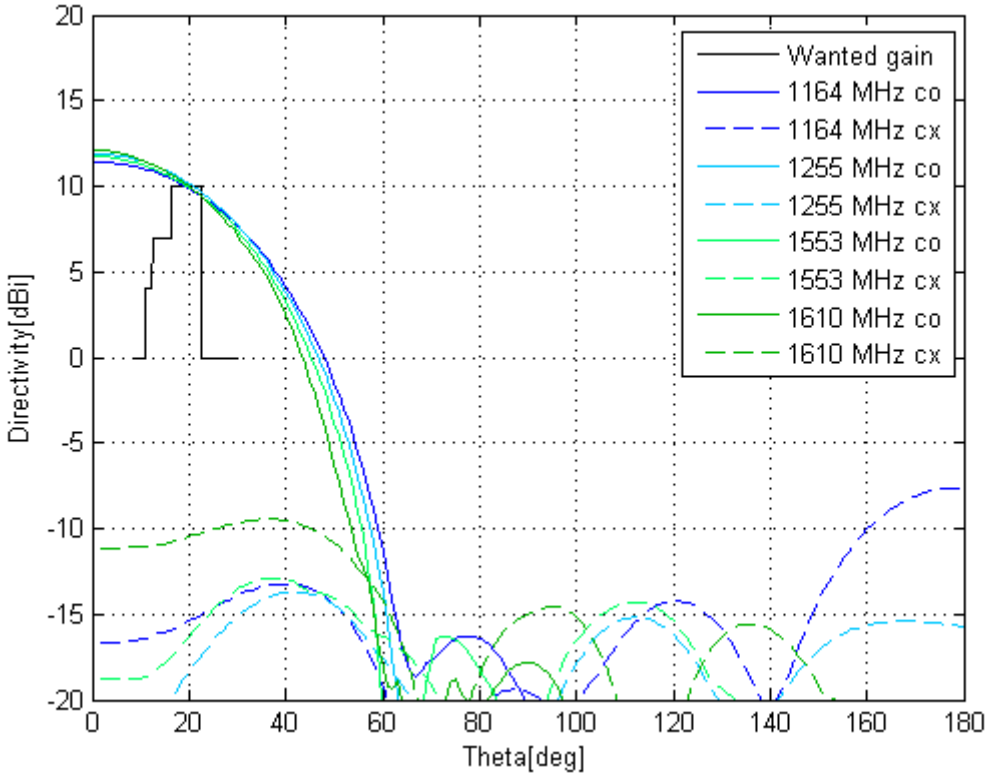


**Figure 46: The minimum directivity for RHCP (co) and maximum directivity for LHCP (cx) of the resulting monofilar helix antenna with ground plane.**

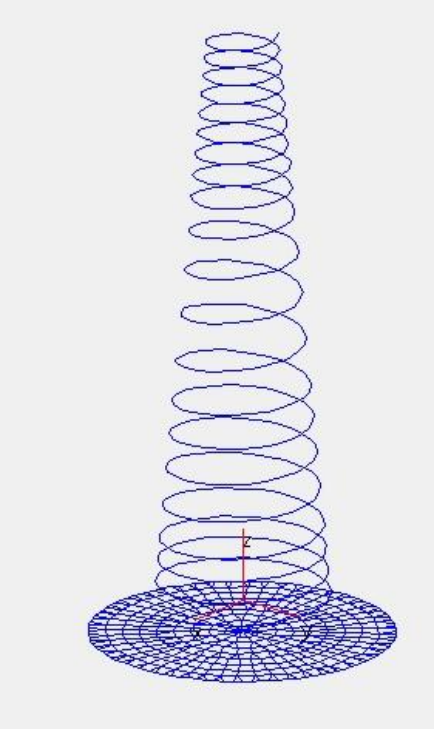

**Figure 47: 3-D representation of the monfilar helix with ground plane model.**

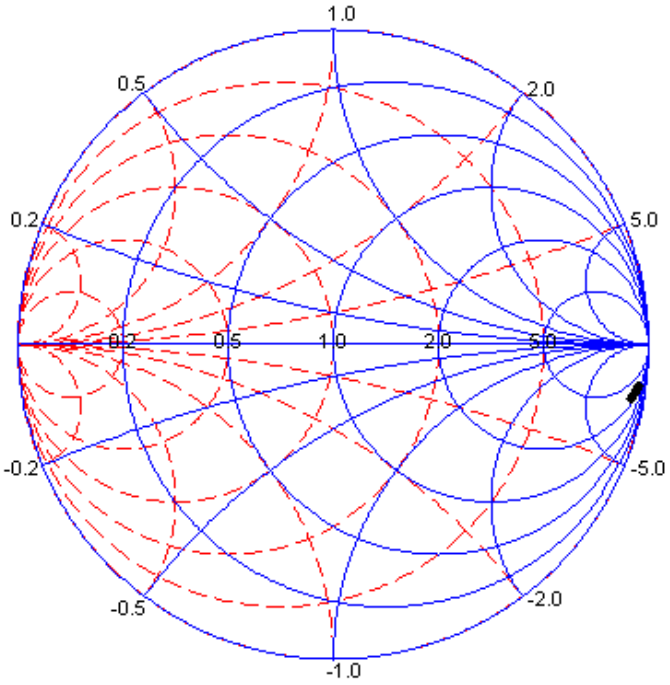


**Figure 48: Smith chart of the monofilar helix antenna with ground plane. The impedance is normalized to 50 Ω which is the impedance for the distribution net.**

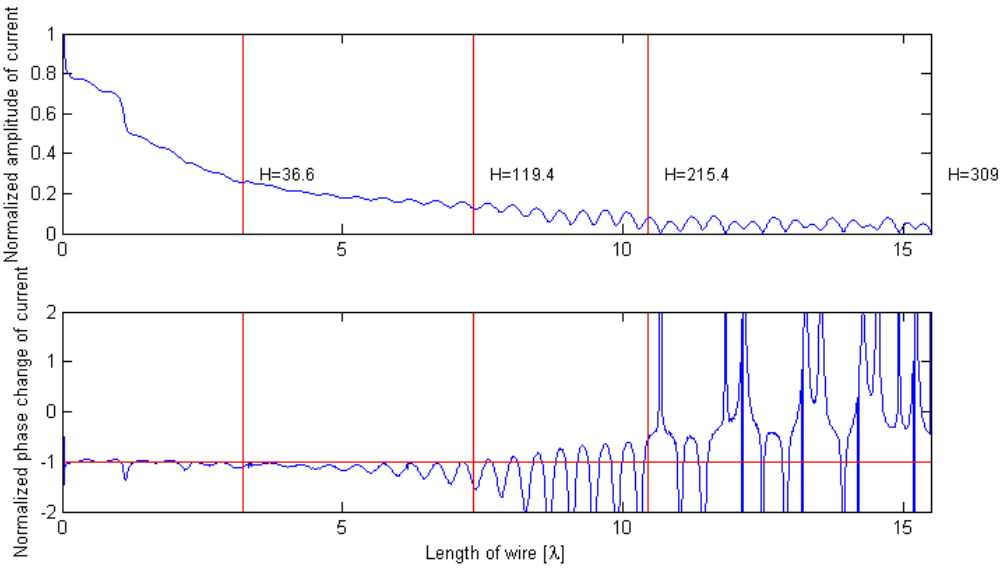


**Figure 49: The amplitude and phase change of the current on the monofilar helix arm for 1164 MHz. The amplitude is normalized to one and the phase change is normalized so a TEM wave in free space along the wire is -1/1 depending on direction. The horizontal red lines mark the different sections of the helix.**

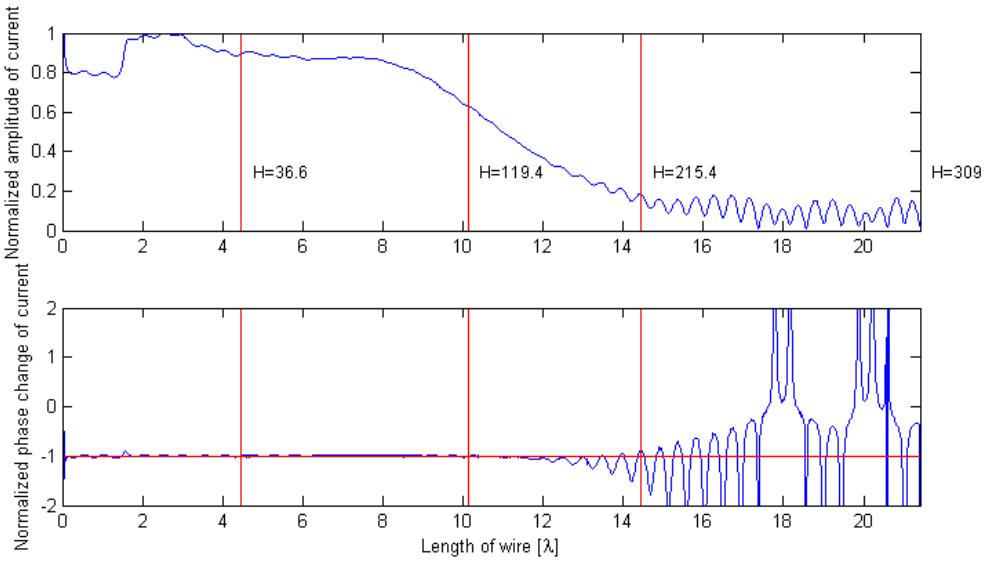


**Figure 50: The amplitude and phase change of the current in the monofilar helix arm for 1610 MHz. The amplitude is normalized to 1 and the phase change is normalized so a TEM wave in free space along the wire is -1/1 depending on direction. The horizontal red lines mark the different sections of the helix.**

### 3.4.3.2 Monofilar helix antenna with cone and changing cone angle

To minimize the size and maximize the performance of the monofilar helical antenna, the ground plane was allowed to be shaped into a truncated cone or a cup. In [64] it is presented that a cup and in even greater extent a truncated cone can increase the gain of a helix antenna. Djordjevic explains that the increase in gain is due to that reflections in the bottom ground plane going out in horizontal directions are diffracted/reflected by the cone/cup upwards which increases the gain of the antenna.

The helix is also allowed to be tapered at the top and bottom sections. [66] shows that by changing the cone angle and the pitch angle for the lowest part of the helix, among other things, the performance without ground plane could be the same as with infinitive ground plane. Tapering the open end of the helix results in an increased axial ratio but also increases the half power beam width, and thus decreases the gain some, according to [67].

The optimizer was run with these options included and the resulting parameters are presented in Table 22 and a 3-D representation is shown in Figure 51. During the optimization small costs were put on the geometric parameters, mainly the ground cones top radius, to see if it was possible to make the antenna slightly smaller and as presented the top cone radius is 69 mm which is smaller than the ground radius of 79 mm for the monofilar helix without the cone or changes in the cone angle.

The directivity for the generated design is presented in Figure 52 and as presented the result is very similar compared to the monofilar helix with just a ground plane. As the gains are so small compared to the extra complexity of the helix with a cone and different cone angles the decision was to continue with the simple monofilar antenna with ground plane.

**Table 22: The parameters for the monofilar helix antenna with conical ground plane along with changes in cone angle, generated by the optimization algorithm.**

| Parameters | Value | | | |
|---|---|---|---|---|
| Wire radius | 0.5 mm | | | |
| Bottom radius, helix | 48.5 mm | | | |
| Bottom ground radius | 65 | | | |
| Top cone radius | 69.1 mm | | | |
| Distance between ground plane and start of helix | 9.2 mm | | | |
| Total Height | 317 mm (326.2 mm including distance to ground) | | | |
| Total number of turns | 19.1 turns | | | |
| | #1 | #2 | #3 | #4 |
| Height of segments | 33.6 | 85.6 | 114.3 | 83.7 |
| Turns per segment | 2.99 | 4.44 | 4.90 | 6.78 |
| Turns/Height×100 | 8.90 | 5.19 | 4.29 | 8.1 |
| Cone angle per segment | 4.9 | 5.4 | 5.4 | 3.2 |

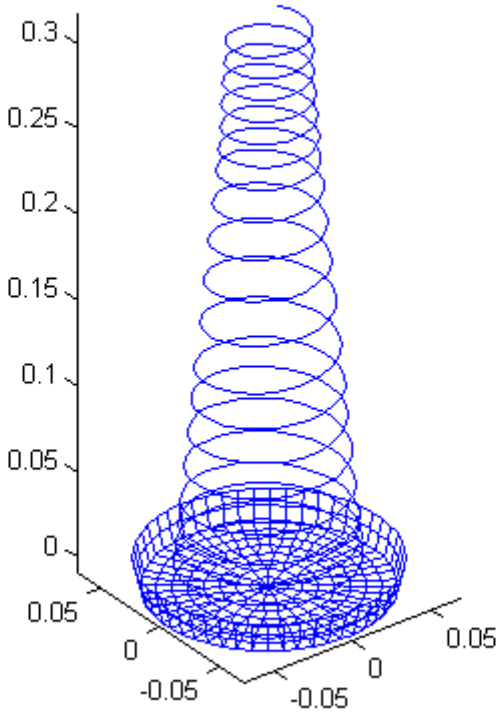


**Figure 51: The monofilar helix antenna with conical ground plane along with changes in cone angle**

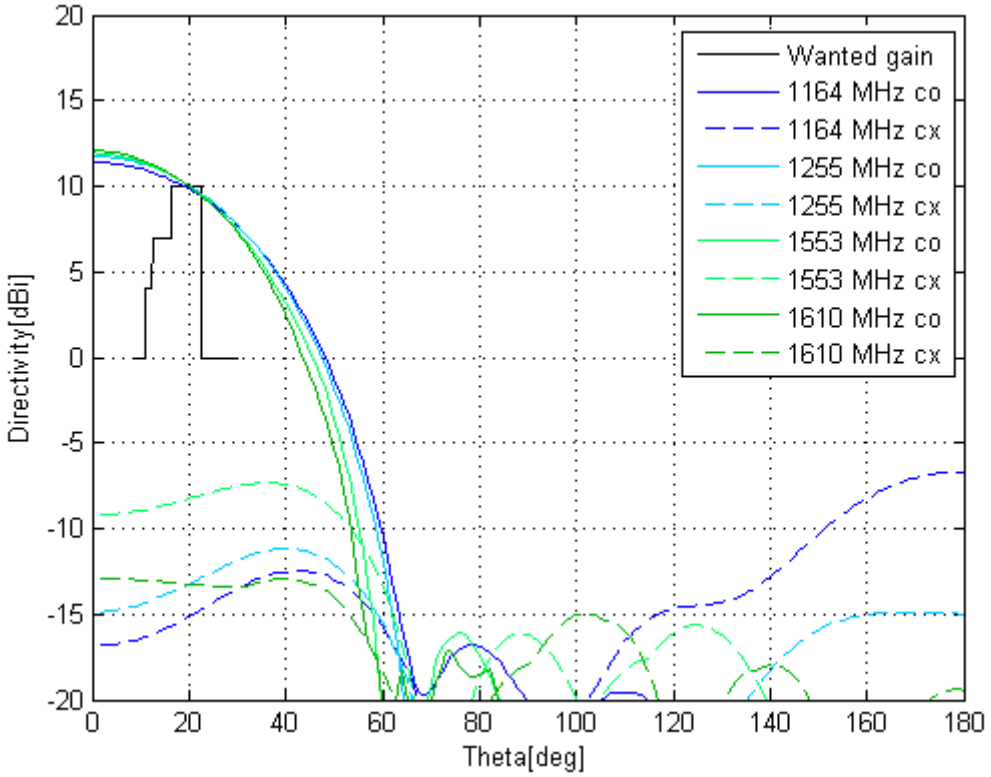


**Figure 52: The minimum directivity for RHCP (co) and maximum directivity for LHCP (cx) for the monofilar helix antenna with conical ground plane along with changes in cone angle.**

### 3.4.3.3 HFSS Simulation of monofilar helix antenna with ground plane

The monofilar helix antenna with a circular ground plane was further simulated in HFSS which uses FEM. The model is presented in Figure 53 and consists of three main parts; the ground plane/structure, a dielectric sheet shaped like a cone on which the helix is printed and the helix trace itself. As presented, the ground plane is separated in two parts where the cone is inserted in between. The dimensions are the same as presented in Table 21 with the addition that the dielectric cone is 0.5 mm thick, the trace is infinitely thin and 0.6 mm wide, the dielectric cone continues 20 mm after the helix arm has ended and the structure continues 91 mm below the ground plane. The ground plane and the trace are modelled as PEC and the cone has a relative permittivity of 3.66 and a dielectric loss tangent of 0.004, the surroundings are modelled as vacuum.

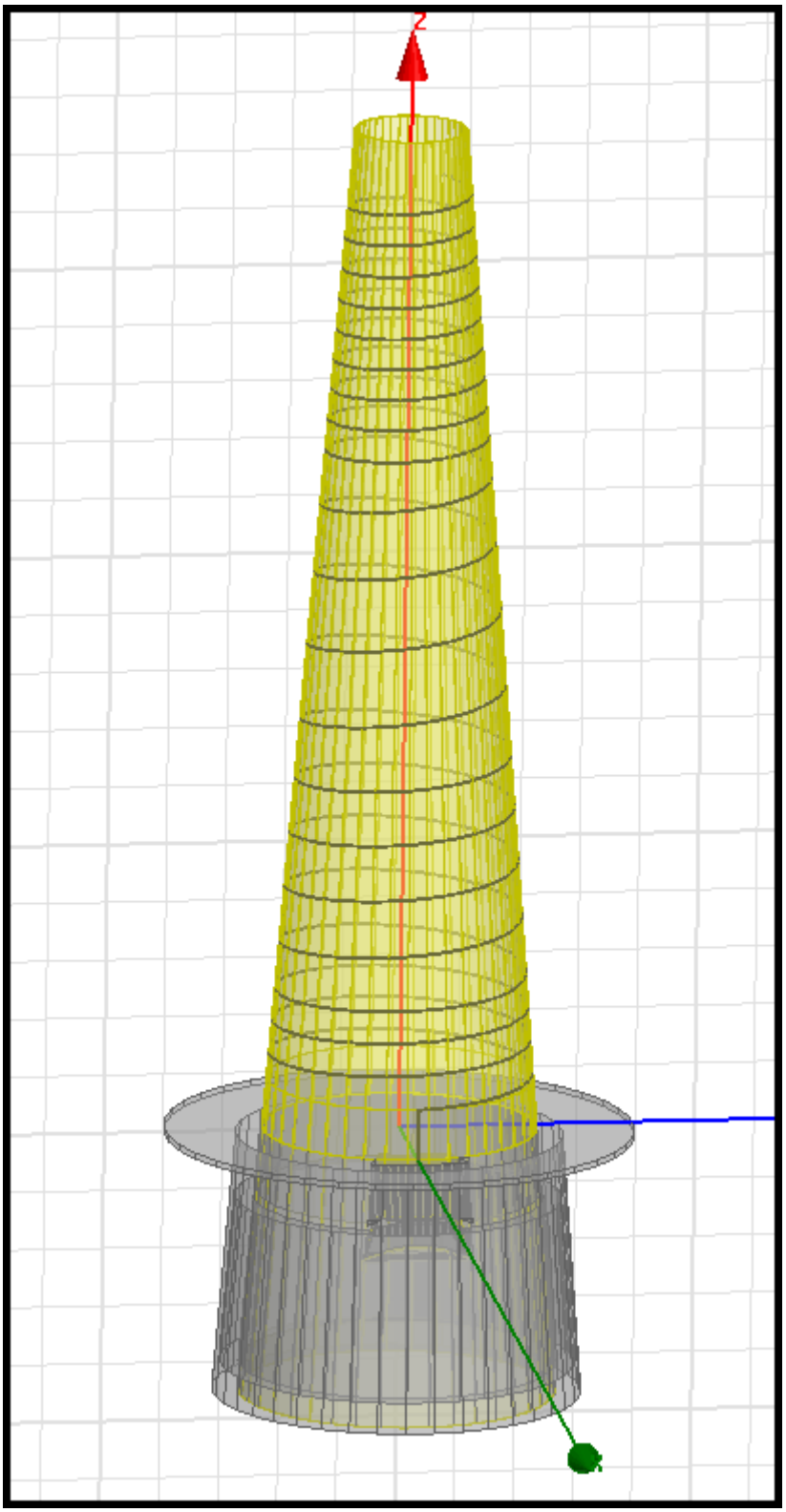


**Figure 53: The HFSS model of the monofilar helix with ground plane which consists of three parts: the dielectric cone, the helix trace and the ground plane/structure.**

In Figure 54 a close-up of the port and feed is shown. The distance from the outer part of the cut-out to the cone is 6.1 mm and the distance from the inner part of the cut-out to the cone is 7 mm, the feed stretches over 36°. In the figure, the electric field in the port is also presented which looks as expected. The Smith chart is presented in Figure 55 with a zoom-in on the interesting area in Figure 56 and shows the reflection at the port which is 20 mm below the ground plane and the impedance is normalized to 50 ohm in the figure. The impedance is significantly different from the MoM model and is easier to match.

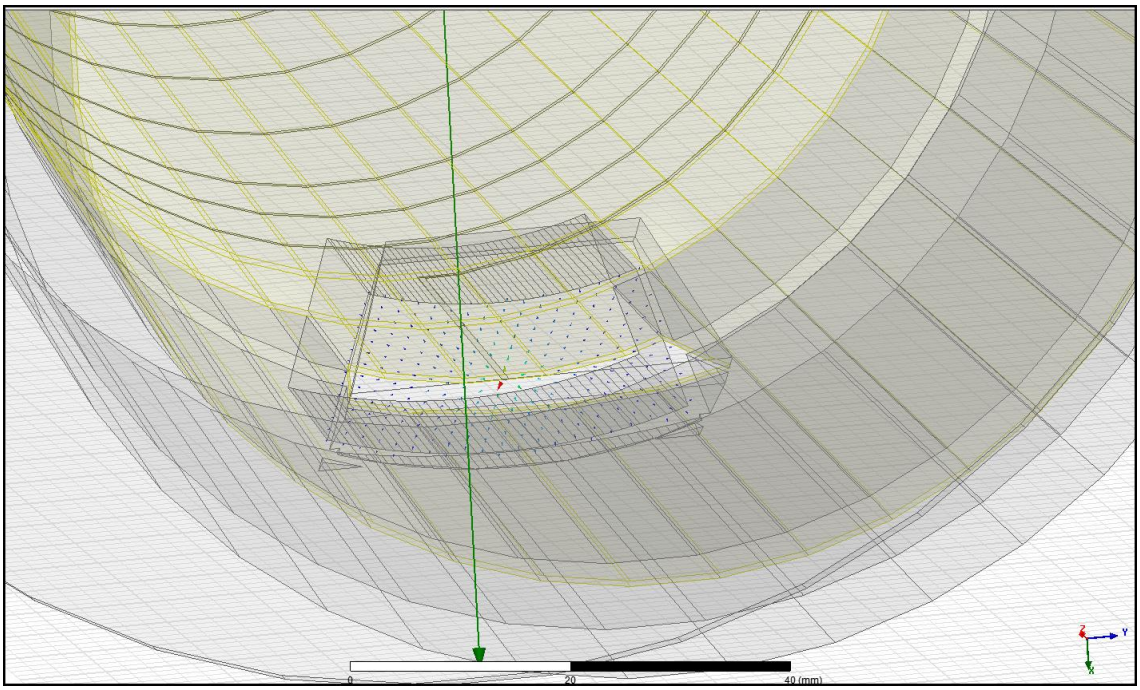


**Figure 54: The port in the HFSS model of the monofilar helix antenna with ground plane. The electric field in the port is also included.**

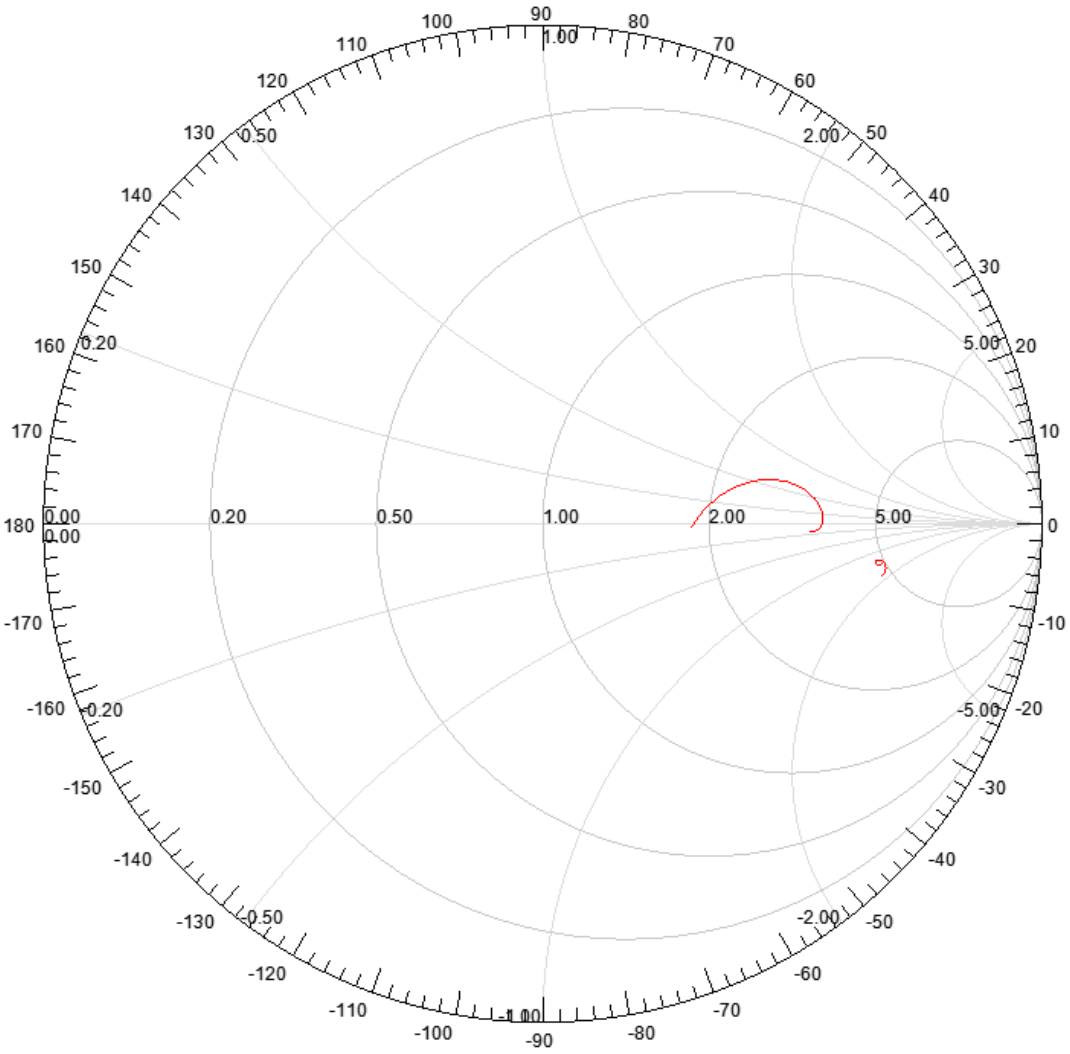


**Figure 55: The Smith chart for the frequencies 1164 - 1249 MHz and 1559 - 1604 MHz for the HFSS model of the monofilar helix with ground plane. The impedance is normalized to 50 Ω which is the impedance of the distribution net.**

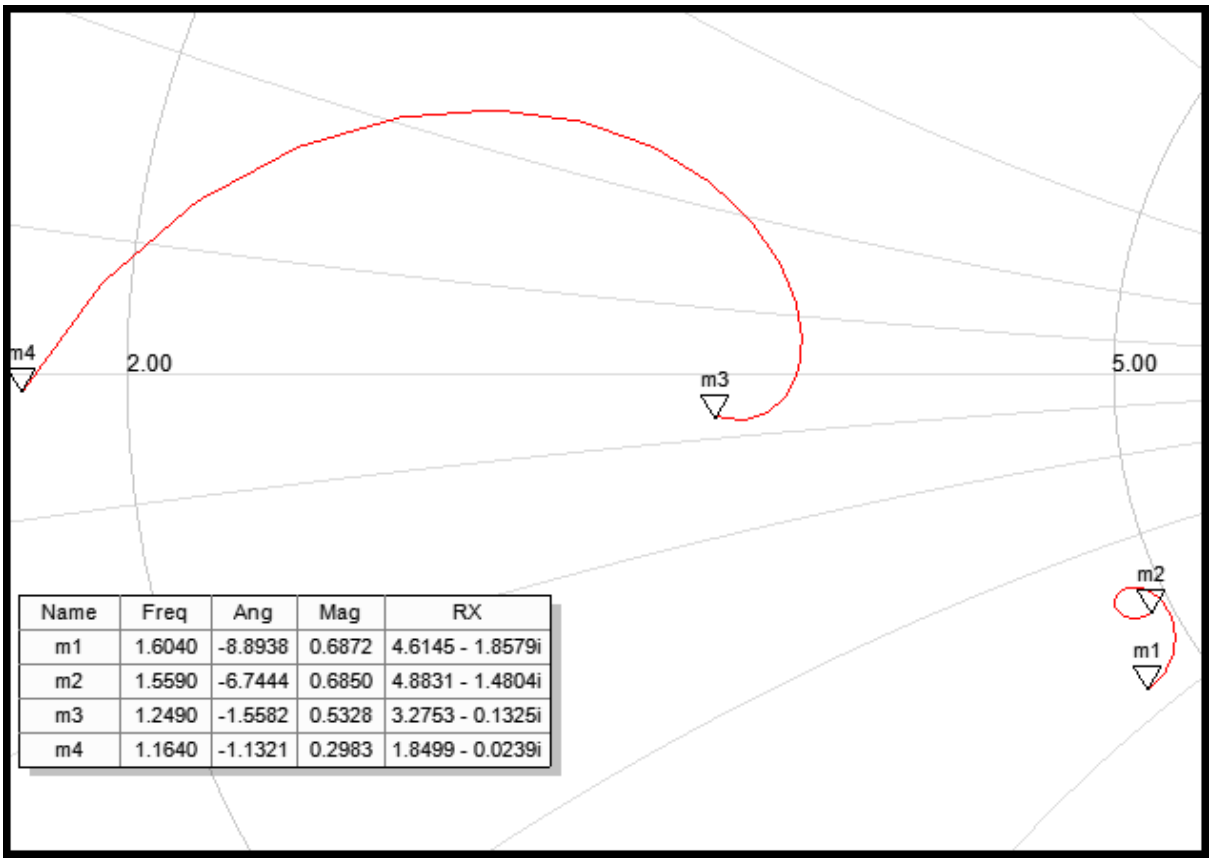


| Name | Freq | Ang | Mag | RX |
|---|---|---|---|---|
| m1 | 1.6040 | -8.8938 | 0.6872 | 4.6145 - 1.8579i |
| m2 | 1.5590 | -6.7444 | 0.6850 | 4.8831 - 1.4804i |
| m3 | 1.2490 | -1.5582 | 0.5328 | 3.2753 - 0.1325i |
| m4 | 1.1640 | -1.1321 | 0.2983 | 1.8499 - 0.0239i |

**Figure 56: Zoom in on the Smith chart, Figure 55, of the monofilar helix with ground plane simulated in HFSS. The impedance is normalized to 50 Ω which is the impedance of the distribution net.**

The computed RHCP gain is presented in Figure 57. The gain fulfils the minimum requirement. The XPD presented in Figure 58 is greater than 15 dB from 0° - 32° theta for 1164 MHz with a maximum at 0° of 25.8 dB for 1605 MHz the 15 dB in XPD is only fulfilled at 0° and is 11.6 at 32°.

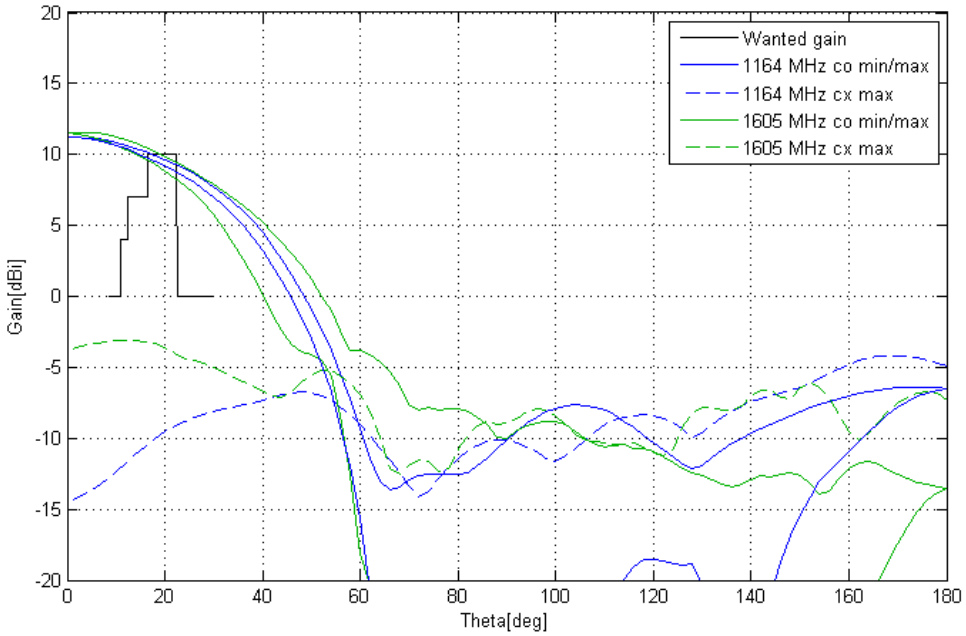


**Figure 57: The min/max gain for RHCP (co) and the maximum gain for LHC polarization (cx) of the monofilar helix model in HFSS.**

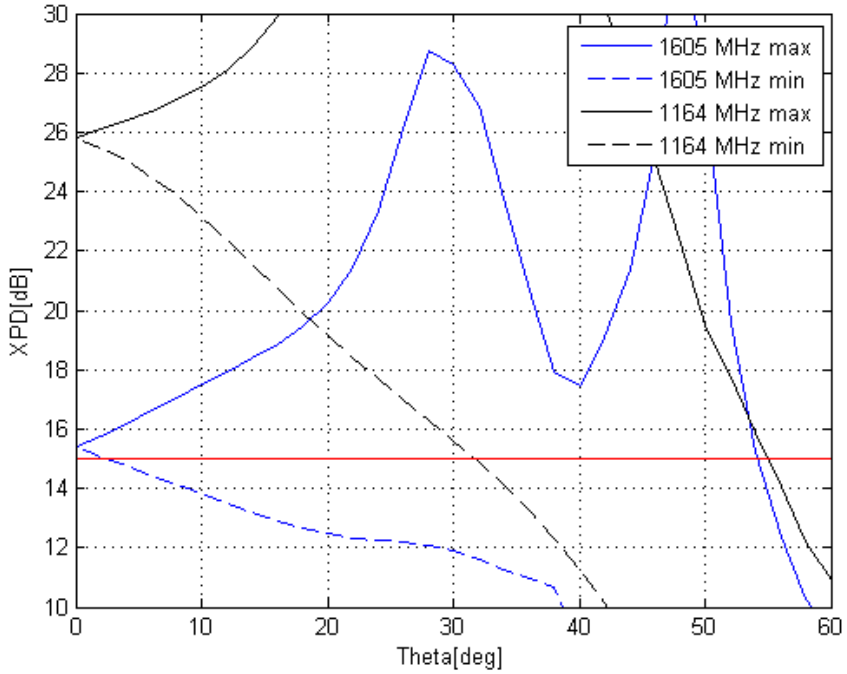


**Figure 58: The minimum/maximum XPD for RHCP at 1164 MHz and 1605 MHz for the HFSS model of the monofilar helix antenna with ground plane.**

### 3.4.3.4 Phase centre and group delay

The phase centre for the antenna was found by finding the position along z-axis where the phase difference over -40° – 40° in theta was as small as possible, where the wave looks as close as possible to a spherical wave. At 1164 MHz the phase centre was located at 127 mm above the ground plane and at 1605 MHz it was located 243 mm above the ground plane. As the shift of phase centre was only 116 mm between the highest and lowest frequency it can be assumed that the phase centre variation over frequency fulfills the specifications. The phase difference from a perfect spherical front at the phase centre is calculated, phase radiation pattern, and presented in Figure 59 for 1164 MHz and in Figure 60 for 1605 MHz. A difference of 10° is observed at 1164 MHz which corresponds to a difference of 7 mm in position, for 1605 MHz the largest deviation was 20° which corresponds to 10 mm in position difference.

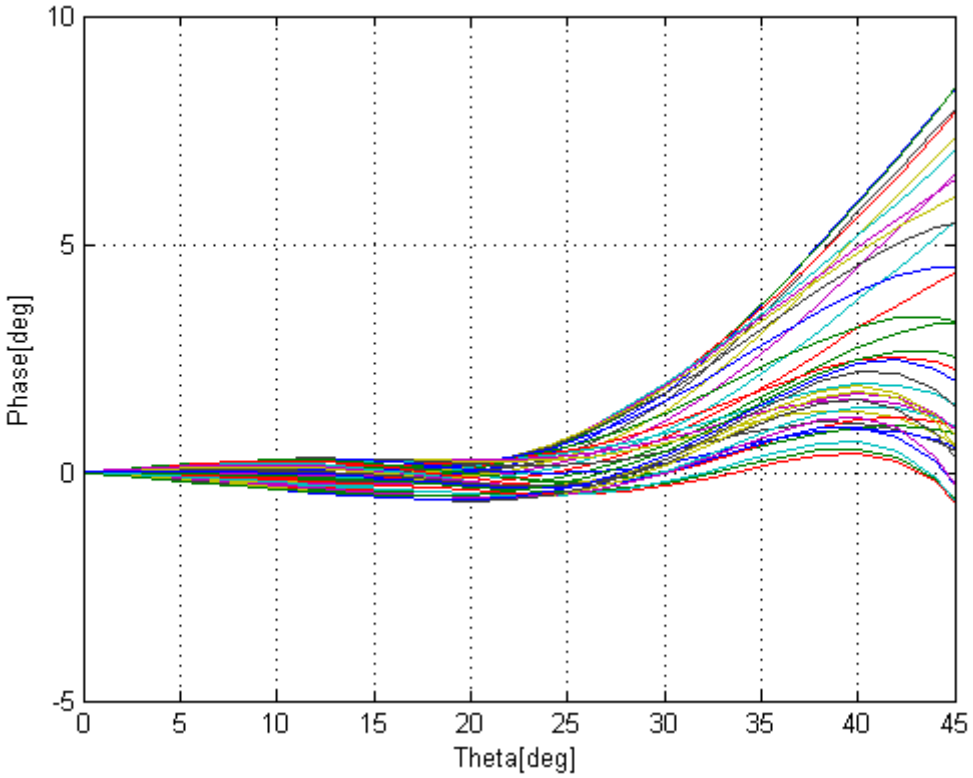


**Figure 59: The phase radiation pattern of the monofilar helix antenna at 1164 MHz. Colour represents different phi cross sections, with a step of 10 degrees.**

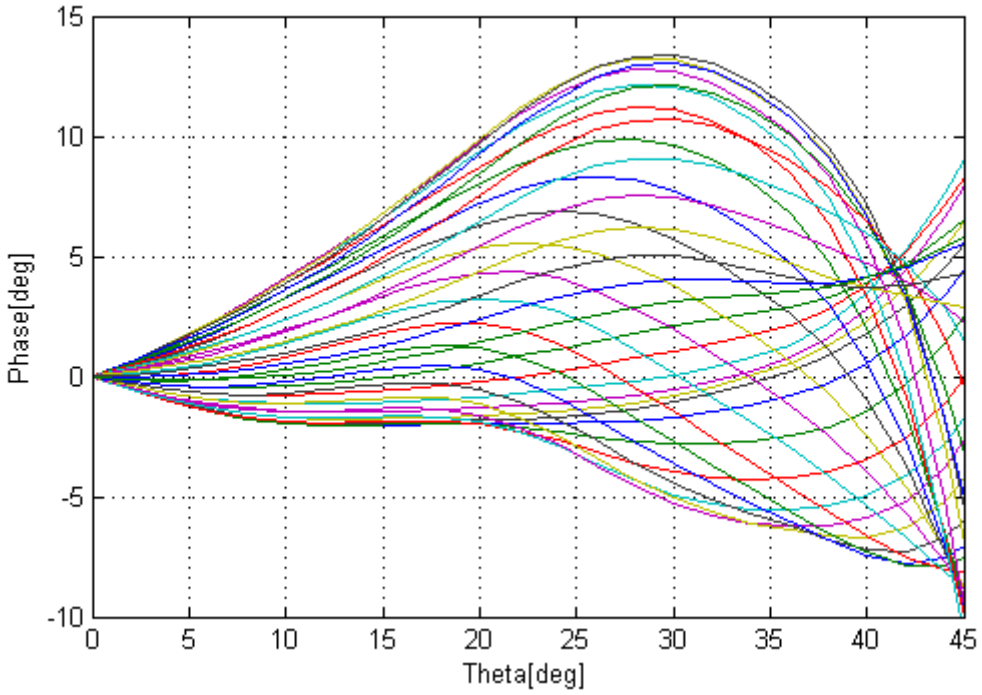


**Figure 60: The phase radiation pattern of the monofilar helix antenna at 1605 MHz. Colour represents different phi cross sections, with a step of 10 degrees.**

The group delay can vary both over frequency and theta. The group delay over theta is presented in Figure 61 and 62 for 1164-1188 MHz (L5 band) respectively for 1598 - 1605 MHz (L1OC band). The group delay variation is below 0.4 ns at 20° and is just slightly below the specification at 40° for 1164-1184 MHz. Between 1598-1605 MHz the group delay over theta is within specification at 20° but is considerably above specification at 40°. The group delay variation over frequency is discussed in Section 3.4.4.

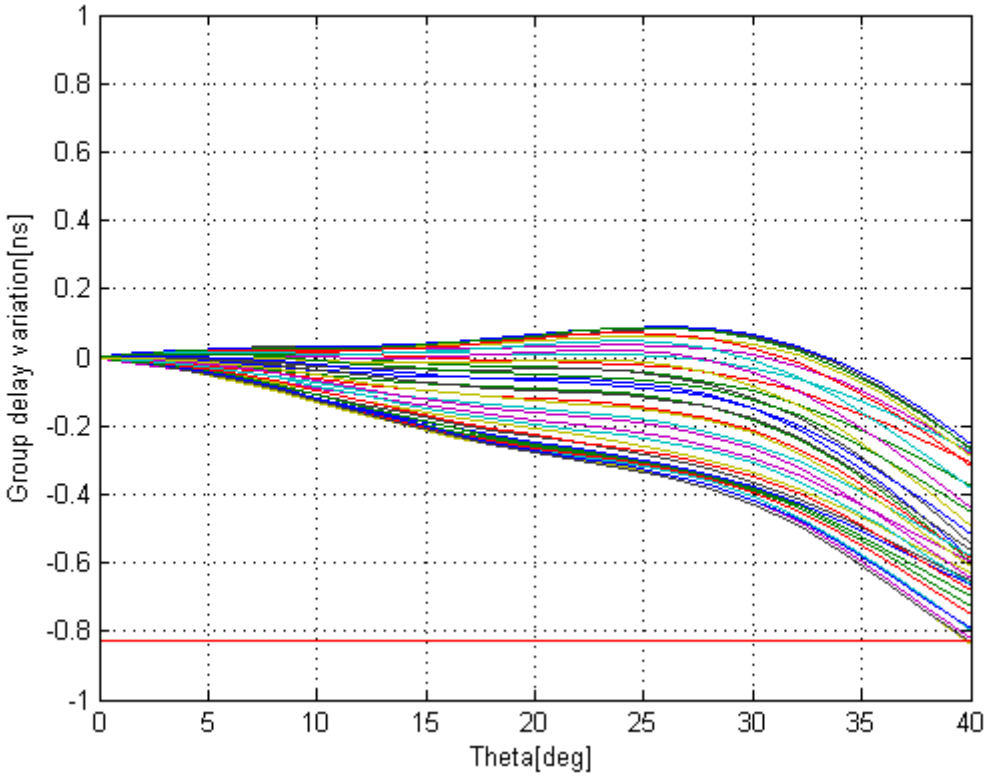


**Figure 61: The group delay difference over theta on the GPS L5 band (1164 - 1189 MHz) for the monofilar helix antenna. The red line marks the specification on max 0.83 ns in group delay difference. Colour represents different phi cross sections, with a step of 10 degrees.**

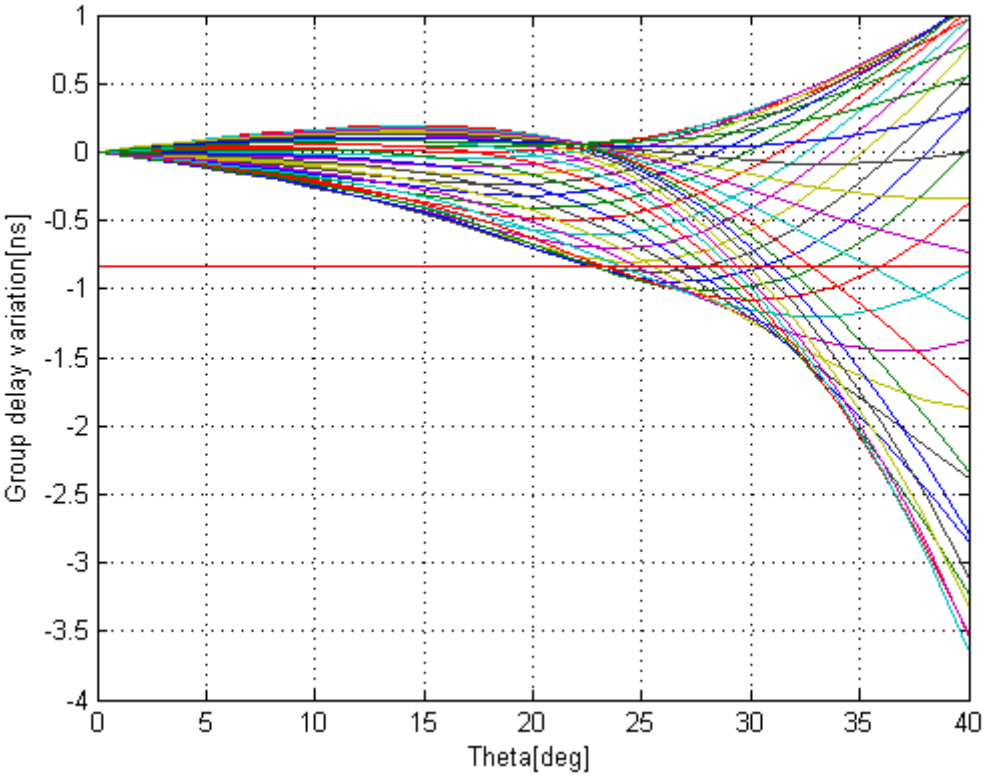


**Figure 62: The group delay difference over theta on the GLONASS L1OF band (1597 - 1605 MHz) for the monofilar helix antenna. The red line marks the specification on max 0.83 ns in group delay difference. Colour represents different phi cross sections, with a step of 10 degrees.**

### 3.4.4 Feed network

As presented in Figure 55 the monofilar antenna with ground plane is not well matched and would need a matching circuit to be used. The matching network is intended to be printed on the same cone as the helix is printed on, to make the antenna easy to manufacture. The matching circuit is here simulated and thought of as a micro strip with the inner side of the bottom structure as ground plane. There is vacuum between the matching circuit and the ground plane and therefore the relative permittivity was set to 1 and losses set to 0, there is also a thin slab of the dielectric material of the cone above the trace but that is neglected here.

First it was investigated if a single network would be able to match over the full spectrum for the WireMoM result but as no solution was found, a design involving a diplexer was selected. Using the diplexer design means that the antenna has two ports one for the upper frequency band and one for the lower frequency band. Normally there is a diplexer just before the filter, which in turn is before the LNA itself. Using this configuration means that the diplexer at the filter could be removed which could lead to a small improvement in the noise figure but would also mean that two coax cables would have to be routed from the antenna to the filter.

In the matching circuit presented in Figure 63, transmission lines, T-section and radial stubs are the used components. Radial stub was selected as they are less complex then couplers and it can achieve better bandwidth than normal stubs [68]. ADS was used to simulate the circuit.

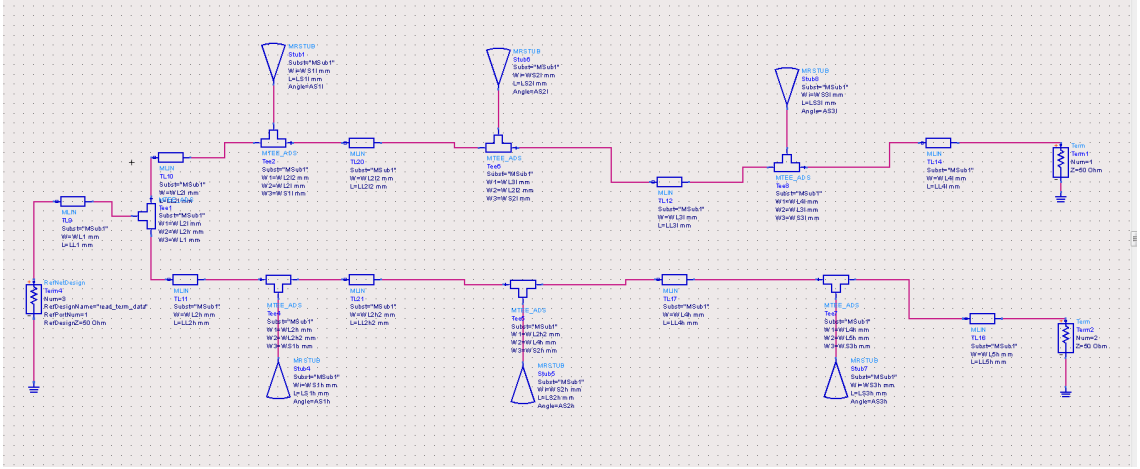

**Figure 63: The matching network for the monofilar helix antenna with ground plane. The antenna is to the left and the port for the lower band is to the upper right corner and to the bottom right corner is the port for the upper band.**

Yield optimization was used on the model where the distance to the ground plane and the length of the first transmission line after the antenna port were given a variation of +-0.1 mm and the other parameters were given a variation of +-0.01 mm. The result was that if the coupling (S12) was restricted to -18 dB and the reflection (S11, S22) for the output ports were restricted to -18.5 dB it was possible to get a 100 % yield, for -19 dB on S11 and S22 there was a 90 % yield and for -20 dB there was a 80 % yield. The S-parameters for the nominal configuration of the -18.5 dB yield optimization case is presented in Figure 64 where port 2 is for the higher frequency band and port 1 is for the lower frequency band. The insertion loss is presented in Figure 65.

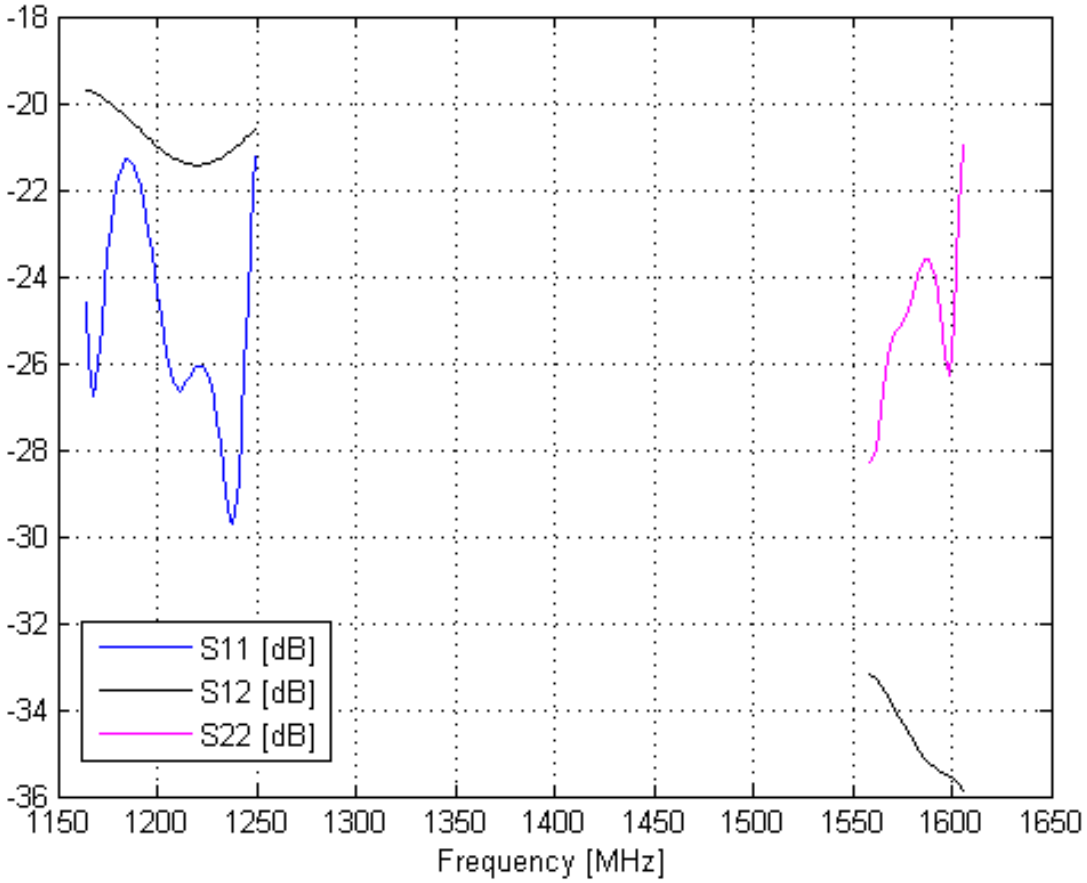


**Figure 64: The S-parameters of the matching network for the monofilar helix where port 1 is for the lower frequency band and port 2 is for the upper frequency band. The simulation is with the nominal values from the yield optimization to -18.5 dB with 100% yield.**

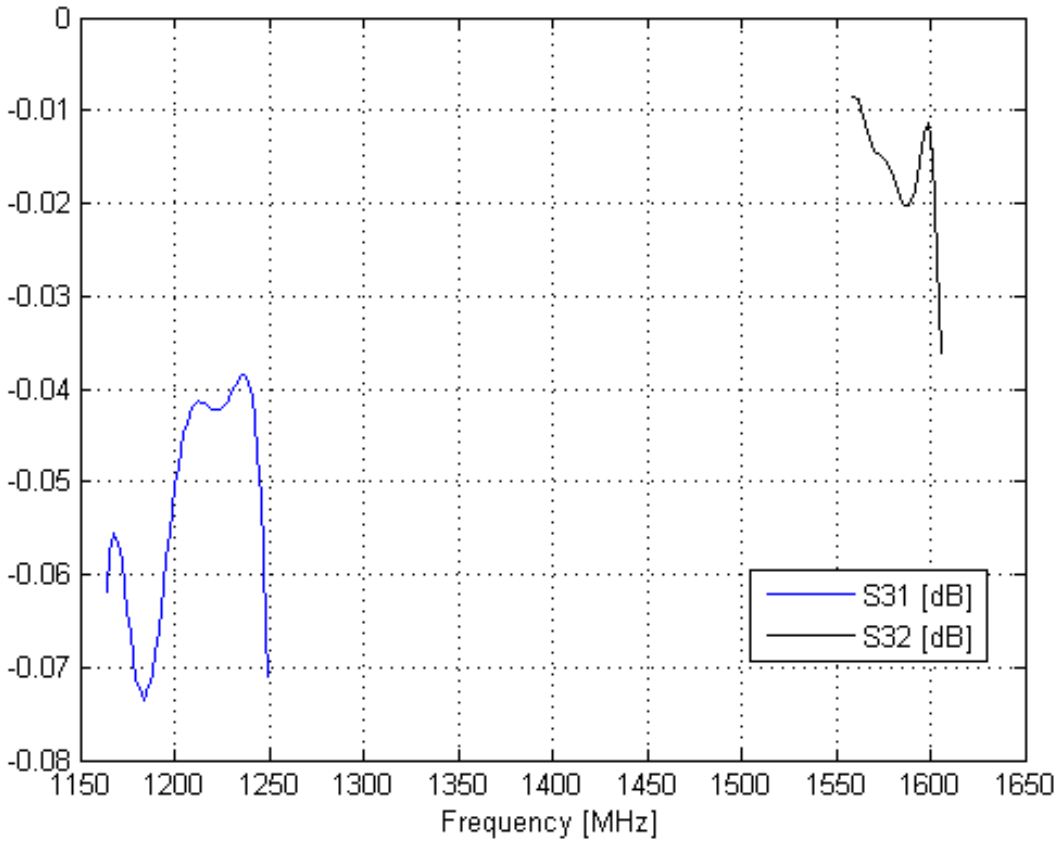


**Figure 65: The insertion loss for the two frequency bands for the matching circuit for the monofilar helix antenna with ground plane. The simulation is with the nominal values from the yield optimization to -18.5 dB with 100% yield.**

The matching circuit has a group delay variation over frequency as does the antenna and both the group delay from the antenna and matching circuit and the combined group delay over frequency is presented in Figure 66. The group delay variation from the matching circuit are somewhat opposite to the group delay variation from the antenna but the resulting group delay variation is still larger than the wanted specification over the B2I, E5B and L1 C band, observe that the group delay variation over L1 and E1 is within specifications. Over B21 the group delay variation is 1.40 ns which correspond to an error of 0.4 m, over E5B the group delay is 1.23 ns and over L1 C the group delay is 0.90 ns.

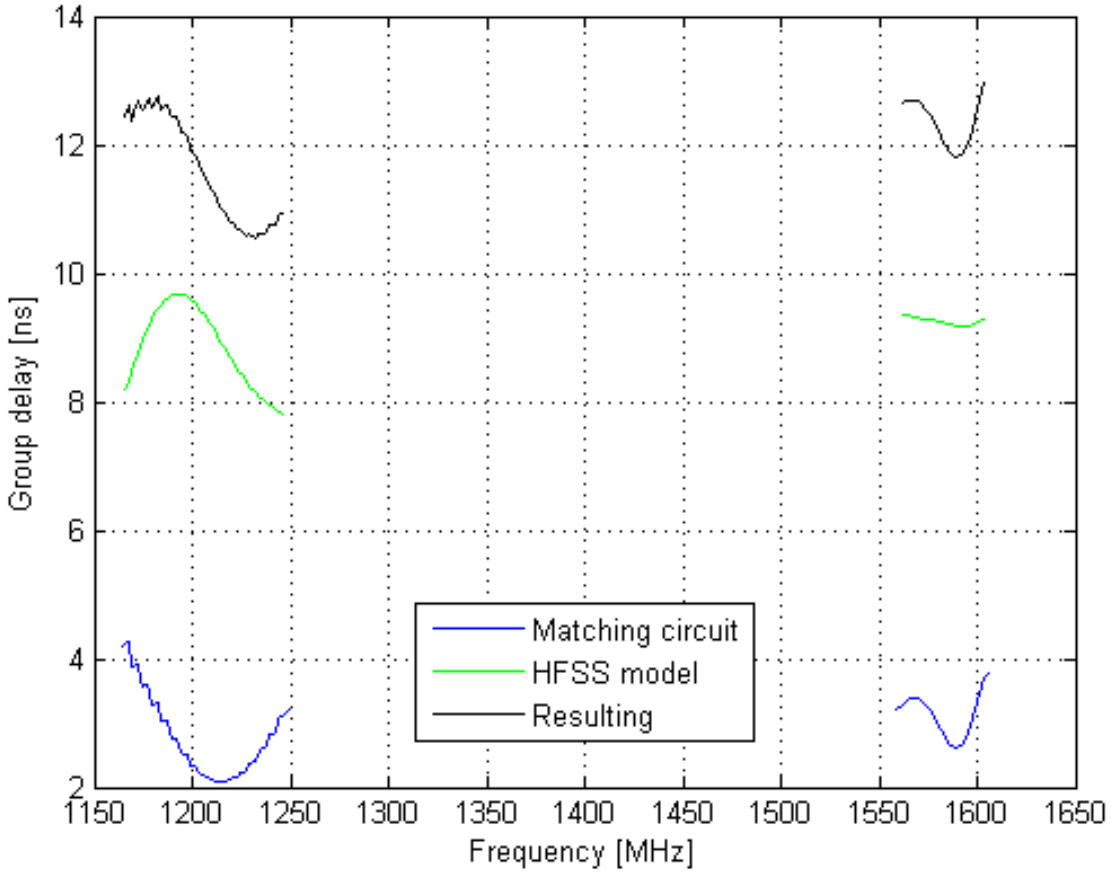


**Figure 66: The group delay for the matching circuit, the monofilar helix antenna simulated in HFFS and finally the resulting group delay from both sources combined.**

In this design the matching network goes down 80 mm from the ground plane which would mean that the network is close to a notch as presented in Section 3.4.5 in Figure 67. This would mean that the matching network might not act as expected and it could be preferable to increase the height of the base or decrease the height of the notch. As the circumference at the place where the matching network is placed is only 336 mm and the matching network is 348 mm long, a bend in the outer end of one/both transmission line/lines before the port is necessary but this is not included in the model.

### 3.4.5 Mechanical construction

The monofilar helix antenna consists of three parts, excluding screws and connectors: the sheet where the helix and matching network is printed upon, the inner ground plane and the outer ground plane. The sheet itself can be 0.2 mm thin and has a relative permittivity of 3.63. The sheet is rolled up over a model cone and glued with epoxy. On the sheet the helix is printed in intervals and not in one full loop, the helix is printed so it is on the outside of the cone. After the dielectric sheet has been rolled up to the cone the helix is soldered together.

The two parts which make up the ground plane are made out of aluminium, are manufactured using CNC and have a mass of 672 g. A cross section of the antenna is presented in Figure 67 showing how the cone is placed corresponding to the other parts along with showing the groove for the matching circuit. The dielectric cone is glued to the bottom and the top of the outer ground structure. The inner ground structure is connected by screws to the outer ground structure.

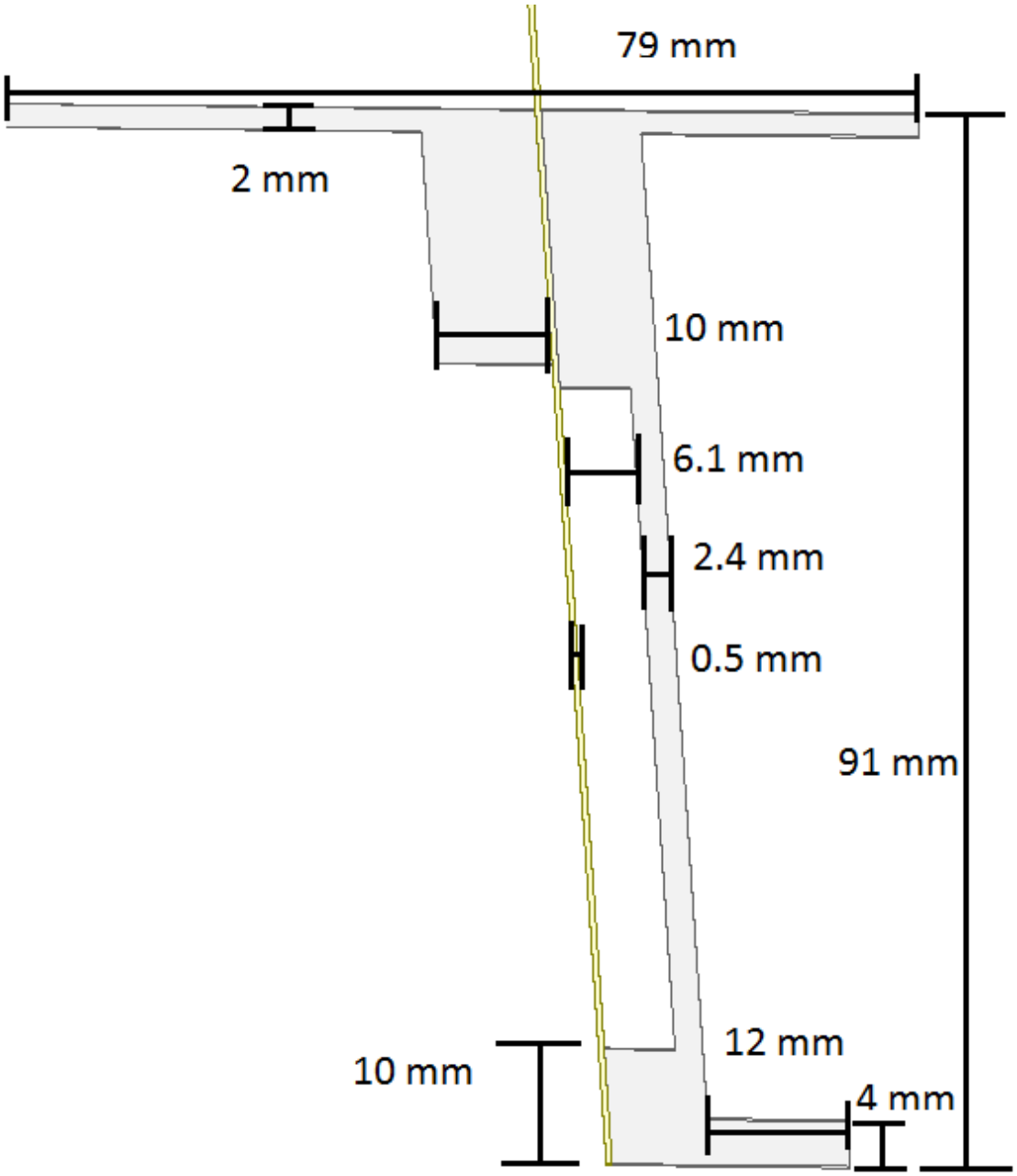


**Figure 67: A cross-section of what the bottom structure of the helix antenna would look like. Some of the features like the notch in the bottom on the outside are not in the simulated HFSS model.**

In reality the ground piece would need stilts on the outer side but the thickness of the skin could probably be reduced to 1.5 mm from 2.4 mm so the mass would not change drastically. The helix antenna is in total 437 mm high with a diameter of 148 mm. The extra plate of 12 mm at the bottom allows the antenna to be fixed to a satellite and is not in the simulated HFSS model. The Helix antenna is estimated to need eight m5 screws to attach it to the satellite, six screws to connect the inner ground plane to the structure and two SMA connectors. The mass is estimated to be 740 g and the breakdown of weight for each part is presented in Table 23.

**Table 23: The estimated weight of different parts and the total weight of the helix antenna.**

| Item | Number | Weight addition each [g] | Total Weight [g] |
|---|---|---|---|
| Metal structure | 1 | 672 | 672 |
| Cone | 1 | (1750 kg/m^3) | 86 |
| Paint and glue | 1 | 10 | 10 |
| Screws to satellite | 8 | 3 | 24 |
| Screws to ground plane | 6 | 3 | 18 |
| SMA connector | 2 | 4 | 8 |
| Screws for SMA connector | 2×4 | 1 | 8 |
| Total weight | | | 826 |

## 3.5 Hispasat AG1 GPS Antenna

RUAG has already delivered a GPS antenna for use in GEO orbit. The antenna was for the Hispasat AG1 satellite, the first using the European small geostationary satellite platform. The antenna is a PEC antenna and is shown in Figure 68 and the gain is presented in Figure 69. The antenna is <0.191 m high, has a diameter of <0.215 m and weighs <585 g.

**Figure 68: An Image of the PEC antenna used for GPS reception on Hispasat AG1.**

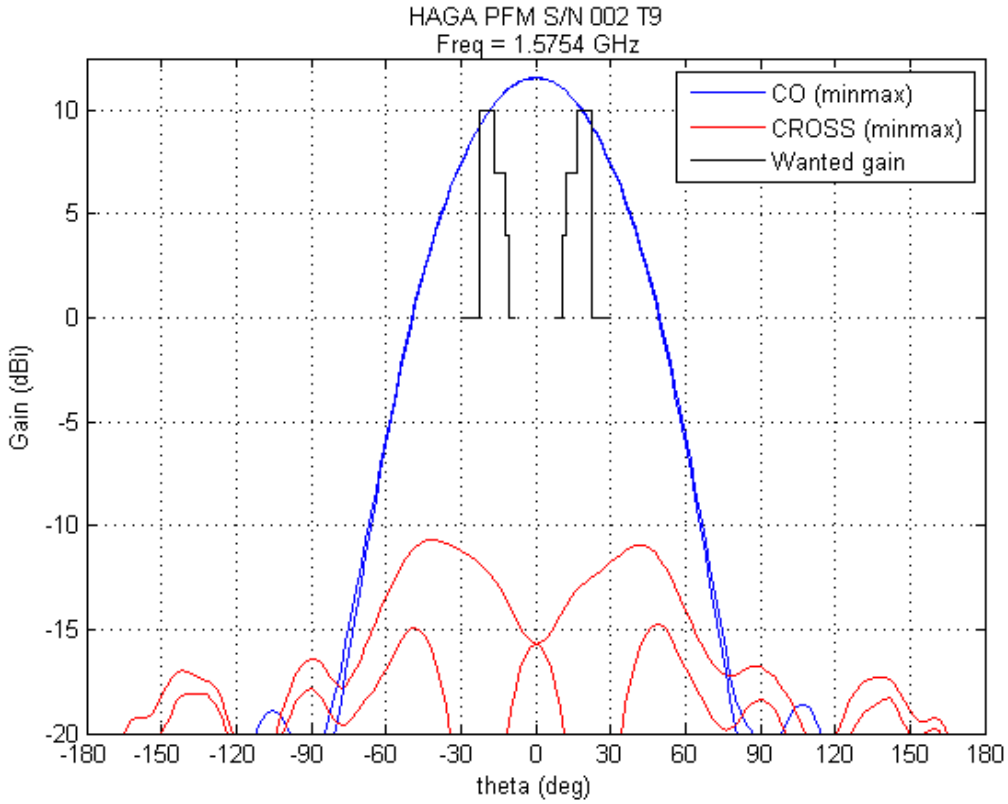


**Figure 69: The min/max gain of the RHCP (co) and the LHCP (cx) for the PEC antenna for Hispasat AG1 in HFSS.**

# 4 DISCUSSION

First in Section 4.1 the methods used is discussed in some detail; namely optimization which was used a lot, and different error sources; both of which cause the results to be different between different simulations and some of how accurate the results are. In Section 4.2 the choice of 30 dBHz as acquisition threshold and the choice of conical radiation pattern during antenna type selection are discussed. The results are discussed in Section 4.3 and the fulfilment of the specifications is discussed in Section 4.4. Possible future improvements are discussed in Section 4.5 and the preferred choice of antenna for different situations is presented in Section 4.6.

## 4.1 Methods used and error sources

Optimization was used during the project for both testing out different array setups, designing the quad and mono helix antenna and for the matching net. When using optimization it is important to remember that the optimization algorithm searches for the solution with the minimum cost within a specified parameter interval. This means that if the parameters are not limited correctly you might get something that is not possible to build or you might for example get something narrow banded if you only have the cost function for a certain frequency. One more thing to remember is that you might not find the best solution which satisfies your cost function, you might find a local minimum even if you use a genetic algorithm. Another part to remember is the computing time, having too wide parameter span might take too long to get the optimization to start to converge. For example for the helix optimization, some created geometries took two hours to simulate while 10-30 min was more common for an geometry.

### 4.1.1 Array field calculations

For the array case the result was calculated by multiplying the element factor by the array factor. This does not take into account the coupling of elements which is of major importance, moreover no antenna design has of course been tested on a satellite.

### 4.1.2 The helix HFSS model

For the monofilar helix there was quite big difference between the result for the matching between the MoM model and the HFSS model, even if the radiation pattern was consistent. A reason for this could be that in the generated monofilar helix model with ground plane the feed did not go all the way down to the ground plane in the MoM model, which it did in the HFSS model. Furthermore in the HFSS model the feed is 20 mm below the ground plane. This might explain the difference in calculated impedance.

The HFSS model also includes the bottom structure while the WireMoM model only has a circular ground plane. Moreover in the HFSS model the trace was created by doing two sheets, one sheet was not enough to be able to create the helix all the way to the top, which were wrapped around the dielectric cone and this has not created an exact copy of the WireMoM model. There are some very small differences in the trace and the total number of turns is not exactly the same as for the WireMoM case. This can be due to that the cone is not actually a cone but 40 flat segments making up something close to a cone or that the start of the helix was slightly miss-placed. Furthermore the helix is a round wire in the MoM model while it is a flat trace, which is infinitely thin, in the HFSS model.

The HFSS model was only meshed at two frequencies the highest and the lowest frequency. There was quite some difference among the two, at the higher frequency the trace higher up in the helix was more heavily meshed which probably was because of the very different current distributions. The differences should be small within the bands but the accuracy is probably lower at the other ends of the bands.

It should also be noted that the array field calculations of the array was done at the highest and lowest frequency of the wanted frequency band and not at the centre frequency of the L1 and L2 GPS bands. The difference in result would be small as the transition of the radiation pattern from 1164 MHz to 1605 MHz is smooth. Presenting the results at the highest and lowest frequency of the wanted region also makes the results easier to compare to the helix if a more wideband element would be used and as stated before the coupling between elements is not taken into account and that the element was not matched in the HFSS simulation.

## 4.2 Assumptions made

In this report it is assumed that the receiver can acquire signals at a $C/N_0$ level of 30 dBHz and based on this the specifications were made which resulted in the antennas presented here. The choice of 30 dBHz was based on the fact that several space GNSS receivers have a threshold in that region and that the small geo satellite uses the Mosaic receiver which has that threshold. If a receiver with a much lower threshold is used, 20-25 dBHz, it might be useful to put specifications so to allow second side lobe reception. On the other hand the second side lobe, I think, might have larger omnivariation.

The antennas presented here could probably already receive the signal at the second side lobe if the threshold was set to 22 dBHz as is the threshold for Navigator GPS receiver. But if the reception requirement would be lowered it would probably be desired to increase the gain further out, which might mean to reduce the peak gain for the helix and the three element array and move the lobe outwards for the twelve element array. For the helix this might be accomplished by using the optimizer with a goal of lower gain but out to 30 degrees with parameters close to what it currently has. For the array the most obvious way to do this by reducing the distance between the element, but this is probably not possible as they sit very close already. Reducing the gain of the elements might be a way to solve this.

Another assumption made, when the antenna type was selected, was that the antenna would have a conical radiation pattern. As the pattern in the end, for two of three antenna alternatives, ended up being high gain pattern other antenna types as horns could possibly be considered to be used as GNSS antennas.

## 4.3 Results

Some of the results presented in the report were not as expected or is worth to discuss in some detail. For example the reason why there was a comparison between having no cable and 3 m cable in the link budget is discussed in Section 4.3.1. In Section 4.3.2 the reason why the XPD is the same for the element and the array is discussed. In the last section, Section 4.3.3, the helix results are discussed including the difference in results between the single and double layer quadrifilar helix and the current distribution on the monofilar helix.

### 4.3.1 Link budget

When calculating the link budget and investigating how the losses from the cable affected the performance, it was thought that maybe the LNA could be placed outside the satellite close to the antenna. When looking on the interface temperature of a GEO satellite, -100 to 120°C, it is clear that this is not possible as the LNA has active semiconductor components, and most semiconductor components cannot handle that temperature span. The filter, on the other hand, could perhaps be placed on the outside and give the opportunity to have only one coax cable from the filter on the outside to the LNA. This would reduce noise figure for the LNA module, which includes the filter, as one diplexer could be removed.

### 4.3.2 Array results

The XPD for the arrays were the same as the XPD for the element. This is probably because the elements in the arrays are turned in the same direction. By turning the elements toward the centre of the array the XPD would probably be improved at least for the twelve element array. The phase patterns could perhaps also be affected.

### 4.3.3 Helix results

It was quite surprising that the quadrifillar double layer helix was so different from the single layer case. According to theory, the cases should be the same and thus give the same results. As I have not done any bigger investigation into the matter I do not have any good reasons for why the results are as they are. The single layer quad helix showed promise but would need to be matched somehow to be useable.

The monofilar helix results were good though. The gain patterns on both frequencies are very similar and bell like. At first there was hope that perhaps a conical pattern could be created, as helixes are capable to produce conical patterns. The reason is probably that it is not possible to have adequate pattern on both frequencies if the radiation pattern is conical on one band/frequency. Furthermore as the patterns are as similar it indicates that the specification was at the border of what was possible to do with a helix.

The current along the helix trace for the monofilar case is also interesting. It seems that the helix starts to radiate higher up at the higher frequency and the current is just propagating along the lower part. The length in wavelengths of the radiating part of the helix seems to be approximately the same over frequency. It should be noted that the position where the helix starts to radiate moves smoothly over frequency. The strict requirement on the gain might be the reason why the helix turned out like this, to allow the radiation pattern to be the same over frequency.

The monofilar helix antenna design was also tried with a cone and to allow the cone angle to change for the different sections. The improvement over the case with just a ground plane was small, only 10 mm in radius. The thought regarding adding the cone and change of cone angle option was that the antenna could be made as directive as the monofilar with only the ground plane but in an even smaller size. The reason why that was not possible can be that the change of pitch angle might have had the same effect as those new changes. For example the pitch angle at the top is very low and this might have the same effect as indenting the top of the helix.

In Section 3.4.4 the yield of the matching network for the helix was discussed. A yield of 85 % of course means that 3 of 20 will not satisfy the specifications. This does not necessarily mean that they have to be thrown away, if means for trimming have been implemented. One option could be to have trim screws in the ground plane or that perhaps the cone could be regulated along the height.

## 4.4 Fulfilment of specifications

All specifications were not fulfilled for all antennas; there were problems with the reflection at the port, bandwidth and the group delay variation. The reflection at the port for the helix case was higher than specified and ideas of how to get above 20 dB are presented in Section 4.5. For the group delay variation over frequency, both the helix and the array does not fulfil the specifications. For the array this is because the element is not matched, for the helix it is after matching.

### 4.4.1 Bandwidth

The ring element is not able to cover the full wanted bandwidth. It covers possibly the full upper band and the L2 band. The frequencies that can be used are though not only decided by the antenna but the rest of the system, and if the receiver does not support one signal there is no loss not to be able to receive it on the antenna ether. It is good though to have an antenna which works on all frequencies so it can be offered as a GNSS antenna to all customers.

### 4.4.2 Group delay

There is also a problem with the group delay variation over theta for the twelve element array and the helix even if the range is to be taken to be the same as for the phase variation, over ±40° theta. First it should be noted that the range over ±40° might be a bit on the top as when the GEO satellite sees a GPS satellite at 39° in theta, it is a little more for GALILEO because of the higher orbit, the GPS satellite sees the GEO satellite at 90° and it is well past the second side lobe. The range ±40° was chosen to be a bit more consistent toward [48] but a more realistic number would probably be at the end of the first side lobe which the gain is specified at 22.5° or end of the second lobe at 30°. Secondly the group delay over theta and the group delay over frequency should probably be added together when deciding if the antennas pass the specifications.

For the twelve element array the group delay is within specification to 30°, but the helix is does still not meet specification at the upper frequency. The question is if the group delay, and phase centre stability, really has to have so strict requirements. The reason to choose these specifications was to not introduce more error than [9] had found, +-0.5 m, for their best case scenario on position error. At the same time it should be noted that one of the stricter specifications on position in GEO, for GOES-R, was 100 m. Another thing to note is that it is true that the satellite will look like it is 1 m further away with an error of 1 m but for a navigation solution the position of several satellites are used with a least square method and the final error might not be 1 m. It might also be possible to correct for the phase centre and group delay variation in the receiver.

### 4.4.3 Cross polarization

The XPD had not any specifications over which range it should be fulfilled but it would be reasonable to have it up to 22.5 or 30 degrees. The helix at the highest frequency does not satisfy this. The loss is 0.15 dB higher at 11.9 dB XPD compared to the specified 15 dB XPD which has a small impact on the performance, but it needs to be clarified that the XPD is below 15 dB at only some phi values so the affect on the navigation performance is probably negligible. Another concern regarding the XPD is the suppression of multipaths, as when a wave is reflected the polarization changes. Reflections from earth are not a problem as the XPD is 15 dB and the wave would have to travel through the atmosphere twice which would dampen the wave. Multipaths from other satellites are extremely unlikely so than it is only multipaths on the satellite itself that can be a problem. The multipaths would than come from outside the -40° to 40° theta region and the important parameter would be the minimum strength of the wanted signal, co-polar gain at 22 degrees theta, compared to the maximum strength of a multipath, cx-polar gain, which is 13 dB for the helix. 13 dB would be the worst possible scenario and it would probably be enough suppression of multipaths to not affect the performance.

## 4.5 Future work

Only the ring element with the somewhat poor bandwidth was tested with the array setup but this should give an indication on what performance is possible with the arrays even if other elements are used. It is possible that another element which covers a wider bandwidth but is a bit bigger could be used instead, which of course would make the array a bit bigger and it might be necessary to lower the gain on the elements as discussed in Section 4.2. One possibility would be to use the RUAG PEC element or design a new element, perhaps a small helix. Furthermore the coupling between the elements has to be investigated to get a better approximation on how the array performs.

For the helix, the height could probably straight away be reduced by 20 mm by removing the extra pieces of cone at the top. Moreover if the height is ranked higher than to keep the number of parts down, a PCB could be attached to the bottom of the ground plane with the matching network and the height could further be reduced. This solution of course would mean that the material of the PCB might need to have quite high dielectric constant to make the network fit and the material of the PCB need to be able to survive in space. If the current design is kept it is probably necessary to simulate the helix with the matching network included to get an accurate result as the there are some irregularities in the ground plane.

It might also be worth investigating if the matching network can be simplified further or if the reflection coefficient at 100 % yield could be improved. One suggestion would be to instead of covering the full bandwidth on both bands, to cover only where the wanted signal is as there exists some space in the frequency plane between L1C and L1OF in the upper band and some smaller spaces at the lower band. Another thing to consider is if the requirement on the coupling between the ports could be a bit lower, for example 15 dB, which might allow for a better solution. Another way would be to investigate if the feed of the helix itself could be tweaked in a way that would produce a case which is easier to match.

It might be worth to consider combining the filter and the matching net. The matching network and the helix in themselves will most likely (as presented in Figure 64 I did not simulate the full band) suppress unwanted parts of the band to some degree and would perhaps allow the filter + matching network to have less components than if they were separated.

The weight has been estimated quite well for the monofilar helix case but for the arrays there has been more guessing. For the arrays the weight can probably be reduced as the arrays do not necessarily have to have a circular shape and some material could be removed from the edges. Furthermore the feed network was very roughly estimated and it would be useful to have better estimation regarding this.

## 4.6 Choice of antenna

Of the different antennas presented here there is none which suits all cases. When choosing an antenna there are a number of criteria that need to be considered:

- **Size and weight is the most important parameter.**

For some cases a small footprint is required to fit on the satellite, which would mean the helix antenna is the viable solution. In other cases the height is restricted and the array antenna solution would be the only possible one. The choice between the different array antennas would beside footprint also be affected by how much the antenna is allowed to weigh, if the antenna is restricted to 1 kg or if it can weigh more. The standalone PEC antenna is somewhere in between the helix and the array in size.

- **What frequencies are supported is the next most important parameter to consider if several antenna options fit the satellite.**

This is because I would prioritize be able to see more satellites at the same time over precision of measurement to a single satellite, I also think that supporting more frequencies is better than higher gain for getting more satellites visible. Some satellites might use a single frequency receiver though, as for example the first iteration of the European small geo satellite platform which only uses the GPS L1 band, which would mean that there would be no advantage in supporting more frequency bands. Then the current PEC antenna would work just as well as the helix in this respect. There are quite a few receivers that can handle frequencies on both bands on the other hand which would mean that in cases where they are used the helix or the array could be the best solution. In regards to the array case, as stated in Section 4.5, it is probably possible to create an array with the same bandwidth as the helix antenna.

- **The other performance parameters are then considered**

The last consideration would be the rest of the criteria which would allow greater precision in the measurement for each satellite and the gain. So if neither size nor frequency makes the array choice inferior to the helix solution, the array solution would probably be the best. Which array to choose would be decided on weight and size limitation. The cost of the different solutions is unknown to me but that could of course also be a limitation.

## 4.7 Impact on society and sustainability

The GNSS antenna is a part of a system which enables the satellite to be navigated autonomously which for the society means that less resources, here as time for operators and facilities for deciding the position of the satellite, needs to be used to keep the satellite within its designated box. As the traditional manoeuvres, with the satellite drifting from one side of the box to the other, not necessarily have to be used perhaps the fuel consumption could be further optimized. If less fuel is used the satellites could be made lighter or perhaps allow for a greater life span of the satellite. A greater life span would mean that replacement satellites can be launched later which reduces the amount of launches. In the case of lighter satellites the rockets could perhaps carry more satellites per launch or be loaded with less fuel.

A GNSS navigation system can further allow for better position accuracy then the standard on the ground positioning systems. Greater position accuracy could be needed for scientifically experiments placed on environmental satellites which for example could improve wheatear forecasts and help climate research. With a GNSS navigation system these experiments could be made with reasonable costs.

The GNSS antenna itself of course has to be built to last as there is no cheap way to replace or repair it in space. Because of this the antenna concepts presented in this report is intended to be made out of materials which can handle the conditions in space. Furthermore from a system perspective several antennas can be used for redundancy.

# 5 CONCLUSION

There are currently two fully operating GNSSs, GPS and GLONASS, and two more in the making, GALILEO and COMPASS. Currently these systems are widely used on earth and in LEO for autonomous navigation. Autonomous navigation is also preferable for satellites in GEO, to reduce cost and perhaps improve accuracy, and there are several planned missions which intend to use GNSS for navigation. Several studies have shown that it is possible to use GNSS navigation in GEO and there are several different receivers for GNSS reception in space.

The task for this master thesis is to design an antenna for GNSS reception in GEO orbit and to do that the specifications were first decided. All the GNSSs use several frequencies and it was decided that the requirement for the antenna was to cover all the open bands. A link budget was also created and the threshold for the gain was decided to be at least 8 dBi, but preferable 10 dBi, over the first side lobe of the GNSS antennas. The antenna is not supposed to weigh more than 1 kg.

It was decided that array and helix antenna types were the best options. For the array case a three element circular array and a twelve element solutions were chosen to be investigated further. Together with a ring element the antennas were simulated, using array factor times element factor. The results showed that they fulfilled most of the set requirements and would be an option for use as GNSS antenna in GEO.

For the helix case, a quadrifilar helix antenna was first investigated but judged not suitable. Instead a monofilar helix antenna was investigated, first with MoM simulations. A monofilar helix with a ground plane fulfilled the gain requirement. It was possible to reduce the size by using a truncated cone instead of a ground plane and allow changes in the cone angle of the helix, but the benefit was judged to be too small compared to the added complexity. The monofilar helix with a ground plane was then simulated in a full wave simulator using FEM, the program was HFSS, and the result showed that the requirements were fulfilled well enough to be considered as an alternative as a GNSS antenna for GEO.

The best antenna is based on the specific requirement for a mission. For missions which requires a flat antenna the array antennas are the best option but if a small footprint is preferred the helix antenna is better. What frequencies the GNSS receiver onboard supports can also affect the choice of antennas where the helix supports all open frequencies while the array element which was used here only supports the L1 and L2 GPS frequency (and possible frequencies close to the L1 GPS frequency as E1).

# 6 REFERENCES

[1] ”History of GPS: Global Positioning Systems: National Park Service,” National Park Service, USA, [Online]. Available: http://www.nps.gov/gis/gps/history.html. [Accessed 10 February 2014].

[2] ”Space Segment: Systems: GPS,” U.S. government, [Online]. Available: http://www.gps.gov/systems/gps/space/. [Accessed 10 February 2014].

[3] S. Revnivykh, *GLONASS Status and Modernization,* Beijing, 2012, [Online]. Available: http://www.oosa.unvienna.org/pdf/icg/2012/icg-7/3-1.pdf. [Accessed 25 June 2014].

[4] China Satellite Navigation Office, ”BeiDou Navigation Satellite System Signal In Space Interface Control Document Open Service Signal B1I (Version 1.0),” China Satellite Navigation Office, 2012.

[5] China Satellite Navigation Office, “*BeiDou Navigation Satellite System and International Activities [Power Point],”* Presented at Workshop on Space Applications for Disaster Risk Reduction and Management &Second Workshop on the Use of Multi-Global Navigation Satellite Systems for Sustainable Development, Bangkok, 2013.

[6] A. Bhaskaranarayana, *Indian IRNSS and GAGAN,* Montreal, 2008, [Online]. Available: http://www.oosa.unvienna.org/pdf/icg/2008/expert/2-3.pdf. [Accessed 25 June 2014].

[7] JAXA, “*Quasi-Zenith Satellite System [Power Point],”* Presented at Workshop on Space Applications for Disaster Risk Reduction and Management &Second Workshop on the Use of Multi-Global Navigation Satellite Systems for Sustainable Development, Bangkok, 2013.

[8] M. Moreau, P. Axelrad, J. Garrison, M. Wennersten och A. Long, ”Test Results of the PiVoT Receiver in High Earth Orbits using a GSS GPS Simulator,” in *ION GNSS*, Salt Lake City, 2001.

[9] DEIMOS Engenharia S.A, ”Feasibility of GNSS sensors for AOCS Applications in GEO and Higher Altitudes,” DEIMOS Engenharia S.A, 2011.

[10] C. Smith, S. Habinc, M. Bandecchi, D. Hardy och P. Sinander, ”Low cost,ASIC based telemetry and telecommand systems - the TEAMSAT experience,” ESA, 1998.

[11] N. Lemke, B. Eissfeller, O. Balbach, W. Enderle och M. Schmidhuber, ”Results from the GPS Experiment on Equator-S,” in *RTO MP-43*, St. Petersburg, 1999.

[12] T. D. Powell, P. D. Martzen, S. B. Sedlacek, C.-C. Chao, R. Silva, A. Brown och G. Belle, ”GPS Signals in a Geosynchronous Transfer Orbit: “Falcon Gold” Data Processing,” in *Proceedings of the 1999 National Technical Meeting of The Institute of Navigation*, San Diego, 1999.

[13] J. D. Kronman, ”Experience Using GPS For Orbit Determination of a Geosynchronous Satellite,” in *Proceedings of the 13th International Technical Meeting of the Satellite Division of The Institute of Navigation (ION GPS 2000)*, Salt Lake City, 2000.

[14] M. C. Moreau, E. P. Davis, J. R. Carpenter, D. Kelbel, G. W. Davis och A. Penina, ”Results from the GPS Flight Experiment on the High Earth Orbit AMSAT OSCAR-40 Spacecraft,” in *Proceedings of the 15th International Technical Meeting of the Satellite Division of The Institute of Navigation (ION GPS 2002)*, Portland, 2002.

[15] Surrey Satellite Technology US LLC,“*Retired GIOVE-A satellite helps SSTL demonstrate first High Altitude (Press release),”* 2012, [Online]. Available: http://www.sstl.co.uk/Press/Retired-GIOVE-A-satellite-helps-SSTL-demonstrate-f. [Accessed 25 June 2014].

[16] P. Zentgraf, S. Berge, C. Chasset, H. Filippi, E. Gottzein, I. Gutiérrez-Cañas, M. Hartrampf, P. A. Krauss, C. Kuehl, B. Lübke-Ossenbeck, M. Mittnacht, O. Montenbruck, C. Müller, P. R. Boldo och A. Truffi, ”Preparing the GPS-Experiment for the Small GEO Mission,” in *Proceedings of the 33rd Annual AAS Guidance and Control Conference*, Breckenridge, 2010.

[17] ESA, ”SmallGEO: Telecommunications and Integrated and Applications,” ESA, 24 May

2013. [Online]. Available: http://www.esa.int/Our_Activities/Telecommunications_Integrated_Applications/SmallGEO. [Accessed 13 February 2014].

[18] NASA, ”MMS: Missions: Nasa,” NASA, [Online]. Available: http://mms.gsfc.nasa.gov/index.html. [Accessed 13 February 2014].

[19] NASA, NOAA, ”Goes-r,” NASA, NOAA, [Online]. Available: http://www.goes-r.gov/. [Accessed 13 02 2014].

[20] NASA, ”GPS at Geosynchronous Orbit,” NASA, 2010, [Online]. Available: http://www.navcen.uscg.gov/pdf/gps/news/Apr2010/Navigator_Space_Receiver _info_04212010_rev4.pdf. [Accessed 25 June 2014].

[21] D. Chu, S. Chen, D. Early, D. Freesland, A. Krimchansky, B. Naasz, A. Reth, K. Tadikonda, J. Tsui och T. Walsh, ”GOES-R Stationkeeping and Momentum Management,” in *Proceedings of the 29th Annual AAS Guidance and Control Conference*, Breckenridge, 2006.

[22] B. Chibout, C. Macabiau, A.-C. Escher, L. Ries, J.-L. Issler, S. Corrazza och M. Bousquet, ”Investigation of New Processing Techniques for Geostationary Satellite Positioning,” in *Proceedings of the 2006 National Technical Meeting of The Institute of Navigation*, Monterey, 2006.

[23] M. C. Moreau, P. Axelrad, J. L. Garrison och A. Long, ”GPS Receiver Architecture and Expected Performance for Autonomous Navigation in High Earth Orbits,” *Journal of The Institute of Navigation,* vol. 47, nr 3, pp. 191-204, 2000.

[24] L. Qiao, S. Lim, C. Rizos och J. Liu, ”A Multiple GNSS-based Orbit Determination Algorithm for Geostationary Satellites,” in *Proceedings of the IGNSS Symposium 2009*, Qld, 2009.

[25] J. J. Miller,”*GPS Modernization Update & NASA’s GNSS Activities [Power Point],”* Tokyo: NASA, 2010, [Online]. Available: http://www.gps.gov/multimedia/presentations/2010/05/japan/miller.pdf. [Accessed 25 June 2014].

[26] M. Mittnacht, E. Gottzein, M. Hartrampf, J. Heim och P. Krauss, ”The MosaicGNSS Receiver Family Orbit and Attitude Determination in various Orbits,” 2004(?).

[27] Thales Alenia Space, ”GPS RECEIVERS SOLUTIONS,” 2012, [Online]. Available: https://www.thalesgroup.com/sites/default/files/asset/document/GPS_receivers _Solutions092012.pdf. [Accessed 25 June 2014].

[28] Astrium, ”Lion navigator,” 2012, [Online]. Available: http://www.astrium.eads.net/media/document/astrium_pdh9_mdef.pdf. [Accessed 28 August 2013].

[29] Surrey Satellite Technology LLC, ”Surrey SGR-GEO Space GPS Receiver,” 2010.

[30] J. Gerner, J. Issler, D. Laurichesse, C. Mehlen och N. Wilhelm, ”TOPSTAR 3000 – An Enhanced GPS Receiver for Space Applications,” *ESA bulletin,* vol. 104, pp. 86-91, 2000.

[31] W. Bamford, L. Winternitz och M. Moreau, ”Real-Time Geostationary Orbit Determination Using the NAVIGATOR GPS Reveiver,” NASA(?), 2005(?), [Online]. Available: http://www.emergentspace.com/assets/1/7/Final_GEO_copy.pdf. [Accessed 25 June 2014].

[32] O. Montenbruck, A. Hauschild, F. Zangerl, W. Zsalcsik, P. Ramos-Bosch och U. Klein, ”Onboard Real-Time Navigation for the Sentinel-3 Mission,” in *Proceedings of the 22nd International Technical Meeting of The Satellite Division of the Institute of Navigation*, Savannah, 2009.

[33] D. Kelbel, T. Lee och A. Long, ”Autonomous Navigation of Geosynchronous Satellites Using GPS: Maneuver Recovery Study,” NASA(?), 2002, [Online]. Available: http://www.emergentspace.com/assets/1/7/5547_05d_GoesManeuverAnalysis.pdf. [Accessed 25 June 2014].

[34] G. Gibbons, ”BeiDou to Restart Satellite Launches Next Year, Shift B1 Signal Frequency after 2016,” INSIDE GNSS NEWS, 1 May 2013. [Online]. Available: http://www.insidegnss.com/node/3537 [Accessed 10 April 2014].

[35] J. Auerbach, *U.S. GPS Program and Policy Update (PP 2013 IGNSS),* Gold Coast, 2013, [Online]. Available: http://www.gps.gov/multimedia/presentations/2013/07/IGNSS/auerbach.pdf. [Accessed 25 June 2014].

[36] Global Positioning Systems Directorate, ”IS-GPS-200G,” 2012, [Online]. Available: http://www.gps.gov/technical/icwg/IS-GPS-200G.pdf. [Accessed 25 June 2014].

[37] Global Positioning Systems Directorate, ”IS-GPS-705C,” 2012, [Online]. Available: http://www.gps.gov/technical/icwg/IS-GPS-705C.pdf [Accessed 25 June 2014].

[38] Global Positioning Systems Directorate, ”IS-GPS-800C,” 2012, [Online]. Available: http://www.gps.gov/technical/icwg/IS-GPS-800C.pdf [Accessed 25 June 2014].

[39] Galileo, ”European GNSS (Galileo) Open Service Singal In Space Interface Control Document,” 2010, [Online]. Available: http://ec.europa.eu/enterprise/policies/satnav/galileo/files/galileo-os-sis-icd-issue1-revision1_en.pdf. [Accessed 25 June 2014].

[40] ESA, ”Next Steps : Galileo: Navigation: Our Activities: ESA,” ESA, 14 January 2013. [Online]. Available: http://www.esa.int/Our_Activities/Navigation/The_future_-_Galileo/Next_steps. [Accessed 14 February 2014].

[41] Russian Institute of Space Device Engineering, ”Interface Control Document Navigational radiosignal In bands L1, L2 (Edition 5.1) (GLONASS),” Moscow, 2008, [Online]. Available: http://www.onlinegnss.com/Links/ICD_GLONASS_5_1.pdf. [Accessed 25 June 2014].

[42] K. Berstis, *NOAA GPS Receiver Impacts Near LightSquared Transmission Towers & Follow On Testing,* Norfolk, 2011, [Online]. Available: http://www.gps.gov/multimedia/presentations/2011/10/HSRP/berstis.pdf. [Accessed 25 June 2014].

[43] ”Skyterra 1: Satellites :Satbeams,” Satbeams, [Online]. Available: http://www.satbeams.com/satellites?norad=37218. [Accessed 14 February 2014].

[44] C. Ho, A. Kantak, S. Slobin och D. Morabito, ”Link Analysis of a Telecommunication System on Earth, in Geostationary Orbit, and at the Moon: Atmospheric Attenuation and Noise Temperature Effects,” *IPN Progress Report,* vol. 42, nr 168, 2007.

[45] D. Le Vine och S. Abraham, ”Galactic noise and passive microwave remote sensing from space at L-band,” *Geoscience and Remote Sensing,* vol. 42, nr 1, pp. 119-129, 2004.

[46] S. Slobin, C. Ho, A. Kantak och S. Asmar, ”Solar Brightness Temperature and Corresponding Antenna Noise Temperature at Microwave Frequencies,” *IPN Progress Report,* vol. 42, nr 175, 2008.

[47] Gore, ”Gore Spaceflight Microwave Cable Eassemblies,” 2003, [Online]. Available: http://www.gore.com/MungoBlobs/823/355/gore_spaceflight_microwave_cable_assemblies_catalog.pdf. [Accessed 25 June 2014].

[48] ESA, ”Antenna for GNSS-based orbit determination system (Activity Ref. 4C.026),” 2012.

[49] D. S. Coco, S. R. Dahlke och C. Coker, ”Effect of GPS System Biases on Differential Group Delay Measurements,” Geophysics Laboratory, 1988.

[50] J. S. Chatterjee, ”Radiation Field of a Conical Helix,” *J. Appl. Phys.,* vol. 24, pp. 550-559, 1953.

[51] A. V. Praveen Kumar, V. Hamsakutty, J. Yohannan och K. T. Mathew, ”A Wideband Conical Beam Cylindrical Dielectric Resonator Antenna,” *Antennas and Wireless Propagation Letters,* vol. 6, pp. 15-17, 2007.

[52] K. Žmak och Z. Šipuš, ”Radiation Pattern of Arrays Mounted on Conical Structures,” in *Proceeding of the 18th International Conference on Applied Electromagnetics and Communications*, Dubrovnik, 2005.

[53] Y. J. Guo, A. Paez, R. A. Sadeghzadeh och S. K. Barton, ”A Circular Patch Antenna for Radio LAN’s,” *Transactions on Antennas and Propagation,* vol. 45, nr 1, pp. 177-178, 1997.

[54] K.-J. Jeon, K.-i. Lee, J.-g. Son, T.-K. Lee, J. W. Lee och W.-K. Lee, ”X-band isoflux pattern antenna for SAR data transmission,” in *Procceding of the 3rd International Asia-Pacific Conference on Synthetic Aperture Radar*, Seoul, 2011.

[55] K.-C. Chen, Y. Qian, C.-K. C. Tzuang och I. Tatsuo, ”A Periodic Microstrip Radial Antenna Array With a Conical Beam,” *IEEE Transactions on Antennas and Propagation,* vol. 51, nr 4, pp. 756-765, 2003.

[56] S.-H. Son, S.-I. Jeon, C.-J. Kim och W. Hwang, ”GA-Based Design of Multi-Ring Arrays With Omnidirectional Conical Beam Pattern,” *IEEE Transactions on Antennas and Propagation,* vol. 58, nr 5, pp. 1527-1535, 2010.

[57] C. Vegni och F. Bilotti, ”Spaceborne Orbito Payload Study and L2c Antenna Design for Precise Geosynchronous Orbit/Time Determination,” in *Proceedings of the European Navigation Conference—Global Navigation Satellite Systems*, Napoli, 2009.

[58] K. Louertani, R. Guinvarc'h, N. Ribiµere-Tharaud och M. Hélier, ”Study of the Radiated Polarization of an Antenna Array With Circular Geometry,” *Progress In Electromagnetics Research,* vol. 24, pp. 173-183, 2011.

[59] H. Ekström, ”Generell GO,” SAAB space (now RUAG space), 2009.

[60] J. Zackrisson och M. Öhgren, ”GNSS Receive Antennas on Satellites for Precision Orbit Determination,” in *Proceedings of the AIAA/USU Conference on Small Satellites, Communications, SSC11-XI-6*, Logan, 2011.

[61] G. Zhou, ”A non-uniform pitch dual band helix antenna,” in *Proccedings of Antennas and Propagation Society International Symposium*, Salt Lake City, 2000.

[62] J. S. Chatterjee, ”Radiation Field of a Conical Helix,” *Journal of Applied Physics,* vol. 24, nr 5, pp. 550-559, 1953.

[63] J. Bäck, J. Zackrisson, M. Öhgren och P. Ingvarson, ”A New Quadrifilar Helix Antenna Family with Flexible Coverage for Space Applications,” in *Antennas and Propagation, 2007. EuCAP 2007. The Second European Conference on* , Edinburgh, 2007.

[64] A. R. Djordjevic, M. M. Ilic, A. G. Zajic, D. I. Olcan och M. M. Nikolic, ”Why Does Reflector Enhance the Gain of Helical Antennas?,” in *Antennas and Propagation, 2007. EuCAP 2007. The Second European Conference on* , Edinburgh, 2007.

[65] H. Nakano, Y. Samada och J. Yamauchi, ”Axial Mode Helical Antennas,” *Antennas and Propagation, IEEE Transactions on ,* vol. 34, nr 9, pp. 1143-1148, 1986.

[66] R. Golubovic, A. Djordjevic, D. Olcan och J. Mosig, ”Nonuniformly-wound helical antennas,” in *Antennas and Propagation, 2009. EuCAP 2009. 3rd European Conference on*, Berlin, 2009.

[67] H. Nakano och J. Yamauchi, ”Characteristics of modified spiral and helical antennas,” *Microwaves, Optics and Antennas, IEE Proceedings H,* vol. 129, nr 5, pp. 232-237, 1982.

[68] P-N Designs, Inc, ”Quarter-wave tricks :Encyclopedia: Microwaves101,” P-N Designs, Inc, 31 December 2011. [Online]. Available: http://www.microwaves101.com/encyclopedia/quarterwave.cfm. [Accessed 25 Februari 2014].